Field Weldability And Hydrogen Assisted Cracking In Hsla Pipeline Steels Including The Arctic Grade.

FIELD WELDABILITY AND HYDROGEN ASSISTED CRACKING IN HSLA PIPELINE STEELS INCLUDING THE ARCTIC GRADE

by

Ramaswamy Vasudevan

A Dissertation
Presented to the Graduate Committee
of Lehigh University
in Candidacy for the Degree of
Doctor of Philosophy
in
Department of
Metallurgy and Materials Engineering

Lehigh University
1979

Approved and recommended for acceptance as a dissertation in partial fulfillment of the requirements for the degree of Doctor of Philosophy.

4 May 1979
(date)

R D Stout
Professor in Charge

Accepted 4 May 1979
(date)

Special committee directing
the doctoral work of
Ramaswamy Vasudevan

Alan W. Pense
Alan W. Pense, Chairman

Ernest A. Jonas

R D Stout
Robert D. Stout

David A. Thomas
David A. Thomas

ACKNOWLEDGEMENT

The author gratefully acknowledges the guidance and constructive criticism of Dr. R. D. Stout and Dr. A. W. Pense during the entire course of this work and for the many stimulating discussions that shaped this study. Sincere appreciation is expressed to the other members of the author's special committee viz., Mr. E. A. Jonas and Dr. D. A. Thomas for their contributions during the course of this work. Special thanks are due to Mr. G. V. Krishna of Air Products and Chemicals, Inc. for his help in conducting acoustic emission studies. Also to be acknowledged is the help rendered by the technical staff of the Metallurgy Department - in particular Messers M. Sheska, W. Mohylsky, D. Conklin, D. Bush and J. Beedle. Thanks are also due to Doris Dillman for typing the manuscript and to Mr. R. S. Wu for making the drawings.

Finally, the author acknowledges the financial support of this research program by the American Petroleum Institute, the American Iron and Steel Institute, and Lehigh University for its support through the Hornor Fellowship.

TABLE OF CONTENTS

LIST OF TABLES

LIST OF FIGURES

ABSTRACT

The present study was aimed at (i) developing a simple, quantitative, reproducible test which is easy to carry out in the field to assess the field weldability of high strength pipeline steels (ii) developing a crack sensitivity formula to account better for the greatly reduced susceptibility to hydrogen assisted cracking of low carbon micro-alloyed steels (iii) correlating the newly developed test with a weldability test already in use such as the Implant test and (iv) a better understanding of the morphology and kinetics of crack growth in high strength pipeline steels using fractography and acoustic emission monitoring techniques.

A 150 x 200 mm specimen cut from formed pipe/ plate with a central machined slot in the girth direction (which is incidentally transverse to the rolling direction) and welded with a cellulosic electrode with welding conditions matching those used in the field was found to develop hydrogen induced cracks. The test was examined for sensitivity and reproducibility by testing a wide range of pipe steel compositions and thicknesses and was found to respond, as expected, to carbon, alloy content and gauge.

The test was also shown capable of establishing welding procedures such as preheat and time lapse between the root pass and the hot pass to ensure crack free welds. For one particular heat the results of the slot weld test were shown to correlate well with

those of the girth shop welded pipes if somewhat conservatively.

A crack sensitivity formula was suggested to account better for the greatly reduced sensitivity to hydrogen induced cracking of low carbon micro-alloy steel. The new formula was shown to be better than the IIW formula but the extent of scatter was about the same as that for the Japanese formula for the limited extent of data available from the present investigation.

Correlation studies of the slot weldability test and the Implant test on a selected number of steels were conducted. The slot weldability test ranked these steels in the same order as the lower critical stress in the Implant test.

Acoustic emission and fractographic studies conducted on Implant as well as slot weldability tests indicated that in a straight 0.26% carbon-manganese steel crack initiation occurred immediately after loading at all hydrogen levels examined, and crack growth occurred during the entire test by relatively fast quasi-cleavage and microvoid coalescence processes with little contribution from intergranular processes. By contrast, in a low carbon micro-alloyed steel, crack initiation occurred immediately after loading at high hydrogen levels for all stress levels examined; but a definite incubation period was noted at lower stress levels when welded with low hydrogen electrodes. The lower the stress, the longer was the incubation period.

The crack growth in the micro-alloyed steel was predominantly intergranular (a relatively slow process as indicated by AE studies) in nature at low stress intensities giving way, progressively, to quasi-cleavage and microvoid coalescence with increase in stress intensity. Both the morphology and kinetics of crack growth were shown to be strongly influenced by microstructural effects.

The results of changes in both fracture mode and crack growth rates in the materials studied in this investigation were associated with the hydrogen-assisted cracking model proposed by Beachem and by the lattice decohesion theory.

Future work was suggested in the way of modifying the Implant test specimen based on a compact tension specimen design which would make possible the application of fracture mechanics principles to the study of hydrogen assisted cracking in weldments. This should go a long way toward a better understanding of the mechanisms of hydrogen assisted cracking in weldments in quantitative terms.

CHAPTER I

WELDABILITY OF PIPE LINE STEELS

I. A. Introduction:

In recent years, a significant increase in energy demand has necessitated the exploitation of energy resources in the arctic and off-shore area. Concurrently the demand for construction of pipelines to transport oil and natural gas to regions where it will be ultimately put to use has also increased dramatically.[1-5] Increases in pipe diameter and wall thickness have been a part of the improvement in gas transportation technology. Concomitantly, yield strengths of pipeline materials have also increased over the years to permit higher pumping pressures and hence greater through put per unit volume of pipe.[6-7] In the construction of pipe lines by the "stove pipe" technique (a large proportion of pipeline fabrication continues to be based on the stove pipe technique although recently semi-automatic and automatic gas-shielded processes are being gradually introduced)[6,8-10] the production of girth welds is often accomplished under difficult conditions of weather and terrain. Further, the desirability to use extremely high hydrogen potential cellulosic electrodes for the root pass, very low heat inputs adopted in the interests of speed and the relatively high carbon equivalents of many traditional high strength pipeline steels have kept the possibility of increased potential of hydrogen

induced cracking a matter of great concern to the constructor. Hydrogen assisted cracking, also referred to in literature as cold cracking, delayed cracking, underbead cracking, hard cracking and internal hydrogen embrittlement in general, is probably the most important potential source of defects in the welding of hardenable materials (indeed, it has recently been referred to as "the only really severe defect"[11]) which might ultimately lead to leakage in or brittle fracture of a pipeline. Hence it is easy to see how "weldability" has come to be regarded as virtually synonymous with the degree of susceptibility to cold cracking (hydrogen induced cracking). Since the stove pipe technique is still the mainstay in production of pipelines, the development of new types of high strength steels, viz low-carbon micro-alloy steels, with a markedly reduced suspectibility to cold cracking has assumed considerable significance. Even though the metallurgical knowledge on which mirco-alloyed steels are based was established at least a decade back,[12] their widespread application has come about only recently with increasing demand for higher-strength, thicker-walled linepipe which is typical of the latest developments in the pipeline industry.[13-15]

The damaging effects of hydrogen first in ferrous and later on in non-ferrous materials has been recognized and researched for more than a century.[16-18] Yet, there is considerable controversy over the mechanism and kinetics of hydrogen-induced cracking

and a complete understanding of the problem has remained highly elusive; especially in the field of welding. The reason for this lack of understanding will become apparent when the complexity of hydrogen embrittlement phenomenon is elaborated upon in a later chapter. Nevertheless, the conditions under which hydrogen-induced cracking in steel weldments can occur have been clearly established. This phenomenon results from a combination of the following three factors acting simultaneously. (i) stresses applied to a welded joint, including the residual stresses arising from the differential expansion and contraction as the weld metal and heat affected zone go through the weld thermal cycle. (ii) a source of hydrogen which provides a concentration of hydrogen in the molten weld metal introduced by electrode moisture, an organic coating or contamination in the weld joint. (iii) an unfavorable low-temperature transformation product in the heat affected zone and/or weld metal which depends upon the chemistry of the base metal and filler metal.

Since hydrogen induced cracking is so important to weldability, there has been a proliferation of tests proposed to evaluate this tendency, and designed to evaluate one or more of the aforementioned factors. All the weldability tests can be broadly classified into two groups: viz., self-restraint tests and external-restraint tests. A serious drawback of these weldability tests is that all of them utilize elaborate laboratory techniques including metallography to study the extent of cracking in steels and hence

they are deemed unsuitable to field pipe fabrication conditions.[19] Moreover, some of these tests do not match welding conditons used on pipe construction and others lack the unique configuration of pipes. For the assessment of field weldability of pipeline steels it is necessary to have available a test which is simple, reliable and easy to carry out in the field. Also, the potpouri of weldability tests has led to international efforts to correlate the various weldability tests so as to contribute to a better understanding of individual tests conducted to date. Hence it is imperative that any new weldability test developed should be correlated with a well established weldability test already in use.

As pointed out earlier, both chemical and physical factors influence the susceptibility of steels to hydrogen-induced cracking, the base metal composition being very critical. The effect of composition has been incorporated in the "carbon equivalent" formula as an index of hydrogen cracking tendency. One of the most commonly used formula adopted by IIW[20] is

$$C\ E = C + Mn/6 + (Cr+Mo+V)/5 + (Ni+Cu)/15$$

The Japanese investigators have proposed a more elaborate formula, the cracking parameter being a linear combination of carbon equivalent (Pcm), intensity of restraint and diffusible hydrogen.[21]

In using the carbon equivalent formulae to predict the weldability of steels, it should be realized that all these formulae were developed for straight carbon manganese and/or conventional low alloy steels

with carbon content not less than 0.07%. These formulae have become increasingly suspect in predicting the weldability of the newly developed family of micro alloyed steels which are essentially very low carbon (0.03-0.06%) high strength alloy steels of the arctic grade combining high strength, excellent toughness and good weldability.[22-24] A need exists for an expression for carbon equivalent which places greater emphasis on carbon level [25-27] to account for the greatly reduced susceptibility to hydrogen induced cracking of arctic grade steels.

I. B. Objectives of the Present Study:

1. To develop a weldability test which is simple, reliable and easy to carry out in the field to assess the field weldability of pipeline steels (slot weldability test)
2. To employ the slot weldability test to establish procedures such as preheat and time lapse between root pass and hot pass in susceptible steels so as to ensure girth welding of pipelines free from hydrogen assisted cracking
3. To develop a new carbon equivalent (cracking sensitivity) formula applicable for very low carbon high strength steels
4. To correlate the new test with a weldability test already in use such as the Implant test
5. To characterize the mechanism of hydrogen-assisted cracking in susceptible steels by
   (i) Fractography on Implant and slot weld test specimens
   (ii) Metallography, and

(iii) Study of initiation and kinetics of propagation of hydrogen assisted cracking in Implant as well as slot weld test specimens.

CHAPTER II
THE PROBLEM OF HYDROGEN EMBRITTLEMENT

II. A. Background:

Hydrogen embrittlement, in general, refers to the severe degradation of physical and mechanical properties of materials by the action of hydrogen which renders the material unattractive, unreliable or dangerous. Hydrogen embrittlement is encountered in most materials of engineering importance in one form or the other over a wide range of environmental conditions.

Hydrogen-metal interactions studied to date can be broadly classified into three categories (1) Hydrogen reaction embrittlement (2) Hydrogen environment embrittlement and (3) Internal hydrogen embrittlement (also called hydrogen assisted cracking).

II. A. 1. Hydrogen Reaction Embrittlement (HRE)

Also sometimes called as high temperature hydrogen attack, this form of hydrogen-metal interaction is based on chemical reaction of hydrogen with itself, with the matrix or with a foreign element in the matrix. Once hydrogen is absorbed, (the source of hydrogen can be one of many possibilities such as the atmosphere during melting, pickling, electroplating, welding etc) it may react near the surface or diffuse substantial distances before it reacts. The new phases (hydrides) formed by these reactions are found to be quite stable [18] and embrittlement is not reversible during room temperature aging treatments.

Hydrogen in the atomic form can react either with the matrix or with an alloying element and assume specific lattice positions within the metal to form hydrides (MH_x). Examples of this type of hydrogen-metal interaction are hydride formation in Titanium, Nickel, Aluminum, Zirconium and also in a number of other materials.[16] Atomic hydrogen can also react with itself to form molecular hydrogen generating high pressures to form defects. Examples of this type of hydrogen-metal interaction are found in steel processing and welding and have been termed "flaking" or "fish eyes". Another possibility is that atomic hydrogen can interact with a foreign element to form a gas. An example of this is the degradation of mechanical and structural integrity of carbon steels brought about by the high temperature reaction of hydrogen with the carbon to form methane (CH_4) bubbles.[17-18] Another example is the formation of blistering or blow holes by the reaction of atomic hydrogen with oxygen in copper to form steam (H_2O).[18] This type of hydrogen embrittlement is not considered in the present study.

II. A. 2. Hydrogen Environment Exbrittlement (HEE)

This form of hydrogen-metal interaction encompasses the group of environment-sensitive problems caused by the exposure of the metal to hydrogen bearing or hydrogenous environment resulting in severe degradation of strength and toughness of the material. HEE occurs typically in the temperature range from $-100^{o}C$ to $400^{o}C$. HEE appears to be most severe near

room temperature. A group of HEE problems based on the embrittlement of high strength materials by gaseous molecular hydrogen has been referred to in literature as gaseous hydrogen embrittlement (GHE). Another form of HEE results from the interaction of metal with aqueous (3.5% Nacl solution, H_2O etc) hydrogen producing environment - commonly referred to as a class of stress corrosion cracking (SCC) problems. The theory that is most subscribed to is that molecular hydrogen must dissociate to atomic hydrogen for embrittlement to occur. Both adsorption (physisorption, dissociation and chemisorption) and absorption have been postulated to take place for HEE to occur.[16-18] The necessity for subsequent lattice diffusion for HEE has brought about considerable controversy.[18] The seemingly similar mechanisms of HEE and internal hydrogen embrittlement (which will be discussed next) has brought about marked disagreement as to whether HEE is just another form of IHE or truly a distinct type of embrittlement.[18] Hydrogen environment embrittlement is considered in this study only to the extent of its similarity to IHE.

II. A. 3. Internal Hydrogen Embrittlement (IHE)

Also known variously as internal reversible hydrogen embrittlement, slow strain rate embrittlement, delayed cracking and hydrogen assisted cracking which is probably the most generally descriptive term, IHE refers to that group of embrittlement problems wherein reduction of strength and toughness of a material is induced by hydrogen (either in atomic or protonic form)

dissolved in the crystal lattice or trapped at sites in the microstructure. This type of hydrogen-metal interaction forms the basis of the present work with particular reference to embrittlement (cracking) in high strength low alloy pipeline steels accompanying the welding process-one of the major methods of fabrication. Hydrogen can be introduced or charged into the material by any number of industrially important processes such as electro-plating, melting, pickling, welding etc, which might later cause unexpected catastrophic failure of the component in service. For the embrittlement process to be completely reversible, it is necessary that hydrogen should not undergo any type of chemical reaction (as in HEE or HRE) after it has been absorbed within the lattice.

One of the major differences between HEE (including GHE) and IHE resides in the fact that environmental pick-up of hydrogen, as in HEE, usually involves an inexhaustible supply of hydrogen plus the possibility of variations in both environment and surface condition relevant to hydrogen entry into the material; whereas in fabrication and processing, the pick-up of hydrogen, as in IHE, involves a fixed quantity of hydrogen (note that local hydrogen concentrations can be substantially greater than average global values).

As complicated as the problem of HEE may be, hydrogen embrittlement problems resulting from processing and fabrication (IHE) particularly due to welding operations become vastly more difficult and complex to understand. During welding of steels, the weld metal

while in the molten state has a high capacity for dissolving hydrogen. During subsequent cooling after solidification takes place, the austenite which has a high solubility for hydrogen decomposes to products (with the attendant transformation expansion and many different microstructures possible viz martensite, bainite etc and their mixtures) in which hydrogen is virtually insoluble. Because of the very nature of welding, there has to be a heat affected zone. If the weld metal is less hardenable than the base metal (which is usually the case), hydrogen will diffuse towards the heat affected zone from the early transforming weld metal. If the reverse is true, the base metal will transform first and tends to reject the hydrogen towards the weld metal. In case of hardenable steels under sufficiently rapid cooling rates (promoted by low heat input, thick plate and low ambient temperatures) austenite decomposes into brittle low temperature transformation products such as martensite. Thus the last portion of austenite to decompose to martensite under high transformation microstresses and at relatively low temperature can be highly concentrated in hydrogen resulting in internal cracking. Welding thus presents a highly complicated problem of the synergistic embrittling influence of hydrogen on material that may have suffered loss of toughness for other reasons.

As complex as the IHE may seem to be, solutions to the problem have been necessarily empirical and fortunately simple, although they may be expensive and time consuming. The solutions are typically based on the removal of dissolved hydrogen during

fabrication and/or prior to placing the component in service. For example, in welding of hardenable steels the sample is preheated before welding so as to lower the cooling rate after welding, thereby allowing more time for hydrogen to diffuse out of the weld metal and thus reduce or eliminate the insidious effects of hydrogen. In electroplating, the hydrogen is driven out of solid solution by a baking treatment which involves heating the material, after electroplating, to a moderate temperature for a sufficient period of time.

The various factors in welding viz material, welding and design, which ultimately control the resulting microstructure, hydrogen level and stress state (and hence the susceptibility to hydrogen assisted cracking) in a weldment are presented in Fig. 1.

In the following paragraphs, the various weldability tests that have been designed to study the behaviour of steels in hydrogen environment and the effect of each of the major variables, viz., hydrogen, stress and microstructure on weldability of steels will be discussed.

II. A. 3.1 Weldability Tests

The term "weldability" seems to be capable of many different definitions depending upon individual viewpoints and particular applications.[28] One of the more frequently used definitions of the term is that it is "the capacity of a metal or a combination of

metals to be welded under fabrication conditions into a specific, suitably designed structure, and to perform satisfactorily in the intended service.[29] A very important aspect of the weldability of a given steel is its ability of being welded without cracking. Although there are various forms of cracking, delayed cracking (hydrogen assisted cracking) is probably the most important and the most insidious variety. Since delayed cracking is so important to weldability, there has been a proliferation of tests designed to evaluate this tendency. Because HAC occurs due to a combination of stress, hydrogen and a susceptible microstructure, weldability tests are usually designed to evaluate one or more of these factors. The numerous weldability tests available to date can be classified, in general, into two categories (a) indirect tests and (b) direct tests. A brief description of these tests and several studies in this area to date merit mention in a general discussion of the delayed cracking phenomen.

(a) Indirect tests: This category of tests includes metallographic examination, hardness tests, hardenability tests, transformation determinations including both isothermal and continuous cooling transformation using high speed dilatometry, heat treatments that simulate the weld thermal cycle and notch tension tests with hydrogen charging during austenitizing in some of these tests.

These tests have been dealt with in great detail along with an excellent criticism of their

merits elsewhere.[30] The indirect tests for weldability have proved invaluable aid to a better understanding of the characteristics of different zones in a weld. But they suffer from the inability to account for residual and reaction stresses, the composite nature of the weld, hydrogen pick up and other conditions which are unique to welding. Hence one is left with no choice but to rely on direct welded-specimen tests to establish weldability. The most intensive research in the field of weldability has been done using direct tests.

(b) Direct tests: This category of tests can be subdivided into self-restraint tests and external-restraint tests. Self restraint tests include the bead-on-plate test, the circular patch cracking test, the controlled thermal severity test, the cruciform test, the Lehigh restraint, the keyhole restraint cracking test,[30] the H-type restraint cracking test, the Tekken (Y grooves) test[31,34] and the Rigid Restraint Cracking (RRC) test.[35,36] The external-restraint tests particularly applicable to the study of hydrogen induced cracking are the Tensile Restraint Cracking (TRC) test[37] and the Implant test.[38-50] The direct tests have been described adequately elsewhere.[30-38] For the evaluation of weldability, the direct tests as a group offer the most promise. As they measure directly the effect of welding on the soundness of steel, the results are more amenable for correlation with fabrication requirements. Nevertheless, both direct and indirect tests have been used

over the years to better understand the effect of the three factors viz hydrogen, restraint stresses and composition (carbon equivalent) on the susceptibility of steels to HAC. Some of the significant work done in this field will be discussed.

II. A. 3.2 Effect of Hydrogen

Sieverts[51] established that the gas dissolved atomically and Zappfe[52] in 1940, established that at equilibrium and at 1 atm pressure the solubility of hydrogen in iron at room temperature is only 20% that of the austenite before it transforms at 910°C. The resulting cracking was attributed to the supersaturation of hydrogen in the ferrite matrix. Since then a number of investigations using various tests have established the effect of hydrogen on the susceptibility of weldments to cracking. Suzuki et al[37] using the TRC test showed that the critical stress for cracking varied inversely with the diffusible hydrogen content. This type of relationship between lower critical stress and hydrogen content (diffusible hydrogen in some studies and total hydrogen in others) has been shown recently by a number of investigators[41,46] utilizing the Implant test. Beachum, Johnson and Stout[53] have reported that as little as 2ppm of total hydrogen was sufficient to cause delayed cracking. It was also shown in this work that the time for cracking increased at lower aging temperatures, indicating the role of diffusion rate in the phenomenon. Interrante and Stout[54] using the Lehigh Restraint test showed that susceptibility to delayed cracking was directly proportional to the hydrogen

content in the welding atmosphere. They also showed that, by providing a "reservoir" for hydrogen, such as an austenite filler wire, delayed cracking could be eliminated but this procedure would produce a lower strength weldment. This study brings out a very important point in the study of HAC, viz., quantifying the critical concentration of damaging hydrogen. A major limitation that plagues all hydrogen studies involves the inability to quantitatively analyze for the critical concentration of damaging hydrogen. Hydrogen can exist in a number of different locations in a metal, including voids, discontinuities, lattice, etc., not all of which represent mobile hydrogen. On this regard, several investigations[46,55-59] have reported on the beneficial effect of sulphides which, acting as hydrogen sinks, tend to lower the susceptibility to hydrogen cracking. However, it has also been reported[60] while conducting test in short transverse direction, that if microcracks or voids form around inclusions, they can act as stress risers. This together with the occluded hydrogen can give rise to increased susceptibility to hydrogen cracking.[57,60] Studies[32,54] on weldments have also shown that any austenite that does not transform during cooling can serve as a sink for hydrogen. Subsequently, if the retained austenite transforms to martensite at or near room temperature, cracking can occur as hydrogen is rejected. The entire process hinges on the availability of hydrogen. It is precisely this quantity of hydrogen available for

damage that regular methods of analysis can give little indication of. Unfortunately, the situation is even more complicated because the critical hydrogen concentration is a function of both the microstructure and stress whether it be internal stress (as in residual stress and transformation stress) or externally applied stress. A brief review of work pertaining to the effect of stress (restraint) and microstructure (composition and carbon equivalent) is as follows.

II. A. 3.3 Effect Of Stress On Weldability

In weld cracking there is a number of factors, both mechanical and metallurgical, which influence the initiation of weld cracking. However, the mechanism of cracking may be simply stated from the mechanical aspect by saying that the weldment crack initiates when the stress and strain induced at a certain point reach critical values. Hence the stress, strain and ductility at each point during the entire course of weld thermal cycle are important. This, however, involves a full three dimensional thermo-elasto-plastic analysis requiring a knowledge of factors such as joint configuration, fixturing and surround structures as well as a number of thermo-mechanical-metallurgical interactions that take place during welding of structural elements. Recently, a number of attempts[61-66] have been made, using finite element methods, to calculate thermal and restraint stresses generated during welding taking into consideration the effect of various temperature dependent

properties such as elastic modulus, yield stress, linear expansion co-efficient, specific heat etc. Although such analysis are based on many simplifying assumptions, studies of this nature have contributed enormously to the understanding of the mechanical aspects of weld cracking.

The stresses in a weldment arise, basically, from two sources:

(a) thermal stresses due to internal restraint

(b) reaction stresses due to external restraint.

(a) Thermal Stresses: The differential expansion and contraction of the joint because of the extreme thermal gradients inherent in welding, give rise to local strains in weld metal and heat-affected zone which are inhibited by the surrounding continuum leading to thermal stresses in the weldment. The magnitude of the peak local stress and strain can approach the ultimate strength of the material although the average can be in the plastic or even in the elastic range depending upon the yield strength of the steel. The final magnitude of stress and strain vary inversely with respect to the yield stress of material and are also a function of the length of weld, welding sequence, electrode and joint geometry[29] although the peak local stresses exceed the yield value along the weld center line regardless of the welding conditions and process.[67,68] The thermal stresses tend to be maximum in those regions which experience the highest temperatures and are the last to cool. Hence, high tensile stresses are produced at regions in and near the weld

and compressive stresses at regions away from the weld.[67] The expansion accompanying the austenite transformation during cooling tends to decrease the thermal stresses in the HAZ. The magnitude of this decrease depends on the nature of phase transformation, which in turn, is controlled by the base metal composition and cooling rate.[69]

(b) Restraint Stresses: For welded joints under external restraint, the reaction force induced, or the "intensity of restraint" proposed by Satoh et al,[70] enables weld crack initiation to be predicted without detailed knowledge of the stress and strain history at the point where weld cracking is expected as in the case of welds with internal restraint alone. The "intensity of restraint" is defined as "the magnitude of force per unit weld length necessary to give a unit displacement (elastic) across the weld". Thus the "intensity of restraint" refers to the degree of stiffness exhibited by the structure surrounding the weldment. For a simple butt joint fixed at both ends at a distance l apart, (R.R.C. test), an elastic stress E/l will be developed in the base metal when the root gap is contracted by a unit length (where E is the elastic modulus). The restraint force per unit weld length, i.e., the intensity of restraint (K) is then given by

$$K = \frac{Eh}{l} \quad \text{(elastic range)} \quad \ldots\ldots \; 1$$

where h = plate thickness.

If the magnitude of contraction across the weld is S, the restraint force P = S. K. Hence the average restraining stress in the weld is given by

$$\sigma_w = \frac{P}{h_w} = \frac{S}{h_w} \cdot K \quad \ldots\ldots 2$$

where h_w = weld height.

The above analysis holds when a weld is deposited at the neutral axis of the base plate. For the case where the weld is deposited away from the neutral axis (top or bottom of the plate are extreme cases), the effect of bending will have to be considered. Such a situation has been dealt with by Matsui et al[65] based on beam theory. The intensity of bending restraint K_B is given by

$$K_B = \frac{\sigma_B}{\theta} \quad \ldots\ldots 3$$

where σ_B = nominal skin stress of weld joint due to the moment M and θ = angular distortion of the weld in radians

The intensity of restraint due to eccentricity (γ) is defined as

$$K_\gamma = \frac{P}{S_T + S_B} \quad \ldots\ldots 4$$

where S_T = displacement due to tension

S_B = displacement due to bending

$$\text{Eccentricity } \gamma = \eta / (h/_2) \quad \ldots\ldots 5$$

where η = distance between neutral axis of plate and that of weld bead

h = thickness of plate

The relation between the various intensities of restraint is given by

$$\frac{1}{K_\gamma} = \frac{1}{K} + \frac{3\gamma^2}{K_B} \quad \ldots\ldots 6$$

For the case of R.R.C. test

$$K_\gamma = \frac{1}{1+3\gamma^2} K \quad \ldots\ldots 7$$

which indicates that the intensity of restraint is reduced due to eccentricity of weld.
But the stress and strain at the root of the weld where weld cracking usually occurs is also changed by bending introduced due to eccentricity. The stress at the root of the weld based on beam theory[65] is given by

$$\sigma_\gamma = \frac{m}{H\ 3\gamma^2} \quad 1 + 3\ \frac{L}{H^2}\ \gamma \quad K \ldots\ldots 8$$

where m = constant

$$L = \frac{l}{l_w} = \frac{\text{weld restraint length}}{\text{breadth of weld metal}}$$

$$H = \frac{h}{h_w} = \frac{\text{thickness of base plate}}{\text{thickness of weld metal}}$$

From Eqn 8 it is seen that when the weld bead is laid at the bottom of the plate ($\gamma < 0$), the stress at the root of the notch decreases and vice versa.

Matsui et al[65] using slit type test on HY 80 steel showed that when $\gamma = 0$, the specimen had to be preheated to $50^{o}C$ to get no cracking whereas when $\gamma = -0.75$ no preheating was necessary and when $\gamma = +0.75$ preheat up to $80^{o}C$ was necessary to avoid cracking. (Fig. 2)

For the case when $\eta = 0$, although the free contraction, S, (Eqn 2) is dependent only on the welding conditions, its rate at any instant depends on the nature of heat transfer from the weld. Satoh and Matsui[70] have shown it to occur in three stages (Fig. 3). The first stage occurs within a short time due to three-dimensional heat flow. This is followed by a period (second stage) during which no contraction occurs despite a continuous drop in temperature. The second stage has been attributed to the cooling of parent plate by two dimensional heat flow after it has attained an equilization temperature. The contraction again takes place (third stage) as a result of overall heat loss from the plate. The second stage is shortened as the restraint length is reduced.

The contraction progresses in different welding processes according to whether plate thickness h is larger or smaller than a critical plate thickness h_{cr} given by

$$H_{cr} = \frac{Q}{CP\,\theta_{ws}}$$

where Q = welding heat input (Cal/cm)

C = specific heat of material ($Cal/gm^{b}C$)

P = density of material (gm/cm^{3})

θ_{ws} = temperature of weld metal at the start of contraction (nearly equal to fusion temperature of weld metal) in ^{o}C

The critical plate thickness is proportional to the square root of heat input and ranges between 10 and 20 mm for typical manual metal arc welding conditions on steels.[70]

When $h \geq h_{cr}$, the final contraction $S_{t \to \infty}$ is independent of h and proportional to h_{cr} (or Q) as given by

$$S_{t \to \infty} = \alpha \theta_{ws} h_{cr} \quad \ldots\ldots 10$$

where α = Coefficient of thermal expansion.

When $h < h_{cr}$, only the third step appears in the contraction process.

The criterion for susceptibility to cracking may be represented either by a critical restraint intensity for a given joint contraction (welding condition) or by the "critical joint displacement" at a given level of joint restraint. The critical restraint intensity may be obtained by either increasing the plate thickness or by decreasing the restraining length (R.R.C. test).

Since the concept of intensity of restraint was introduced, investigators [61,63,71] have calculated this parameterfor a number of weldability tests developed over the years and also for real-structures such as spherical pressure vessels, water turbine casings etc.[71-73] Most weldability tests are designed to provide variable restraint by changing the specimen dimensions while the contraction is dependent on the welding conditions. The concept of restraint has been applied to provide a simple quantitative measure of susceptibility to

various forms of cracking by using TRC, RRC and H-type tests.[35-37] Even before the concept of intensity of restraint was introduced, the effect of restraint and residual stresses on cracking were well understood.[54,75,76]

Briefly, perhaps the single most definitive characteristic of hydrogen assisted cracking, whether in weldability tests (both direct and indirect) or in base metal tests (a number of tests have been devised which are not discussed herein) involving no welding or welding cycle, is the existence of a lower critical stress (applied or residual) below which HAC will not occur. In particular regard to weldability tests, since there have been a proliferation of tests to assess susceptibility of steels to HAC, there has been considerable confusion as to what the results of one particular test means with respect to those of other tests. Recently,[77-81] however, international efforts have been directed to correlate the various weldability tests in order to understand the interplay between them. A complete review of the results thereof is beyond the scope of the present study. The existence of a lower critical stress for HAC has virtually become a design number which in modern fracture mechanics can hopefully be related to a stress-intensity factor. Unfortunately, because of the very nature and complexity of problems associated with welding processes, some of which have been alluded to previously, the application of fracture mechanics principles to the study of HAC in weldments has proved to be extremely difficult.

II. A. 3.4 Microstructural Effects (Carbon Equivalent) On Weldability

It is well known that under constant welding conditions (the brand of electrode, heat input, plate thickness, preheat and joint preparation), steels of different composition (i.e., having different austenite-transformation characteristics for a fixed thermal cycle) would show different susceptibility to hydrogen cracking. The effect of composition, or strictly speaking, the effect of microstructure has been incorporated in the so called "carbon equivalent" formula. In principle, the carbon equivalent formula is similar to other statistical formulae in physical metallurgy, such as those that relate steel chemistry to the hardenability, the M_s (martensite start) and AC_3 (upper critical cooling) temperatures, and so on. Of the alloying elements, carbon is critical to the phenomenon because it controls the nature and properties of the low temperature transformation products. The other elements contribute to cracking sensitivity essentially by increasing hardenability, i.e., by lowering the critical cooling rate needed to form martensite. The concept of carbon equivalent is based on the observation that sensitivity to hydrogen-cracking increases progressively as the M_s temperature becomes lower. Most commonly the formula is a simple additive one, such as that given below:[30]

$$C.E = C + Mn/6 + (Cr + Mo + V)/5 + (Ni + Cu)/20$$

The assumption in using such a formula would be that danger of cracking in welds made at room temperature can be expected, for the above forumla, when C.E exceeds 0.4 for cellulose electrodes and 0.5 when low hydrogen electrodes are used for welding. Japanese investigators have proposed much more elaborate formula taking into account restraint stresses and hydrogen; the cracking parameter suggested being a linear combination of carbon equivalent (P_{cm}), intensity of restraint and diffusible hydrogen.[21] Winterton[20] and Miyoshi[82] have discussed the various formulae proposed to date along with the composition limits, weld tests and the criteria on which each of these formulae was based. However, it should be mentioned that the drawback of such formulae is that they can only be applied to the type of steel which was used for their derivation. All these formulae were developed for straight carbon manganese and/or conventional low-alloy steels with carbon content not less than 0.07%. These formulae have become increasingly suspect in predicting the weldability of the newly developed family of micro-alloyed steels,[22-24] which are essentially very low carbon (0.03-0.08%) high strength alloy steels of the arctic grade combining high strength, excellent toughness and good weldability.

The hardness of the resulting microstructure after welding has been frequently proposed as an easily determined indicator of cracking susceptibility. In general, susceptible microstructures have been found to be those with an as quenched hardness greater than

300 V.H.N.[30] But the problems and pitfalls of such an approach are obvious and have been dealt with by Stout[83] in great detail. Thus, the susceptibility to hydrogen cracking should be related directly to the microstructure itself. Boniszewski and Watkinson[84] using constant-load rupture (CLR) test on simulated microstructures with hydrogen charging during austenitizing noted the extreme embrittlement of twinned martensite as compared to slipped martensite even though the hardness of the former was only marginally higher. Such extreme embrittlement was attributed to the presence of twinning itself[84,85] although no particular mechanism was proposed. Bainites which form as sheaves of narrow, parallel ferrite laths have an intermediate susceptibility to hydrogen cracking. Slipped martensite, auto tempered low carbon martensite and granular bainite are least embrittled.[84-86] Small amounts of twinning in slipped martensite increased the index of embrittlement considerably.[84] Increasing prior austenite grain size also increased embrittlement,[84] as the size of both martensite crystals and baintic colonies is enlarged. Fractographic analysis by Boniszewski[84-86] and others[87-89] tends to support the observation that hydrogen embrittlement in steel does not result in cracking of a specific morphology, but exploits the crack nucleation mechanism which is the easiest in a given microstructure.

II. B. Theories Of Hydrogen Assisted Cracking

To date, basically five mechanisms have been proposed to explain the embrittling effect of hydrogen on the iron-iron bond.

(a) Planar pressure theory of Zapffe and Sims[90] modified by Tetelman and Robertson[91]

(b) Surface adsorption theory of Petch and Stables[92,93]

(c) Lattice Interaction theory proposed by Trioano[94]

(d) Lattice decohesion theory advanced by Oriani[95]

(e) Mechanism based on modification of dislocation mobility proposed by Beachem[96]

The planar pressure theory postulated that molecular hydrogen can precipitate into internal voids in the lattice thereby building up pressure sufficient to cause premature fracture. Due to straining, the voids enlarge resulting in a decrease in hydrogen pressure. For further damage to occur, continued precipitation of hydrogen to the voids is necessary. If the rate of straining is greater than the restoration of necessary pressure, embrittlement should decrease. The effect should be similar if test temperature is reduced because the rate of hydrogen delivery into the void and gas pressure inside the void would both decrease with decrease in temperature.

The surface adsorption theory of Petch and Stables suggests that the hydrogen already in a metal lattice diffuses to the crack tip and reduces the fracture stress by adsorbing on the crack surface. They reported the delay time needed for diffusion of

hydrogen to the crack tip. Their model was based on Griffith's criterion using energy considerations and thus plasticity effects were ignored.

The "lattice-interaction theory" proposed by Troiano suggested that the "true fracture strengths of the lattice" was lowered, by hydrogen diffusing under the influence of a stress gradient to regions of high triaxial stress within the lattice, causing a loss in lattice cohesion ("perfect cleavage" was made easier). Troiano postulated that the electrons in the hydrogen atoms (or ions) would enter the d bands of the metallic cores in the transition metals, and that the increase in the electron concentration of these bands produced an increase in the repulsive force between the metallic cores, or in other words, a decrease in cohesive strength of the lattice.

The recent theory by Oriani and Josephic called "lattice decohesion theory" is based on Troiano's model described above. The decohesion theory suggests that the maximum cohesive strength of the lattice (F_m) is reduced by an amount proportional to an undefined function of the hydrogen content at the crack tip. Embrittlement (cracking) occurs when the local tensile stress (σ_Z) is increased above the hydrogen modified cohesive strength (F_m). The rate of crack advance is controlled by the kinetics of hydrogen entry to the highly elastically stressed region to achieve the concentration necessary to cause F_m to equal σ_Z.

In 1972, Beachem first introduced the term "Hydrogen Assisted Cracking" to draw attention away

from the traditionally held concept that hydrogen enhances the separation of atomic bonds by a non-deformation type decohesion mechanism. Beachem's theory was based on fractographic results obtained on two grades (4315, 5330) of alloy steel tested in gaseous hydrogen and in 3.5% Nacl solution. Based on the presence of microscopic plasticity in the fracture morphology, Beachem proposed that the presence of sufficiently concentrated hydrogen dissolved in the lattice just ahead of the crack tip aids in whatever deformation processes the microstructure will allow. Intergranular, quasicleavage or microvoid coalesence fracture modes will operate depending upon the microstructure, the crack tip stress intensity and hydrogen concentration. This model was later modified[97] to include a necessary second effect, namely, that this plastic deformation aids the entry of hydrogen into the critical volume of material. This latter effect had been noted previously by several investigators.[95,97]

Various other theories have been proposed, but they are all, essentially, variations of the theories cited above. The evolution of these theories along with the controversy that still exists has been detailed by many.[16-18,91] It will suffice to mention that, to date, a large body of controversial evidence has been produced which supports or disproves the various theories. It seems that each of these theories is applicable to certain materials tested under specific conditions. There exists no single mechanism which can explain all the experimental results to date. Nevertheless, in

recent years, more credence is being given to hydrogen-dislocation interactions in determining the material's susceptibility to hydrogen assisted cracking at least in high strength steels. Recent studies[98,99] in weldments have supported such a model at the expense of planar pressure theory.

CHAPTER III
DEVELOPMENT OF A FIELD WELDABILITY TEST

III. A. Experimental Procedure.

III. A. 1. Materials:

In order to develop and characterize candidate specimen designs, it was necessary to obtain a variety of compositions and thicknesses of pipe steels that would provide a range of responses to hydrogen induced cracking. The compositions and gages of steel pipes and plates obtained are listed in Table 1. The steel grades ranging from 5LX - 52 to arctic grades included precipitation hardening steels. The mechanical properties of these steels are presented in Table 2. The microstructure of these steels varied from those of polygonal ferrite plus islands of pearlite or bainite, more or less banded, to those of acicular ferritic structures. Representative microstructures of selected steels are shown in Fig. 4.

III. A. 2. Specimen design:

Because a shop type weldability test was sought, the laboratory tests requiring elaborate mechanical or microscopic equipment were not approrpiate. An early design was a Specimen 150 mm by 200 mm cut from the pipe/plate with the 200 mm dimension in the curved direction which, incidentally, is transverse to the rolling direction. A central through thickness slot 2.4 mm wide and 90 mm long was cut into the plate by milling as shown in Fig. 5.

In initial tests, the weld was commenced and ended within the slot length. This procedure produced a preponderence of weld metal cracks, starting in the crater and running through the weld metal. Subsequently the weld was initiated 25 mm in front of beginning of the slot and continued 25 mm beyond the end of the slot, where upon total weld metal cracking was eliminated in almost all cases and HAZ, or combinations of HAZ-fusion zone-weld metal hydrogen induced cracking was consistently obtained in sensitive heats of steel.

III. A. 3. Welding Apparatus and Procedure:

Welding was done with semi-automated shielded metal arc welding process (also called manual metal arc welding) with individual controls for current, voltage and travel speed. For this experimental program the welding conditions were standardized to match representative field practice. A 4 mm diameter E7010 electrode (HYP)* generally used for the root pass in girth welds was welded at 150 amps and 300 mm/min travel speed. Before welding, the oxide layer on the specimen was removed by grinding and the surface and slot of the specimen were thoroughly cleaned by acetone to remove any grease and other contaminants. To facilitate easy starting of the weld arc, a small ball of degreased steel wool was placed on the specimen surface immediately beneath the tip of the electrode. In the trial runs, to discover the response of the test to variations in steel, welding was performed at 20^{o}C plate temperature (room temperature) and the aging period was 24 hrs.

*A proprietary electrode designed for pipeline welding

Welds were also made on selected steels with 4 mm diameter E7018 electrode using the same heat input. The E7018 electrodes were baked at 370°C for 1 hr. and stored at 100°C for at least 8 hrs. before welding. This procedure facilitated the study of the effect of low hydrogen concentration in the weld on the susceptibility of the steels to hydrogen induced cracking.

The next step was to develop a simple technique for measuring the extent of hydrogen-induced cracking. After aging for a desired period of time, up to 24 hrs. the specimen was reheated to 400-500°C in a furnace to temper the steel, dissipate the dissolved hydrogen from the weld and thus to obviate cracking in later processing. It was intended that reheating would also heat tint any hydrogen induced cracking already present and therefore reveal the extent of cracking when the weld was broken open. By sawing slits from one side of the plate toward the ends of the slot, it was possible to place the specimen in a vice and hammer off the flap generated by slitting. The notch effect of the central slot assured fracture at the weld because the hammer bending put the weld root in tension. As Fig. 6 shows, the extent of hydrogen cracking was clearly delineated by oxide discoloration in the fracture and could be reported quantitatively.

III. A. 4. Testing Program:

The main testing program consisted of 1. calibration tests to demonstrate the response of the test to variations in steel composition and thickness

2. tests to examine the combined effects of elapsed time after welding and preheating on the extent of cracking 3. effect of type of electrode on the extent of cracking 4. exploration of means of varying the specimen constraint should it be necessary.

III. B. PRESENTATION AND DISCUSSION OF RESULTS

III. B. 1. Test Response:

The heats of steel listed in Table 1 were tested under standard conditons, as described above, with the results presented in Table 3. A few of the heats were also subjected to bead on plate tests welded with E6010 electrode. It is evident that cracking levels from 0 to 100% were exhibited by the group of steels and that the slot-test results are compatible with the bead-on-plate tests. If the results are plotted against the carbon equivalents, as in Fig. 7, the correlation is about as good as that typically observed in laboratory tests. The high level of cracking in H473, a pipe fitting steel, may have been enhanced by its 25 mm thickness. Conversely the lower cracking level in C10113 may be traced to its very low carbon content of 0.05%. Table 3 also shows that slot tests welded with E6010 displayed somewhat greater cracking levels than those welded with E7010 (HYP) electrode and compared closely to the bead on plate tests welded with E6010. No cracking occured in any of the heats tested when welded with E7018 (low hydrogen) electrode. The behaviour of one particular steel, viz., heat No A 68-2, presented in Table 3, deserves special attention. Three specimens of this heat gave 60% cracking whereas three others gave no cracking. Subsequent metallographic examination revealed the presence of lamination in specimens which gave 0% cracking whereas specimens which experienced 60% cracking did not have any lamination (Fig. 8) Note that the lamination is in the crack

arrester configuration. Delamination, in this case, relaxed the stresses to such an extent that no cracking occurred. The dramatic improvement in impact toughness arising from delamination is well documented.[100,101] When delamination occurs, the effective thickness of the sample is reduced. Consequently, the specimen acts like a series of thin plates (thus reducing the triaxiality of stress) instead of a thick plate. The beneficial effects of crack arrester geometry have been utilized in the design of a number of components for many years such as in the manufacture of multi-walled pressure vessels and gun barrels.

III. B. 2. Locus of Crack Initiation and Growth

Metallographic sections were taken from the center of the slot weld test specimens to determine the locus of crack initiation and growth. Results of this survey are presented in Table 5 for several steels investigated. The typical paths of cracking for several steels is illustrated in Fig. 9. The cracks tend to wander between the HAZ, fusion line and weld metal, partly because of the stress pattern and partly because the weld metal itself is not highly crack resistant. This point is confirmed by the presence of microcracks in the weld metal as shown in Fig. 10 for several steel weld metals. The responses of the steels to the weld thermal cycle differ principally because the coarse-grained HAZ's of the higher carbon steels form largely martensitic structures whereas the lower carbon heats develop Widmanstätten ferrite and bainitic structures as shown in Fig. 11.

III. B. 3. Effect of Slot Width On The Extent And Locus Of Crack Growth

During the early period of development of the slot weldability test, additional testing was done to explore the effect of slot width on the extent and locus of crack growth. Two extreme cases, one with slot width of 3.2 mm (since 4 mm dia electrodes were to be used, higher slot widths were impractical) and the other with no gap (two 200 mm by 75 mm plates were abutted together and welded over) were studied. Metallographic sections were taken to examine the crack locus. Fig. 12 shows the crack locus for these two cases together with that of the standard slot weldability test described before for heat 63843. It is seen that total weld metal cracking occured when the gap was too narrow or too wide whereas the appropriate slot width of 2.4 mm gave fusion line - HAZ cracking. This is because in either of the two cases (no gap and 3.2 mm gap) the root of the weld bead and slot together, produce a sharp re-entrant angle into the weld metal. This, together with the bending imposed on the plate (due to welding) during cooling causes the crack to initiate and propagate entirely in the weld metal. Thus it is seen that a slot width of 2.4 mm produces the optimum results.

III. B. 4. Combined Effects Of Time Lapse After Welding And Preheat On The Extent Of Cracking

The effect of time interval after welding on the extent of cracking is of considerable interest

in field welding where the schedule provides that the hot pass be laid shortly after the root pass. Since hydrogen induced cracking is a delayed type of failure occurring by the cooperative action of stress, hydrogen and susceptible microstructure, care is taken in the field to control one or all of these factors by preheating the pipes and controlling the times lapse between the root pass and the hot pass in order to avoid hydrogen induced cracking in high strength steels.

The experimental program consisted of welding the plates and then holding them for a period of 20 mins, 10 mins, 5 mins or 1 min before tempering and heat tinting them to oxidize any crack previously formed. Holding times up to 20 mins were studied to bracket the usual time lapse in the field between the root pass and the hot pass. To study the combined effect of preheat and time lapse after welding, the test plates were preheated to the desired temperature, welded and held for the specific periods of time, as stated above, before tempering. Preheating ranged from $20^{o}C$ (R.T) to $120^{o}C$.

The results of this series of tests is presented in Table 4. Fig. 13 gives a plot of the percentage cracking vs time lapse after welding with a preheat of $20^{o}C$ (R.T) for the different heats investigated. Fig. 14 shows the fracture surfaces of heat B 319 depicting the effect of time lapse after welding on the extent of cracking at a preheat of $20^{o}C$ (R.T). Note that the cracking area appears dark on the fracture surface from oxidation during

heat tinting after welding.

From Table 4 and Fig. 13 it is seen that some steels show 10% cracking within a time lapse of 1 min after welding. The significance of this finding is that in field welding the usual time lapse between the root pass and the hot pass is of the order of 5-8 mins. If cracking does not occur within the time interval between passes, it can probably be avoided since the hot pass provides post heat to the already deposited root pass. The hot pass acts as a tempering treatment which would immediately relax the stress, bring about a less susceptible microstructure and give more time for hydrogen to diffuse out - all of which are effective in reducing the possibility of hydrogen induced cracking. These test results suggest that cracking might already be present before the hot pass is laid in the higher carbon steels. The implication therefore is that, however short (within practical limits) the time interval may be between the root pass and the hot pass, one cannot avoid hydrogen induced cracking in highly susceptible steels without resorting to preheating to an appropriate temperature. Data presented in Table 4 brings out the importance of preheating. Results show that even moderate preheating temperatures of the order of 65^{o}C to 100^{o}C are effective in delaying the onset of cracking long enough to make it practicable to deposit the hot pass before the root pass experiences cracking, even in the more hardenable steels such as Heats 63843 and 492S1871. At 120^{o}C preheat cracking was virtually eliminated. The

data may be summarized in a graph such as Fig. 15 in which allowable time lapse for different levels of cracking at various preheats is shown for heat 492S1871. A more useful way of representing the data would be to show the time lapse that can be tolerated for a specified percentage of cracking (which would correspond to no cracking in the field) at various preheats. Fig. 16 illustrates such a relationship for a critical cracking level of 10% for the various steels tested. A vertical line erected at a practical time lapse between the root and hot passes intersects the curves at the preheat required for each heat of steel. This type of analysis should facilitate establishing a schedule of preheat and time interval between root and hot pass welds that will assure crack-free welds in field girth welding.

III. B. 5. Variable Constraint:

It was found desirable to examine the specimen design for means of varying the restraint so that test results could be "tuned" to match field experience. Several ways of varying restraint were examined. One of the early designs examined which provided a very convenient way of varying the restraint was simply to vary the position of the slot across the breadth of the sample. For this series of tests, Heat 63843 which gave 50% cracking with the slot in the center was chosen. Fig. 17 shows the fracture surface (time lapse of 24 hrs) together with the test plate design for three different restraint levels. It is seen from this that the slot placed 25 mm from the edge (the least

restraint) gave no cracking and the specimen with the slot 50 mm from the edge, the intermediate restraint level, produced intermediate cracking level of about 30%. Other methods of varying the restraint were also examined - notably reducing the width of the specimen and also by cutting side slots into the regular slot weld test specimen to various depths. Heat IF 5913 was chosen for this series of tests for lack of heat 63843 material. Table 6 shows the various plate designs tested together with the extent of cracking in break open test as well as the locus of crack in 12 mm wide metallographic section cut out from the center of the slot. It is seen that by reducing the specimen width from 150 mm to 100 mm, the cracking level falls from 50% to a very low value without any change in heat affected zone and weld metal hardness. Also cutting side slots into the plate reduced the extent of cracking, the reduction in cracking being proportional to the depth of side slots. Thus it is seen that satisfactory methods of controlling restraint have been devised to that the specimen design can be adjusted so as to yield cracking levels to match those encountered in field welded girth joints.

III. B. 6. Correlation of Slot Weldability Test With Full Size Shop Welded Pipe:

If the slot weldability test is to be useful in predicting the girth field welding behaviour of pipeline steels, it is necessary to have available a direct correlation of the behaviour of a given steel in the laboratory tests with its behaviour in actual field welding. Through the cooperation of the API Steering Committee members, especially Mr. White, it was arranged to have such a direct correlation conducted.

The heat of steel used for this investigation was 492S1871. The conditions and procedures followed in shop welding of the pipes were as follows. Full size pipes, with joint preparation and design as shown in Fig. 18, were assembled and welded by three welders. Two welders starting at the top, welded in opposite directions to the 3 and 9 o'clock positions on either side of the top, and the third welder, starting from the 3 o'clock position welded the whole bottom half circumference. Next, after a 5 minute lapse time after the root pass, the hot pass was laid on one of the top quarter sections. The other top quarter section was welded after a time lapse of 20 minutes after the root pass. The pipe was then allowed to cool to ambient temperature and was then cut into half for shipment. Another pipe was welded with the same sequence except that the pipe was preheated before welding to a temperature of 66^{o}C. This procedure yielded six conditions, as follows, for further examination

a. No preheat - 5 mins between root and hot pass
b. No preheat - 20 mins between root and hot pass
c. No preheat - No hot pass after root pass
d. 66°C preheat - 5 mins between root and hot pass
e. 66°C preheat - 20 mins between root and hot pass
f. 66°C preheat - No hot pass after root pass

The shop welded pipes were cut into sections for metallographic examination. Data for the six conditions are presented in Table 7. For each test condition 12 sections were selected randomly to determine whether cracking occurred. Fig. 19 shows photo micrographs of the extent and severity of cracking observed in the girth welds deposited under four conditions in which cracking occurred. It is seen from Fig. 19 (a) that for no preheat - no hot pass conditions, total failure of the root pass occurred. Such complete failures were not found for the other conditions.

Results indicate that the frequency of cracks is closely related to preheat and time lapse after welding - the frequency of cracking is maximum for the no preheat - no hot pass condition and is reduced either by shortening the time lapse between the root pass and hot pass or by preheating. Fig. 20 shows the correlation of test results between the shop girth welded pipe and the laboratory slot weldability test. Since the extent of cracking in the field welded pipe is of the same order of magnitude as that of the laboratory slot test, it appears that the slot weld test is able to assess the field weldability of pipeline steels usefully if somewhat conservatively.

III. C. Summary and Conclusions:

1. A satisfactory shop type weldability test has been developed for measuring the field weldability of pipeline steels. It utilizes a 150 mm by 200 mm specimen removed from formed pipe or plate, slotted centrally in the direction of pipe curvature (transverse to the rolling direction for plates), and welded by depositing the weld bead over the slot and extending 25 mm beyond each end of the slot. The welding conditions are chosen to match field practice.

2. Quantitative measurement of the extent of cracking is obtained with shop tools by aging the specimen up to 24 hrs, and re-heating to about 500^{o}C with a gas torch to arrest cracking and to heat tint any hydrogen-induced cracking. A hammer and vice are used to knock off one side of the weld to reveal the oxidized surface of the hydrogen induced crack already present, which can then be measured.

3. The test was shown to discriminate among various compositions of pipeline steels.

4. The test method was used to show the rate at which cracking takes place over intervals of time following welding. Some of the more crack sensitive steels exhibited cracking within one minute of completion of the weld. Cracking occurred sooner in steels of higher carbon content.

5. The benefit of moderate preheating in preventing hydrogen-induced cracking was demonstrated by the slot specimen.

6. The possibility of laying down welding conditions such as preheat and time lapse between root pass and hot pass to ensure welds free of cracking was demonstrated by the slot weld test.

7. Variable constraint is readily obtained by moving the slot off center toward one side of the specimen, reducing the size of the specimen or by cutting side slots into the specimen.

8. The slot weldability test results were shown to correlate well with those of shop girth welded pipes for heat 492S1871.

9. The slot weld test specimen appears suitable to assess field weldability of pipeline steels, (and more conveniently than tests requiring elaborate laboratory facilities) if somewhat conservatively.

III. D. Difficulties In Conducting Slot Weldability Test In Practice

Since the preliminary results of the slot weldability test were published[102] a number of laboratories have carried out weldability studies using the newly developed test to assess the feasibility of the test as a reliable indicator of the susceptibility of pipeline steels to hydrogen-induced cracking. Although some laboratories[103,105] have reported that the slot weldability test provides a simple and reproducible test to establish welding parameters such as preheat and time interval between root and hot pass welds, others[107,109] have expressed lack of reproducibility of the test, excessive and sometimes total weld metal cracking and the lack of field applicability of the test for which it was intended. Some of the difficulties that have been cited to bring out the lack of field applicability of the test are as follows:

(a) the machined slot in the original test was produced by milling which as been found to be a difficult practice to conduct in the field

(b) although, if a milling equipment is not available, the specimens may be prepared by saw cutting from one end and welding that end with E7018 electrode leaving a 90 mm through thickness open slot, a saw blade capable of producing a slot of the proper width (2.4 mm) was not available in the market.

Possible reasons for the lack of reproducibility excessive and sometimes total weld metal cracking encountered in some of the studies cited above are as follows.

(c) During fabrication of the slot it is possible that the slot width was reduced due to contraction experienced during restraint weld beads so that the final slot width might have been less than the starting slot width of 2.4 mm. The sensitivity of the slot weld test to width of slot has been demonstrated previously in the machined slot (Chapter III) wherein it was shown that a very narrow slot led to severe cracking in the weld metal and a slot 3.2 mm wide also produced extensive weld metal cracking. In either case the slot produced a very sharp re-entrant angle (high stress concentration) into the weld metal. A slot width of 2.4 mm was shown to produce optimum results.

(d) Manual welding of the test weld might produce an erratically shallow and wide bead which would result in higher stresses on the weld and an unfavorable weld configuration at the root of the notch. Note that all the tests conducted at Lehigh were performed using an automatic welding unit wherein the electrode has a tendency to dig in as it passes over the slot producing deep penetration and a narrow bead.

Hence a supplementary program was undertaken to explore possible ways of alleviating the problems mentioned above (except case d) and to better understand significant variable in the fabricated rather than machined specimens.

III. D. 1. Alternative Methods of Fabrication And Test Procedure:

Fabricated test specimens made from 200 mm by 75 mm strips saw cut from pipe, with the 200 mm

dimension in the direction of curvature of the pipe segment, were prepared from four heats included in the previous Lehigh tests using a machine slot. The heats were 492S1871, 88284, B319 and 490S2441 and the heats varied in cracking response from 2-3% for 490S2441 to 80% for 492S1871 after 24 hour time lapse (Table 4). The results are reproduced for convenience in Table 8. Specimens were fabricated according to the procedure shown in Fig. 21. They were first tack welded in place with wire spacers to hold the plates apart at the appropriate 2.4 mm gap. From this point three alternative procedures were followed:

1. The wire spacers of 2.4 mm diameter were removed and the restraint welds were made on both sides (top and bottom) of the plate leaving an open slot length of 90 mm at the Center. The electrodes used for the restraint welds were E7018 which were previously baked at 370°C for 1 hour followed by holding for at least 8 hours at 100°C. A welding current of 190 amps and a travel speed of 150 mm/min was used. This procedure resulted in substantial contraction during restraint welding, leaving a slot width of less than 1.6 mm.
2. The wire spacers of 2.4 mm diameter were left in position during restraint welding. After restraint welds were completed the center spacer was removed. This resulted in a gap of 1.6 mm in the slot. Restraint welding was done as in Case 1.

3. Wire spacers of 3.2 mm diameter, instead of 2.4 mm, were used during tack welding. No center spacer was used. The spacers were not removed during restraint welding but were welded over on each side incorporating them in the restraint weld. This left a gap of 2.4 mm in the slot. Restraint welding was done as in 1.

In order to see if the specimen dimension itself has any effect on the extent of cracking when the width of the slot was varied, additional tests were performed on heat 492S1871 by fabricating the test specimens from 200 mm by 62.5 mm strips so as to obtain a final plate size of 200 mm by 125 mm. Fabrication was performed according to procedure 3 above using 2.4 mm and 3.2 mm spacers to obtain final slot widths of 1.6 mm and 2.4 mm respectively. Tests were also run on heat 492S1871 using the 200 mm by 125 mm regular slot weld test with machined slot of 2.4 mm width to provide a basis for comparison with the fabricated slot. Heat No. 492S1871 was of particular interst because this was the only heat on which full size girth welding was conducted and the extent of cracking thereof was previously compared to that of the standard machined slot weldability test results.

After preparation of the specimens, test welds were made using 4 mm dia E7010-HYP electrode and standard welding conditions and procedure. Time lapses of 10 minutes and 24 hours were studied. Specimens in duplicate were run for all conditions.

III. D. 2. Results and Discussion

The results of the series of tests elaborated upon above is presented in Tables 8 and 9. From these tests, it is apparent that the results are quite sensitive to the width of the test slot. The sensitivity of the test to slot width was not reduced with a reduction in the size of the plate with the concomitant reduction in restraint level (Table 9). It is seen from Table 8 that in Heat 492S1871, which produced extensive cracking in the machined slot weldability test, the fabricated slot which have the slot width of 2.4 mm gave less severe cracking as compared to the machined slot. This is to be expected and is consistent with previous studies elsewhere[110] because the fabricated welds are partial penetration welds which would provide lower restraint as compared to the machined slot. It can also be seen from Table 8 that in other heats wherein the machined slot produced only moderate amounts of cracking, the results of the two tests when the fabricated slot width was 2.4 mm are almost identical. Apparently the effect of reduction of restraint due to partial penetration restraint welds is realized only in cases where the machined slot showed extensive cracking. But in all cases where the slot width in the fabricated slot was much less than 2.4 mm, more severe cracking was encountered consistently with most of the cracking occurring in the weld metal. This result is consistent with that obtained in Tekken Y-groove test[111]

wherein severe weld metal cracking is reported when a slot width of 1 mm was used whereas the standard 2 mm slot width produced essentially HAZ cracking.

III. D. 3. Conclusion:

From the foregoing discussions it can be concluded that alternative fabricating methods are available which can alleviate the problems of applying the machined slot for field fabrication purposes referred to earlier (cases a and b). It has also been shown that the results of fabricated tests compare well with those of the machined slot test for a range of steels with different cracking potentials when the slot width in the fabricated test was maintained at 2.4 mm. One outcome of the study that seems quite important is that no matter what the method of fabricating the test specimen, it must be carefully controlled so that a reproducible slot width of 2.4 mm results. Failure to control this dimension can lead to significant inaccuracies in the test.

CHAPTER IV

CARBON EQUIVALENT AND WELDABILITY

IV. A. Introduction:

The limitations of carbon equivalent formulae, proposed to date, to assess the susceptibility to hydrogen assisted cracking of steels in general and very low carbon microalloyed steels in particular, have been ennumerated earlier (Chapter II). Since hydrogen-induced cracking is due to the three factors, viz., hydrogen, restraint and a susceptible microstructure acting simultaneously, it should be possible to conceive of a crack sensitivity formula to account for all the three variables instead of the carbon equivalent formula. The crack sensitivity formula would then take the form

$$C.S.F = (A)\ \ (H)\ \ (C.E.) \ldots\ldots 11$$

where A = measure of restraint co-efficient or the intensity of restraint. In the present study, it will be expressed as a percentage of free contraction

(H)= Diffusible hydrogen content in the weldment (ppm)

C.E. = Carbon equivalent.

This type of crack sensitivity formula is supported by the argument that as either hydrogen level or restraint goes to zero, cold cracking is not encountered. At the same time, for each type of steel (a particular carbon equivalent) there will be

a critical hydrogen level and restraint below which cracking will not occur. Other carbon equivalent formulae proposed to date are incapable of predicting this fundamental behaviour of hydrogen induced cracking.

In the present study, a carbon equivalent such as the one shown below will be examined.

$$C.E = C^{\frac{1}{2}}\left(1 + \frac{Mn + Cr + Mo + V}{5} + \frac{Ni + Cu + Si}{25}\right) \quad . \quad . \quad 12$$

This carbon equivalent formula is similar to those proposed to date except that greater emphasis is given to carbon by making carbon a multiplying factor, rather than additive, to account for the greatly reduced propensity to hydrogen induced cracking of very low carbon microalloyed steels.

IV. B. Experimental Procedure:

It is apparent from Eqn. 11 that in order to evaluate the factor for restraint, A, measurements of both hindered and free contraction should be carried out.

IV. B. 1 Hindered Contraction Measurements:

Fig. 22 (b and c) illustrates the two types of designs and experimental set up (a) that were employed to measure the expansion - contraction of the plate during and after welding. These two designs will be designated as design 1 and design 2 respectively. The contraction process of a weld joint in arc welding is influenced by the geometry of the weldments (including rotation experienced by the specimen when the bead is laid away from the neutral axis of the plate),

thermal variables, metallurgical factors of the material and cracking that might occur during and after welding.

During the first phase of the investigation, it was intended to examine the effect of plate thickness on the contraction processes. In order to avoid the anomalies due to cracking, heat NKK, which showed no cracking during the early part of the investigation, was chosen. Incidentally heat NKK is a plate material, rather than a section of a pipe, which made it convenient to grind the plate to different thicknesses. Plate thicknesses of 25 mm, 19 mm and 15 mm were employed for this investigation. Since it was also necessary to avoid warping of the plate due to eccentricity of the weld with respect to the neutral axis of the plate, a V groove was cut to mid-thickness in each plate to deposit the weld bead at the neutral axis of the plate. For this investigation design 1 (Fig. 22b) was employed to measure the expansion - contraction across the center of the weld since no appreciable warping is expected. Briefly, the experimental procedure consisted of drilling holes 5 mm in diameter and 12.5 mm from the center-line of the slot to accomodate the prongs of the measuring scissors. Each of the prongs was equipped with a sleeve to minimize the effect of possible warping and to indicate only the expansion and contraction of the weld at mid thickness. The mechanical movement of the weld due to the weld thermal cycle was transmitted through the lever system to the calibrated clip gauge mounted on the far side of the scissor prongs, the electrical output of which is directly proportional to the dilation of the weld. A clip gauge was also

mounted on the bottom of the plate through studs welded on to the plate, as shown in Fig. 22 c), to measure possible warping of the test specimen due to welding. The outputs of both clip gauges were fed to a two-pen strip chart recorder to record dilation against a time base. Both the clip gauges were capable of measuring displacements of the order of 0.0025 mm. Thermal cycles were also recorded for the three plate thicknesses investigated at the center of the weld using a chromel-alumel thermo-couple. Additional experiments were run on 25 mm thick plate by depositing the weld on top of the plate in order to evaluate the effect of eccentricity of the weld on the contraction process.

The second phase of investigation consisted of measuring the expansion - contraction on sections of pipes. During the development of the slot-weldability test, it was shown the restraint could be varied by moving the slot to one side of the specimen. Dilation measurements on off-center slots were carried out on heat B 259 (to avoid contribution due to cracking) to see if the reduction of restraint could be quantified. Since the weld bead was to be deposited on top of the plate, considerable warping of the plate might be expected. Hence, design 2 (Fig. 22c) was adopted for measuring expansion and contraction. In this design, instead of drilling holes in the plate, studs were welded on top of the plate also 12.5 mm from the center-line of the slot. A long sleeve was used to secure the scissor prongs to the studs, the details of which are shown in Fig. 22c. For this series of tests, experimentation

was also carried out using design 1 to see differences due to design itself on contraction measurements. Additional experiments were run using design 2 on heats 492S1871 and C 10113 to investigate the effect of cracking during and after welding on the contraction process. In all cases, welding was performed with standard welding conditions and E 7010 HYP (4 mm dia) electrode.

IV. B. 2 Free Contraction Measurement:

For this, heat NKK, 15 mm thick, with V - groove cut to mid thickness and incorporating the slot was used. Side slots 25 mm apart were cut deep into the specimen up to 6.25 mm from the center of slot as shown in Fig. 23. This procedure produced a specimen with restraint so low that for all practical purposes the contraction measurements on this specimen could be taken as free contraction. Design 1 was used for contraction measurements in this case.

IV. C. Presentation and Discussion of Results

Fig. 24 shows the temperature versus time curves for the center of the weld for the three plate thicknesses examined. The effect of thickness of the plate on the contraction process along with the free contraction for heat NKK (the weld bead was deposited at neutral axis of plate. Hence eccentricity $\gamma = 0$) is depicted by the solid lines in Fig. 25. Also shown in Fig. 25 (dotted lines) is the effect of laying the bead on the top of the plate (positive eccentricity w.r.t neutral axis of plate) for the case of 25 mm plate thickness. Note that considerable warping of the

plate occurs as depicted by the curve representing measurements given by the bottom clip gauge. For the case when $\gamma = 0$ also, some warping was observed. As the bottom clip gauge measurement was made at a distance of 19 mm from the bottom of the plate, the actual expansion registered by the bottom clip gauge can be expected to be much higher than the actual expansion at the root of the notch. Note also that the weld extended 25 mm on either side of the slot. Starting the weld on the base plate away from the slot produced a small build up of weld at the start (and hence a positive γ) which, also, might have contributed to warping. This build up of weld is produced because the arc cannot penetrate into the plate as it does when it passes over the slot. Considering all these factors, when $\gamma = 0$ the actual measurements of the bottom clip gauge were small enough to be neglected in restraint calculations. Since design 1 was used for all measurements when $\gamma = 0$, the top clip gauge measurements were expected to be more representative and were used for further analysis of restraint. It is seen from Fig. 25, that as the plate thickness increased, the final contraction experienced by the specimen reduced or in other words, greater the restraint, smaller was the final contraction experienced by the specimen. The effect of plate thickness on the final contraction, percent free contraction and restraint co-efficient (A) which will be expressed as

$$A = \left(\frac{\text{free contraction}}{\text{hindered contraction}} \right) \quad \ldots \quad 13$$

is shown in Fig. 26, a, b and c respectively. It is also seen from Fig. 25 and 26, that the effect of a positive eccentricity of the weld bead was to

apparently reduce the final contraction and hence increase the restraint, at least, as far as the measurements from the present experimental design are concerned. This effect was considered only apparent and not real, because, although the local stress and strain at the root of the weld will increase due bending imposed on the plate when is positive, the restraint level which is a measure of the resistance to contraction of the surrounding continuum should not change as long as the welding conditions and plate dimensions remain the same. Hence the present experimental procedure did not seem to be adequate to deal with the situation of eccentricity of the weld bead with respect to the neutral axis of the plate and concomitant bending. The effect of positive eccentricity on the stress and strain at the root of the notch have been dealt with before (Chapter III). The situation becomes even more difficult to handle when dealing with measurements on curved plates (sections of pipes).

For the case when $\gamma = 0$, the contraction process proceeds in three steps. In the initial Step AB, in Fig. 25, the slot center experienced a small expansion as the arc is started at position 1 (Inset - Fig. 25) on the solid plate and moved towards the slot. This was followed by step BC when the contraction increased rapidly due to solidification of the weld metal as the arc passed over the slot. Finally, when the arc was extinguished at position 5, there was a small expansion CD due to the last phase of solidification in the crater. From then on, the contraction process proceeded as the temperature of the

plate dropped slowly to room temperature. Note that the possible expansion due to phase transformation was obscured by the contraction of the previously solidifying weld metal.

Figs. 27 (a and b) depict the contraction process on pipe sections of heat B259 when the position of the slot was varied, by using design 1 and design 2 respectively. Since the weld bead was deposited on top of the plate, there was considerable bending experienced by the specimen. The curves of Fig. 27 (a) are similar to those of Fig. 25 except that another small expansion was experienced as the arc passed over the center of the slot. When design 2 was used, (Fig. 27b) the top clip gauge did not experience the expansion during the last phase of solidification that was observed when design 1 was used. In either of these designs, the behaviour of the bottom clip gauge after welding when the slot was 25 mm from the end was vastly different from that of the other two cases. The reason for this was not very clear.

The effect of cracking on the expansion - contraction measurements using design 2 for heats 492S1871 (an example of extensive cracking) and C10113 (an example of moderate cracking) is shown in Figs. 28 and 29 respectively. The measurements of the bottom clip gauge appeared to be more sensitive to cracking than that of the top clip gauge, possibly because of the warping effect of the bead deposited on the top of the slot. For heat 492S1871 (Fig. 28), appreciable cracking about 3 minutes after the end of weld is

suggested by the slope changes in the bottom clip gauge plot, whereas Fig. 29 suggests moderate cracking in heat C10113. This behaviour for these two steels was noted in previous tests broken open for the cracking measurements reported in Table 4.

Only qualitative explanations for the expansion and contraction behaviour during and after welding have been given when the weld bead was deposited away from the neutral axis of the plate and for sections of pipes (curved plates). Quantitative assessment of restraint levels for these cases at least by the experimental techniques conducted in the present study is difficult because of both longitudinal and transverse shrinkage. The longitudinal shrinkage tends to deform the pipe sections against the curvature whereas the transverse shrinkage imparts warping due to the bead deposited on top of the plate. Both of these were very difficult to handle quantitatively by the present methods. For these situations, finite element methods of anaylsis might be needed to get a better understanding of the problem.

The quantity, A, in the equation 11 for the steels investigated in this study, was evaluated for the different thickneses of plates and pipe sections by interpolating, as a first approximation, from the values obtained with flat plate (heat NKK) when = 0 (Fig. 26). For E7010 and E7018 (well baked) electrodes the diffusible hydrogen content was assumed to be 30 ppm and 5 ppm respectively. For the purposes of comparison, two other formulae which have been used widely over the years viz the I.I.W. formula and P_{cm}

formula (due to Ito and Bessyo) were evaluated (Table 10). Fig. 30 (a to g) shows the correlation between extent of cracking and the various formulae. It can be seen from these figures that the extent of scatter is more or less the same in all these cases.

IV. D. Conclusion:

Though the theoretical basis for a formula such as equation 11 is well founded, the extent of scatter in the data obtained from this was not much less than that obtained from other formulae to date. More experimentation and evaluation of data in the literature might help evolve such a formula to predict the weldability of steels in general and low carbon micro-alloyed steels in particular.

CHAPTER V

IMPLANT TEST AND ITS CORRELATION WITH SLOT WELD TEST

V. A. Introduction:

The advantages and drawbacks of both the direct and indirect weldability tests that have been used to date to study the susceptibility of steels to hydrogen assisted cracking have been enumerated in Chapter II. Granjon[38] developed a test called the Implant test, that combines some of the advantageous features of both the direct and indirect type of tests in the sense that is allows independent control of stress, microstructure and hydrogen content possible with indirect tests but imposed on actual weldments instead of simulated structures.

In the implant test, a small cylindrical test specimen containing a circumferential notch near one end (called the implant) is slide-fitted into a hole drilled in a base plate. A test weld is then deposited on the top surface of the base plate to fuse the top end of the test specimen, introduce a controlled amount of hydrogen and create a weld heat-affected zone which contains the cylindrical notch as shown in Fig. 31. The specimen is then loaded in tension and the time to failure is noted for a series of tests conducted at various stress levels.

The implant test has the following advantages 1. stress, microstructure (welding condition) and hydrogen level can be varied independently and

the effect of each of these variables on the susceptibility to hydrogen assisted cracking can be studied independently of each other, 2. the test specimens are small and simple to machine, 3. the composition of the implant may be different from that of the plate into which it is inserted - the latter merely acting as a heat sink. So tests of weldability may be carried out with only a limited quantity of steel available.

A major drawback of the implant test lies in locating the notch in the coarse grained heat affected zone (considered the most susceptible structure) in each implant of a series of tests. To overcome this problem, a modified implant test, which uses a helical notch in place of a single circumferential notch has been introduced.[112] Also it has been shown[41] that the two procedures give identical results. Hence for the present investigation the modified implant test with a helical notch will be cmployed.

V. B. Materials To Be Investigated:

The objective behind conducting implant test was to examine the correlation between the lower critical stress obtained in the Implant test (externally loaded testing method) with the extent of cracking obtained on the same steels in the slot weldability test (self-restraining specimen). Hence it was imperative that steels with widely different cracking susceptibilities, as evaluated by slot weldability test, be selected to see if the Implant test would rank these steels in the same order as the slot weld

test. For this purpose, heats 492S1871, B259 and C10113 (see Tables 1 and 2 for chemical-composition and mechanical properties) were chosen for Implant testing because, from slot weldability test results (Table 3), heat 492S1871 (0.26C-Mn steel) showed extensive cracking and B259 (0.08C-Mn steel) showed no cracking at all whereas C10113 (0.05-microalloy steel) showed moderate cracking even though its carbon-equivalent was about the same as that of 492S1871.

V. C. Experimental Procedure and Testing Equipment

6mm Modified implants with helical notch oriented with their axis in the rolling direction were machined from the test plates. The specimens were prepared to slide fit into the hole drilled in the base plate. The center of the hole drilled in the base plate was carefully located to make sure that the axis of the loading arms and the implant were coincidental so that no eccentricity was introduced during loading. The details of the base plate and implant are as shown in Fig. 32. The base plate dimensions were chosen to closely match the dimensions of slot weld test specimens to keep the cooling rates in the two tests as nearly identical as possible. Since it was also intended that the different heats be capable of being compared against each other by the implant test, a base plate thickness of 15 mm was chosen as a compromise.

The test was conducted for both high hydrogen (HYP E7010) and low hydrogen (E7018)

electrodes. Additional tests were also run after welding by the MIG process using Argon +2% oxygen mixture at a flow rate of 1.42 M^3/hour as shielding gas to produce conditions where hydrogen levels would be negligible. Presumably, the only hydrogen that would be encountered in this process would be the residual hydrogen in the base plate, test piece and the welding wire (bare) themselves which would be exceedingly small. For all the conditions the heat input was maintained the same. E7010 electrodes were used in the as received condition whereas E7018 electrodes were baked at 370^{o}C and stored at 100^{o}C for at least 8 hours before use. In case of welding with E7018 electrodes, welding was performed 2 minutes after taking the electrodes out of the oven.

A creep testing machine was modified to perform as an implant testing machine. Fig. 33 shows the details of the testing equipment used. The testing machine was a dead weight loading machine with a maximum capacity of 5500 kgs load. The machine was equipped with an automatic timer actuated at the instant of loading and stopped by a microswitch on the loading grill when the specimen failed.

Before welding, both the implant and base plate were thoroughly degreased using acetone. Two minutes after performing the weld, which is the time for the weld to cool down to 125^{o}C (Fig. 24), the load was applied to the implant specimen and maintained until either rupture occurred or until it was judged that rupture would not take place (24 hours).

The ruptured specimen fracture surfaces were preserved by coating with Krylon for fractographic examination which is elaborated on in the next chapter. The specimens which did not fail after 24 hours were cut out for further metallographic examination to detect any cracks present.

V. D. Presentation And Discussion Of Results

The stress-time to failure diagrams for the three heats examined at different hydrogen levels are shown in Figs. 34,35 and 36. Stresses were calculated based on the area at the root of the notch. In general the lower critical stress decreased as the hydrogen level was increased in susceptible steels. Fig. 34 brings out the extreme susceptibility to HAC of heat 492S1871. Even when welding was done by GMA process using (Ar + 2% O_2) mixture, the HAZ shows a remarkable drop in stress to failure. It was presumed that small amounts of hydrogen must have been introduced into the heat affected either from moisture on the bare wire or the test plate or from residual hydrogen in the steel itself. Even such small amounts of hydrogen were sufficient in drastically reducing the stress to failure in heat 492S1871. Note that for the same conditions of welding, heat C 10113 showed virtually no reduction in stress to failure (Fig. 35). Heat B 259 (Fig. 36) showed no susceptibility to cracking at any hydrogen level examined. When loaded above the lower critical stress, failure in heat B 259 occurred well away from the HAZ in the base metal after considerable plastic flow.

Fig. 37 shows the stress to failure diagrams for the three heats when welded with E 7010 electrode. From this figure it can be seen that the lower critical stresses for cracking are in the same order as the susceptibilities to cold cracking in the slot weldability test. The steel with the highest susceptibility to cracking in the slot test gave the lowest critical stress in the Implant test and vice versa. Hence the results of slot weld test seem to correlate very well with those of the Implant test.

CHAPTER VI

STUDY OF CRACK INITIATION AND KINETICS AND MORPHOLOGY OF CRACK GROWTH USING ACOUSTIC EMISSION MONITORING TECHNIQUE AND FRACTORGRAPHY

VI. A. Introduction:

Acoustic emission (AE) is defined as the high frequency stress waves generated by the rapid release of strain energy that occurs within a material during crack growth, plastic deformation or phase transformation.[113] This energy may come from elastic stored energy as in crack propagation or from stored chemical free energy as in phase transformation. Since the first documentation of AE monitoring in metals (zinc, steel, aluminum, copper and lead) under stress by Kaiser[113] in 1950, AE analysis of fatigue and fracture toughness tests, stress corrosion cracking, hydrogen embrittlement,[114-118] twinning deformation and martensitic phase transformations,[119] deformation processes in welded joints[120] and other tests is becoming increasingly widespread as a research tool. On a more practical side, AE inspection is used as a non-destructive inspection method and for quality control.[121-125] Because AE inspection is limited to the detection of an active flaw during a change in the stress field that surrounds the flaw, it is not capable of detecting static flaws. For this reason, AE testing must be applied while the material or structure is subjected to stress. Because of its ability to detect dynamic flaws, AE as a tool for monitoring crack

growth, predicting life and monitoring leakage in components under stress such as nuclear reactors, pressure vessels, pipelines etc[126,127] is becoming increasingly important.

Recently, the superiority of AE technique in detecting small, discontinous crack extensions such as in hydrogen embrittlement, stress corrosion cracking and fatigue processes, over other methods has been shown.[117,118] Studies on kinetics of crack growth during hydrogen assisted cracking employing AE techniques, particularly in welding, are very scarce.[128] Even in this study,[128] no source location techniques were used and very few details of the monitoring system are available. Moreover, testing was conducted on a very limited scale and only at low hydrogen concentrations.

Hence, in the present study, to provide additional information on the initiation and progagation of hydrogen assisted cracking, AE monitoring technique was adopted by instrumenting the implant testing machine previously described and also the slot weldability test sample after welding. A description of the AE system used and instrumentation of implant and slot weld test specimens follows.

VI. A. 1. <u>General Description of the System Used And Its Capabilities.</u>

A block diagram of the 12 channel computerized AE system* is illustrated in Fig. 38. The system is designed for locating AE activity regions on a real

*Manufactured by Acoustic Emission Technology Corporation, Sacramento, California.

time basis, that is, AE source location analysis and measurement of signal characteristics (amplitude, ringdown count and v.m.s) are carried out and displayed on a CRT screen as they occur. The system also provides a complete record of the background noise levels during all portions of the test by means of floating threshold concept, enabling the signal to noise ratio of the test to be continually established. The operation of the system is as follows.

Stress wave information from the test sample under consideration, is picked up by the sensors (the AET sensors used are piezoelectric devices with a peak resonant frequency of 375 KHZ nominal with a sensitivity greater than -75 db referred to 1 volt per microbar, operational in the temperature range from $-250^{o}C$ to $+200^{o}C$. The sensors are 19 mm in dia and 22 mm high and are attached to the test piece by means of magnetic mounts). The sensors convert this mechanical stress wave to electrical signals which travel a length of transmission line to a preamplifier which amplifies the low level AE signals and filters out extraneous noise. The signals are then processed in several ways. Signal level monitoring circuitry measures the rms output voltage levels, and AE detection is accomplished by discriminators or signal processors (Gain continually adjustable from 0 to 60 db and threshold adjustable from 10 mv to 10 volts).

The discriminator pulses are used to define time differences for source location and for individual events when counting a total. The parametric data

system transfers variable parameters of interest such as time, pressure, load, temperature etc into the monitoring system which enables the system to present the AE data versus the test parameter of interest. Multiple parameters can be accomodated and this information is available for both displays of source location and graphics as well as for the teleprinter copy. For location of AE sources, the signal arrival time differences are processed by a minicomputer. The source locations are then plotted on a CRT display. Both source locations and event count data are stored on a digital cassette tape in a computer-reusable form. Dual cassette tapes enable program and test data to be easily entered, stored, re-entered and re-analyzed at any time. The system also incorporates a simulator and an audio unit. The simulator unit is used to provide test pulses to AE sensors to check system operation and for source location calibration. The audio unit provides an output for audio perception of the AE activity. The audio output is a tool which is useful to system users since the data can distinguish (with experience) crack noise and plastic deformation from mechanical and extraneous background noises. There are several pieces of additional equipment which may be used together with the basic system. These include an oscilloscope, for visual examination of incoming signals and a strip chart recorder, generally used to record a representative channel of AE counts or other parameter as a function of time.

VI. B. Instrumentation and Procedure:

For the purposes of locating the sensors for source location and identification on CRT, a sensor layout carried out previously on a pressure vessel was used. A hard copy made from the CRT display of the sensors layout is shown in Fig. 39. The display represents a flat map of the cylindrical portion only of a pressure vessel having semi-spherical top and bottom heads. The surface is divided into sections for triangulation purposes.

VI. B. 1. Implant Test:

For the implant testing, sensor positions 2, 4, 5 and 8 were used. The exact position of the center of the sensors on the base plate with respect to the weld and the implant are shown in Fig. 40. In order to secure the positon of sensors on the base plate during testing (note that the sensors make contact with the welded side of the base plate which is facing downwards during testing) the magnetic fixtures were glued to the back-up plate at pre-determined positions and the sensors were placed face up in the hole in the magnet, the holes being just big enough to accomodate the sensors. A rubber cushion was provided between the magnet and the sensor so that some pressure would be exerted when the test plate was secured in place for testing. This ensured good contact between the test plate and the sensors. Copious amount of coupling agent, viz., silicone grease Dow Corning 11 compound was used to ensure good acoustical contact between test plate and sensors.

After welding with the same conditions and procedures as described in Chapter V, the slag and spatter were removed by chipping and the plate surface was cleaned by wire brushing. The test plate was then placed in position in the testing machine by dropping the plate onto the magnets (incorporating the sensors) and against the positioners which made sure that the axis of the implant test piece and that of the loading arms were colinear. The base plate was then bolted onto the backing plate. The entire procedure took approximately 90 secs to perform after welding. Load was applied to the implant specimens exactly 2 mins after welding and acoustic emission monitoring was started the instant load was applied. Testing was conducted for both high hydrogen (welded with E7010) and low hydrogen (welded with E7018 electrode) conditions on heats C10113 and 492S1871 on only specific pre-selected stress levels as shown in Figs. 34 and 35. The stress levels were selected to represent the full range from below the critical stress to the highest which were determined previously.

VI. B. 2. Slot Weld Test:

For the slot weldability test, sensor positions 2, 3, 4, 5 and 6 were used. The exact sensor positions on the test plate with respect to the weld are shown in Fig. 41. The positions of the sensors were pre-marked on the test plate. After welding with the standard welding conditions the plate was cleaned of spatter and slag on the top of the plate and the slag on the bottom of the weld in the slot was also thoroughly removed. (Failure to remove the slag from

the bottom of the weld in the slot resulted in an overwhelming amount of acoustic emissions because the cracking in the plate and cracking of the slag apparently produce acoustic bursts of the same characteristics and frequency range so that the monitoring system has no way of distinguishing between the two. Hence it was absolutely essential that slag from under the slot was also thoroughly removed). The sensors were then placed in pre-determined positions and secured in position by hold-down magnets. This entire procedure took about 140 secs. Crack growth monitoring was started exactly 150 secs after welding. The crack growth monitoring was done for heats C10113 and 492S1871 for only high hydrogen (welded with E7010 electrode) condition since it was previously determined that no cracking occurred in either of these heats when welded with E7018 electrode (low hydrogen).

For the acoustic emission monitoring studies on both implant tests and slot weldability tests, the following instrument settings were used.

Gain = 79 db
Threshold = 0.205 volts
AE sensor used: - Model AC 375 - LM.

The threshold level of 0.205 volts was selected by trial and error. When a threshold of 0.8 volts was used only AE during the final fracture was registered and the rest of the signals were wiped out. A threshold of 0.41 volts also resulted in a significant loss of emission data. A threshold of 0.150 volts resulted in an enormous amount of

spurious signals. A threshold level of 0.205 volts resulted in optimum operating conditions. Such low threshold levels are possible because in the present study a dead weight loading system was used. If hydraulic servo-controlled test system were used, more than an order of magnitude increase in threshold level would be required to eliminate background noise. The result of this on the loss of valuable emission data is readily apparent. In fact, Liptai et al[116] in an extensive review paper concluded that servo hydraulic systems are almost unusable for acoustic emission analysis. This is particularly true where low amplitude acoustic signals are anticipated. This problem can be minimized, as in the present case, by using band pass filters.

Following testing, the fracture surfaces of both implant and slot weld test specimen (a 12 mm section was cut out at the center and broken open) were subjected to fractographic study using ETEC scanning electron microscope (SEM) operated in the secondary electron imaging mode at 20 KV.

VI. C. Results:

VI. C. 1. Acoustic Emission Studies

The results of acoustic emission studies conducted on heat 492S1871 and C10113 on both the implant and slot weldability tests are presented in Figs. 42 to 46; wherein the cumulative total pulse height is plotted as a function of time. The specimen numbers denoted in Figs. 42 to 45 correspond to those in Figs. 34 and 35. Note that the

stresses are also denoted as percent N.T.S (notch tensile strength) which is taken as the stress at which the implant specimen would break within 10 secs after loading when welded with GMA process using (Ar + 2% O_2) mixture as shielding gas. This makes possible the comparison of the two heats studied regarding crack growth rates. A typical source location and total pulse height vs time plot of events during a test as produced by CRT display are shown in Figs. 47 and 48 respectively. The dots in Fig. 47 indicate the located positions of real acoustic emission sources. The dot concentration indicates the activity level and approximate position of the source. The resolution of source location can be vastly improved by using either microsensors (less than 3 mm in dia are available) or a 2 mega cycle electronic clock (for time difference computations) or both.[129] For the present investigation a 1 mega cycle clock was used. The dots aways from the region of high concentration (Fig. 47) could be traced to pulses arising from reflection. Note that these pulses are also taken into account in the plot produced by the CRT display (Fig. 48). However, total pulse height vs time plots in Figs. 42 to 46 represent real stress wave emissions coming from the sample; where in impertinent AE signals due to S.W reflections and other spurious (noise) sources have been eliminated.

With respect to initiation of cracking, it is seen from Figures 42 and 43, that in heat 492S1871 for all hydrogen concentration and stress level examined, there was virtually no incubation time for crack initiation. The same behaviour was seen (Fig. 44) for heat C10113 at high hydrogen concentrations

(welded with E7010 electrode). By contrast in C10113 at low hydrogen concentrations produced by welding with E7018 electrodes, a definite incubation period was noted for crack initiation at lower stresses (Fig. 45). The lower the stress, the longer was the time for initiation of a crack. This incubation period can be attributed to the time required for the critical hydrogen level to accumulate by diffusion to regions of triaxial stress just ahead of the notch.[94] The AE signals from the specimens were discrete events with a large range of amphitudes and pulse widths. In all cases, the high sensitivity of AE in showing the discontinuous nature of hydrogen assisted cracking was evident. The quiet periods are probably the time required for sufficient hydrogen to diffuse to the crack tip. In general, for all the conditions examined, the higher the stress, faster was the crack growth rate and shorter was the time for final fracture. Note also that the energy to failure (square of the pulse amplitude is proportional to energy) in heat C10113, in all cases was significantly lower than that for heat 492S1871. From Figs. 42 to 46 it is also seen that the crack growth rates (for the same percent N.T.S for implant specimens) in heat 492S1871 are faster than that in C10113. A possible explanation for these observations is given later based on fractographic information.

VI. C. 2. Fractographic Studies:

VI. C. 2. 1. Heat 492S1871

Figures 49 and 50 show the scanning electron microscopic (SEM) views of specific areas of the

fracture surfaces in implant specimens of heat 492S1871 when welded with HYP E7010 electrode (high hydrogen) and E7018 electrode (low hydrogen) respectively. It is seen that the fracture mode at crack initiation was essentially trans-granular quasi-cleavage (TGQC) with little contribution from inter-granular (IG) failure. As the crack propagated, the fracture morphology changed from one of quasi-cleavage (Figs. 47 a, 47 c, 48 a, 48 c) to one of TGQC associated with extensive microvoid coalescence (Figs. 49 b, 49 d, 50 b, 50 d). On the other hand, in specimens from the slot weldability test (Fig. 51), crack initiation was associated with microvoid coalescence (MVC) and TGQC and the morphology changed entirely to quasi-cleavage associated with small amounts of IG failure.

VI. C. 2.2 Heat C10113

The fracture morphology in implant specimens of heat C10113 tested to failure when welded with E7010 and E7018 electrodes are shown in Figs. 52 and 53 respectively. It is seen from these figures that the fracture mode at crack initiation was predominantly IG in nature. The amount of IG failure decreased with either an increase in initial stress (Figs. 53 a, b and c) or with continued crack propagation giving way to TGQC (52 b-d), perfect cleavage (53 d) and TGQC associated with extensive MVC (53 b). In slot weld-ability test also (Fig. 54) there was a small region of tear associated with MVC at the root of the notch (Fig. 54 b) with the fracture mode changing immediately to QC (Fig. 54 b) and further to QC and IG (Fig. 54 c and d) as the crack propagated. Note that the proportion of IG process increased rapidly as the

crack propagated in the slot weldability test in heat C10113. Hence in heat C10113 both IG and QC types of failure play a very important role in the hydrogen induced cracking. This was in sharp contrast to heat 492S1871 in which fractographic study showed large areas of dimples and cleavage indicating that hydrogen induced cracking occurred primarily by MVC and QC type of failure with very little contribution due to the IG process.

VI. D. Discussion

Since hydrogen induced cracking in steels occurs due to the combined action of hydrogen, stress and microstructure, the foregoing results should be capable of explanation by considering these three factors. In welding, hydrogen available for the micro-cracking process is determined by the competing factors of hydrogen diffusion to the crack tip under a stress gradient to regions of high triaxial stress and the effusion of hydrogen from the weld metal to the atmosphere. This situation is depicted for both high and low hydrogen concentrations in the weld produced by E7010 and E7018 (properly dried) electrodes respectively in Fig. 55. It is assumed that initially the weld bead and the heat-affected zone next to the fusion zone in the vicinity of the notch, where crack initiates, have a uniform distribution of hydrogen concentration of about 30 ppm in case of E7010 electrode and 5 ppm for E7018 electrode. With the passage of time after welding, the average hydrogen concentration in the matrix (weld metal and coarse grain heat affected zone) will decrease due to the outgassing of the charged

weld metal to the atmosphere and the surrounding base metal in an attempt to attain equilibrium. The regions of high triaxial stress (near voids, just ahead of the notch or near internal cracks as dictated by the microstructure) in the coarse grain heat affected zone and weld metal have a high affinity for hydrogen and the local concentration in this region becomes greater than that of the surrounding matrix. Thus, while the hydrogen concentration tends to increase in the regions of high triaxial stress, there is a decrease in the average hydrogen concentration in the matrix. This situation is depicted in Fig. 55b. When the hydrogen concentration in the stressed region reaches a critical value (the higher the stress, the lower is the critical concentration of hydrogen necessary), either initiation of a crack or the extension of a existing crack takes place. In case of high initial hydrogen concentrations in the weld metal (E7010 electrode), little increase in local hydrogen concentration at stressed regions is necessary to cause cracking; whereas for initially low hydrogen contractions (E7018 electrode), depending on the stress level, considerable increase in hydrogen concentration can be expected ahead of the crack tip (Fig. 55 b). As the crack propagates, part of the atomic hydrogen which had diffused into the triaxially stressed region is lost as molecular hydrogen behind the growing crack. This, together with the continual effusion of hydrogen from the weld metal to the atmosphere with the passage of time, provides a situation wherein, lesser and lesser amounts of hydrogen are available in the matrix for diffusion

to the triaxially stressed regions. Ultimately the local hydrogen concentration at the crack tip will also decrease with time as shown in Fig. 55 b. Finally, when the hydrogen concentration at the crack tip falls below the critical level for the existing local stress at the crack tip, further crack growth should cease to take place. This is the situation for implant test specimens loaded below the lower critical stress as well as for slot weldability test specimens. It is seen from Figs. 42 to 44 that even when the specimens were loaded below the critical stress, cracking started immediately upon loading. But the crack growth rate was slow enough that the increase in stress intensity at the crack tip as the crack advanced, could not keep pace with the decreasing concentration of hydrogen at the crack tip and cracking eventually ceased. The situation is slightly different in the slot weldability test. The test utilizes an internally restrained specimen. Hence,when a crack propagates it produces a relaxation of the load. The fact that a change of fracture mode from one of MVC at crack initiation to QC and further to IG process was observed as the crack propagated in heat C10113 (Fig. 54) supports the view that, the stress intensity at the crack tip decreases with continued crack propagation in the slot weldability test. The situation is similar to wedge-loaded specimen design[96] which also produces a case of decreasing stress and a concomitant decreasing stress intensity as the crack grows. The decrease in stress intensity together with the effusion of hydrogen will cause eventual cessation of cracking (Fig. 46). The need for accumulation

of critical hydrogen concentration at the crack tip can also explain the quiet periods, in Figs. 42-46, between increments of crack growth. Note that the lower the stress, the higher is the critical concentration of hydrogen necessary for crack growth and hence the longer are the quiet periods associated with longer periods of time for diffusion and build up of hydrogen to critical level. Everytime a crack propagates it leaves the site of critical hydrogen concentration. A halt in crack growth occurs until sufficient hydrogen diffuses to the new location of the crack tip. This process gives rise to the discontinuous nature of hydrogen assisted cracking (Figs. 42 to 46).

When welded with E7010 electrodes, the average concentration in the weld metal and coarse grain heat affected zone is so high (Fig. 55 b) that it is probably well above the critical level at all stress levels examined in the implant test (Fig. 42 and 44) as well as in the slot weldability test (Fig. 46) for both heat 492S1871 and heat C10113. Hence there is no necessity for an incubation period and cracking is observed immediately upon loading. But for the case of E7018 electrode, no incubation period was observed at all stress levels examined in heat 492S1871 (Fig. 43). In heat C10113 only the highest stress level registered no incubation period while at lower stresses a definite incubation period was noted (Fig. 45). Of course, the lower the stress the higher was the incubation period for crack initiation. This observation suggests that the critical hydrogen concentration necessary for crack iniation and growth in heat 492S1871 is very small (less than 5 ppm). In heat

C10113, the local hydrogen concentration at the crack tip will have to exceed the initial hydrogen concentration of 5 ppm (when welded with E7018) in the matrix at lower stress levels for crack initiation and hence the necessity for an incubation period in heat C10113 when welded with E7018 electrode. This difference in behaviour between these two steels is explained based on fractographic and microstructural features as follows.

Fractographic studies on fracture surface of the implant as well as the slot weldability tests indicated that for all stress and hydrogen levels studied, MVC and QC type were the major modes of failure in heat 492S1871 whereas IG and QC type were the important modes of crack growth in heat C10113. To explain these observations, it is necessary to consider the microstructural features of the coarse grain heat affected zone in these two heats of steel (Fig. 11 a and b). The HAZ microstructure of heat 492S1871 was untempered martensite whereas that of C10113 was acicular low carbon martensite with auto tempering during cooling. It is not possible to define explicitly the exact form of martensitic (plate, lath or internally twinned etc) structure seen in Fig. 11 a. However, hydrogen induced failure of lath or packet boundary [88,89,130] and hence TGQC mode appears most reasonable in heat 492S1871. Both the hardness (Table 5) and grain size (Fig. 11 a and b) of coarse grain HAZ in 492S1871 were higher than those of C10113. Hence it is also possible that grain size and microstructure might be having synergistic effects. Since the HAZ microstructure of heat 492S1871 was untempered martensite, it is possible that very high

internal stresses were present within the microstructure which was further augmented by the external stress. This might have led to a situation wherein, at all stress levels examined, the internal stresses were significantly higher (and hence lower critical concentration of hydrogen necessary for cracking). Hence, even when this heat of steel was welded with E7018 electrode (low hydrogen) no incubation period was noted at all stress levels examined in implant testing. Note that in heat C10113, the HAZ microstructure was low-carbon martensite with auto tempering. Auto tempering reduced the internal stresses within the microstructure in this heat of steel and hence higher external stresses and higher hydrogen concentrations were necessary for crack initiation and growth. This could explain the necessity for an incubation period (for hydrogen diffusion to crack tip to attain critical concentration) in heat C10113 at lower applied external stresses when welded with E7018 electrode. At the highest stress level examined, however, no initiation period was needed, probably because, at that stress level the critical hydrogen concentration necessary for crack initiation was less than the hydrogen concentration in the matrix (about 5 ppm) at the instant of applying the load. The very low hydrogen concentrations necessary for cracking (high susceptibility) in heat 492S1871 was further evident from Fig. 34 which showed a precipitous drop of stress to failure even when this steel was welded by GMA process using (Ar + 2% 0_2) mixture. Note that C10113 showed virtually no reduction in stress to failure when welded under the same conditions indicating higher hydrogen concentrations necessary for

this steel to exhibit cracking. It is clear from these results that the interaction between hydrogen and microstructure is very important in determining the initiation, the kinetics and the mode of the fracturing process.

The relation between the stress intensity factor, hydrogen concentration at the crack tip and the fracture mode for the two heats studied viz., 492S1871 and C10113 are summaried in Figs. 56 a and 56 b respectively. The stress intensity factors for implant specimens were calculated on the following assumptions. (a) only the first thread in the helical notch takes up all the load so that the effects of other threads can be neglected. This assumption is justified by the observation that tests conducted using both the helical notch and a single circumferential notch gave identical results for the lower critical stress in implant tests[41] (b) Immediately after crack initiation, the situation can be approximated to the case of an infinitely sharp notch in a round bar (Fig. 57). The stress intensity factors thus calculated, have been plotted against hydrogen concentration at the crack tip in Figs. 56 a and 56 b. Note that the stress intensity factor values plotted in these figures are known quantitatively only at the instant of crack initiation (crossed points denoted by numbers) at the various stress levels studied in implant test. The stress intensity factors during further crack propagation and that for slot weldability test should be treated as strictly qualitative (indicates the trend only) in nature. Positions x and y on the abscissa correspond to concentration of hydrogen in the matrix two minutes after

welding (instant of loading in the implant specimen) for E7018 and E7010 electrodes respectively. Note that this is equivalent to hydrogen concentration at the crack tip for cases where no incubation period for cracking is observed. In Fig. 56, it should be appreciated that the fracture process can be one of mixed modes along the leading edge of a crack if the stress level and/or hydrogen concentration change along the crack tip. No cracking would be expected below the lowest curve. In general (for both Figs. 56 a and b) at high stress intensities the failure mechanism is MVC. At lower stress intensitites concurrent with a smaller plastic zone size in which a large number of inclusions are not present the fracture mode is one of QC. At still lower stress intensities the IG mode of failure, a process involving even lesser plastic deformation, occurs. It is also seen that increasing hydrogen concentration at the crack tip decreases the critical stress intensity at which these microfracture processes can occur. These findings are consistent with those of others.[96,97,128]

Acoustic emission studies showed (Fig. 42-45) (i) that the total pulse height to failure for heat 492S1871 was considerably higher than that for heat C10113 and (ii) the crack growth rates (for the same percent NTS) in heat 492S1871 were faster than those in C10113. These ovservations can be rationalized based on the fracture modes in these two steels. Since HAC in heat C10113 was shown to occur predominantly by IG mode (Fig. 52-54) it should be energetically the most favorable process (as supported by AE data) as it involves the least amount of plastic deformation compared to QC and MVC

modes. It has been hypothesized that MVC and QC are relatively faster modes of fracture compared to IG mode.[96] Hence higher crack growth rates should be expected in heat 492S1871 since QC and MVC were shown to be the dominant modes of failure (Fig. 49-51) in this steel.

The energetically favorable IG process is thought to be superceded at high stress intensities by the kinetically faster QC and MVC processes.[96]

For the case when the combination of stress intensity factor and hydrogen concentration at the crack tip corresponds to point 14 in Fig. 56 b, the hydrogen concentration is insufficient to initiate crack growth at the instant the specimen is loaded. Hence, an incubation period is required so that sufficient hydrogen can diffuse to the crack tip. When the hydrogen concentration reaches the level indicated by point A in Fig. 56 b, cracking will initiate and grow intergranularly for a short distance. As the crack grows, the stress intensity at the crack tip will increase and critical hydrogen concentration necessary for further growth of crack reduces. When the combination of stress intensity and hydrogen at crack tip reaches point B, the mode of fracture changes to QC. The stress intensity will again increase until point C is reached where the fracture path assumes mixed mode. Ultimately fracture occurs at point D.

Just below the lower critical stress, as represented by point 11 in Fig. 56 b, cracking occurs immediately upon loading. But the rate of crack

growth is slow and the rate of hydrogen effusion is high enough to deplete the hydrogen level before the ciritcal hydrogen level is reached at the crack tip for further crack growth as represented by point E in Fig. 56 b. Thereafter, no further crack growth takes place. Such is the situation in slot weldability test specimens except that in this test the stress intensity factor also decreases with crack growth as discussed before. This is shown by the dashed lines in Figs. 56 a and b.

Finally, what significance do the results of the present study have on the potential mechanisms of hydrogen assisted cracking? Fractographic observation of MVC, QC and IG processes are compatible with the suggestion by Beachem[96,97] that the presence of sufficiently concentrated hydrogen dissolved in the lattice just ahead of the crack tip lowers the stress required to drive whatever deformation processes the micro-structure will allow. Areas of "perfect cleavage" observed on some fracture surfaces (53 d, 53 f, 50 b, 49 d) also supports the model that hydrogen reduces the binding energy between iron atoms, and therefore, the stress to propagate a crack.[94,95] The inter-relation between these two mechanisms and others[90-93] is not very clear. However, what is quite clear, is that hydrogen can strongly affect the yielding and flow characteristics of high strength steels. Further, the present study demonstrates that hydrogen can react with microstructural features in quite different ways, and that this interaction can strongly affect the kinetics and morphology of crack growth in steels.

VI. E. Summary and Conclusions:

The results of AE and fractographic studies may be summarized as follows.

1. Cracking initiated in heat 492S1871 immediately after loading at all stress and hydrogen levels examined. However, heat C10113 showed no incubation period at high hydrogen levels and a definite incubation period for crack initiation at lower stress levels and low hydrogen concentrations. The lower the stress, the longer was the incubation period.

2. Crack growth rates in heat 492S1871 were higher than in heat C10113 in both implant and slot weldability test specimens.

3. Fractographic studies revealed that crack propagation in heat C10113 was predominantly intergranular; whereas crack propagation in heat 492S1871 occurred by quasi-cleavage and microvoid coalescence, both being relatively rapid fracture processes.

4. Hydrogen assisted cracking is very sensitive to microstructural features and this interaction can dictate the kinetics and morphology of crack growth.

5. The results of this study are compatible both with Beachems's model for HAC and with the lattice decohesion theory. The inter-relation between these two theories is not very clear.

CHAPTER VII
SUGGESTIONS FOR FUTURE WORK

1. During the entire course of the present work, only one heat input (9KJ/cm) was used. The effect of various heat inputs on the extent and locus of crack growth in pipeline steels using the slot weld test should be examined.

2. A correlation test between slot weld test results and shop girth welded pipes was carried out for only one heat of steel viz 492S1871. In order fully to evaluate the usefulness of slot weld test results in assessing the susceptibility of steels to hydrogen induced cracking during girth welding, it is suggested that correlation studies be carried out on several steels with varying susceptibilities to cracking.

3. The desirability to use fracture mechanics principles to study HAC of steels due to welding was mentioned in Chapter II. Unfortunately such an approach has been lacking in the field of welding because of the unique nature of the process. Even the implant test does not lend itself to the application of fracture mechanics because of the small size and cylindrical shape of the specimen which gives rise to multiple crack initiation sites particularly at higher stress values. Implicit in the fracture mechanics application is the assumption that the crack is infinitely sharp. Hence, a modification of the implant test is suggested based on compact tension specimen design as shown in Fig. 58.

The implant (Compact Tension) specimen is fatigue precracked to provide an infinitely sharp crack. The specimen is then cut out along the dotted line as shown in Fig. 58 (a) at a distance x from the fatigue precrack. Distance x, should be predetermined for the heat input and welding process to be used so that the precrack ends up in the HAZ after welding. The heat of welding will, of course, eliminate the cold work at the fatigue crack tip. Since no load is applied on the specimen during the welding operation, no appreciable blunting of the fatigue crack tip is expected. The fatigue crack should still provide an extremely sharp crack to facilitate application of fracture mechanics principles for the study of HAC. The specimen slide fits into a slot cut in the base plate (Note the relief given to the slot in the base plate to allow for the specimen swing during fracture). From here-on the procedure is similar to that used on regular implant testing method. One important but not a serious drawback of the specimen design is the necessity to carefully position the fatigue crack so that it ends up in HAZ after welding in every test in a series. AE and COD techniques can be used to monitor crack growth rates during testing. The position of crack growth is predetermined by the specimen design and the problems associated with multiple crack initiation sites is avoided.

The AE monitoring system using microsensors and 2 Megacycle timer should be capable of locating the regions of AE activity (and hence the crack front) more accurately during testing. The stress intensity factor solution for this specimen configuration is given in Fig. 58 d. If this experimental set up (or variations thereof) is found successful, it is expected to open the door for the application of frature mechanics principle to study HAC in weldments not available to date. This should go a long way in a better understanding of HAC problems in weldments.

TABLE 1. Composition of Pipe Line Steel Materials

Heat	Pipe Dimensions Diam. mm	Wall mm	C	Mn	P	S	Si	Cb	V	Cr	Ni	Mo	Others
63843	900	14.3	0.25	1.30	0.010	0.025	0.01	0.03	-	-	-	-	-
C10113	1200	18.3	0.05	2.04	0.010	0.006	0.29	0.06	-	-	0.25	0.58	Al=0.04
B319	900	15.7	0.24	1.25	0.012	0.024	0.18	0.023	-	-	-	-	-
H471(a)	320	15.7	0.24	1.21	0.060	0.025	0.23	-	0.06	-	-	-	-
98173	900	14.3	0.21	1.30	0.018	0.019	0.02	0.031	-	-	-	-	-
H473(a)	320	25.4	0.19	1.38	0.007	0.015	0.25	-	-	-	-	-	N_2=0.01
88284	900	19.0	0.21	1.19	0.013	0.021	0.01	0.031	-	-	-	-	-
W3134	1050	10.3	0.13	1.60	0.009	0.012	0.29	0.037	0.06	0.092	0.018	0.002	Cu=0.035, Sn=0.004, Zr=0.13
H228	900	11.4	0.17	1.36	0.010	0.026	0.35	0.023	-	-	-	-	-
A210	900	15.7	0.17	1.25	0.030	0.009	0.18	0.028	-	-	-	-	-
59609	750	9.5	0.04	0.46	0.010	0.018	0.28	0.047	-	0.70	0.89	0.21	Cu=1.17, Al-0.056
B259	900	15.7	0.08	1.15	0.020	0.004	0.23	0.050	-	-	-	-	-
Mobil(b)	300	6.4	0.20	0.82	0.004	0.026	<0.01	<0.005	0.002	-	-	-	Al< 0.005
A69-2	900	11.4	0.19	1.38	0.026	0.005	0.08	<0.005	0.002	-	-	-	Al=0.013
A68-2	900	11.4	0.22	1.38	0.025	0.005	0.09	<0.005	0.002	-	-	-	Al=0.011
492S1871	1050	14.6	0.26	1.36	0.011	0.025	0.04	0.031	0.060	-	-	-	-
496S2211	1050	14.6	0.20	1.31	0.007	0.032	0.02	0.029	0.060	-	-	-	-
496S1871	1050	14.6	0.21	1.20	0.008	0.021	0.02	0.025	0.047	-	-	-	-
490S2441	1050	14.6	0.19	1.30	0.007	0.021	0.02	0.026	0.045	-	-	-	-
492S2681	1050	14.6	0.19	1.28	0.010	0.025	0.03	0.027	0.043	-	-	-	-
490S2391	1050	14.6	0.18	1.31	0.008	0.032	0.03	0.026	0.047	-	-	-	-
493S2761	1050	14.6	0.18	1.26	0.006	0.033	0.02	0.027	0.043	-	-	-	-
493S2791	1050	14.6	0.18	1.10	0.006	0.022	0.02	0.022	0.039	-	-	-	-
Italsider(1)	Plate	20.0	0.062	1.53	0.016	0.007	0.30	0.050	-	-	-	0.29	Al=0.03, Ce=0.5 kg/ton
Italsider(2)	Plate	20.0	0.060	1.53	0.016	0.007	0.30	0.039	-	-	-	0.30	Al=0.042, Ce=0.5 kg/ton
1376	Plate	19.0	0.12	1.00	0.008	0.007	0.020	0.019	<0.01	0.58	-	-	Cu=0.34, N_2=0.011, Ce=0.03, La=0.014
IF5913	Plate	19.0	0.12	1.37	0.007	0.004	0.21	0.048	-	0.07	0.04	0.30	Al=0.012
IF5914	Plate	19.0	0.069	1.56	0.007	0.003	0.23	0.050	-	0.06	0.03	0.28	Al=0.013
IF6221	Plate	20.3	0.084	1.44	0.008	0.006	0.22	0.052	-	0.25	0.05	0.27	Al=0.014
2F1665	Plate	20.3	0.066	1.46	0.005	0.003	0.21	0.053	-	0.53	0.05	0.35	Al=0.018
NKK	Plate	25.4	0.040	1.24	0.013	0.003	0.32	0.020	0.050	0.300	0.20	-	Cu=0.34, Al=0.027
B35	Plate	15.9	0.099	1.39	0.004	0.005	0.33	0.025	0.095	0.024	0.161	0.156	Cu=0.017, Sn=0.002, Ce=0.007
B229	600	15.0	0.180	1.21	0.012	0.009	0.22	0.019	0.020	-	-	-	Ce=0.014
B268	600	16.0	0.100	1.41	0.010	0.002	0.26	0.035	0.065	-	-	-	Al=0.056, N=0.008, Ce=0.017

TABLE 2. Mechanical Properties of Some of the Pipe Line Steels Studied (in transverse direction).

Heat	Yield Stress (MPa)	Tensile Strength (MPa)	% El in 50 mm
63843	470.9	675.0	33
C10113	574.3	772.2	39
B319	503.3	601.9	31
H471	415.1	530.9	42
98173	460.6	630.9	36
H473	423.3	581.9	30
88284	457.1	638.5	37
W3134	503.3	646.0	35
A210	493.0	581.2	36
59609	573.6	637.1	36
B259	448.2	507.5	42
492S1871	547.4	688.1	25
1376	419.9	574.3	35
IF5913	490.2	645.3	--
IF5914	417.8	564.0	--
IF6221	386.1	602.6	--
2F1665	404.0	626.0	--
N.K.K.	513.7	591.6	54
835	486.0	595.7	44
B229	416.4	583.3	33
B268	577.8	635.0	--

TABLE 3. Hydrogen Assisted Cracking Test Results with Slot-Specimen and Bead-on-plate Specimen After An Elapse Time of 24 hrs.

Heat	Carbon Equivalent[1]	Percent Cracking			
		HYP E7010	E6010 Welds		E7018 Welds
		Slot Test	Slot Test	Bead-on-plate	Slot Test
63843	0.467	50	80	80	Nil
C10113	0.461	25			Nil
B319	0.448	40	90	30	
H471	0.442	90			
98173	0.427	25	30	40	
H473	0.420	100			
88284	0.408	20	40	50	
W3134	0.408	2			
H228	0.397	15			
A210	0.378	10	15	20	
59609	0.281	Nil	Nil	Nil	
B259	0.272	Nil	Nil	Nil	Nil
Mobil	0.337	Nil			
A69-2	0.420	3			
A68-2[2]	0.450	0-60			
492S1871	0.487	80			Nil
496S2211	0.418	2			
496S1871	0.410	1			
490S2441	0.407	5			
492S2681	0.403	3			
490S2391	0.398	3			
493S2761	0.390	1			
493S2791	0.363	Nil			
Italsider(1)	0.346	Nil			
Italsider(2)	0.345	Nil			
1376	0.354	0-70			
IF5913	0.389	50			
IF5914	0.365	Nil			
IF6221	0.379	0-10			
2F1665	0.400	0-3			
N.K.K.	0.287	Nil			
835	0.357	0-10			
B229	0.382	30-35			
B268	0.335	15-20			

1. Carbon Equivalent = C + Mn/6 + Ni/20 + (Cr +Mo)/10 + Cu/40
2. Showed 0% cracking in plates with lamination and 60% cracking in sound plates.

TABLE 4. Combined Effect of Preheat and Time Lapse After Welding on the Extent of Cracking

Heat	Percent Cracking																				
	R.T. (20°C)					52°C	66°C					80°C					93°C				120°C
	24 hrs	20 mins	10 mins	5 mins	1 min	24 hrs	24 hrs	20 mins	10 mins	5 mins	1 min	24 hrs	20 mins	10 mins	5 mins	1 min	24 hrs	20 mins	10 mins	5 mins	1 min	24 hrs
63843	50	50	40	40	10	50	40	1-30	15-20	5-6	1-2	35	1-25	2-3	1-2	Nil	30	~10				1.0
C10113	25	5		3			20	Nil														
B319	40	35-40	30	15	3-5	30-40	15	1.0	1.0			~1.0					~1.0					Nil
H471	90	50	30	2-4	Nil																	
98173	25	15	5-10	5-10	2-3	5	5	3-5	2-3	2-3		3-5	Nil	Nil			1.0	Nil				Nil
H473	100	20	5	1	Nil																	
88284	20	20	20	10	2	~ 13	10	2	2-3	2-3	Nil	~5	~5	~3	Nil		3-5	0-2	Nil			Nil
W3134	2	Nil				Nil	Nil															
H228	15	Nil	Trace	Trace	Nil	Nil	Nil															
A210	10	1	1	1	Nil	1-2	Nil															
A69-2	3	Nil				Nil	Nil															
A68-2	60	1																				
492S1871	80	50	50	40	10	70	45	4-6	4-6	3-5	1-2	45	0-1	1-2	~1	~1	3-40	1-3	1-2	~1		~1
496S2211	2					Nil																
496S1871	1					<1.0																
490S2441	4-5					1-2																
492S2681	3					~1.0																
490S2391	2-3					2-5																
493S2761	1					Nil																
1376	0-70	1-2		Nil			Nil															
IF5913	50	40-50		5-10			0-40	Nil				Nil										
IF6221	0-10	5					0-1															
2F1665	0-3																					
835	0-10	Nil					Nil															

TABLE 5. Locus of Crack Growth and Hardness of HAZ in Some of the Steels Studied

Heat No.	Coarse grain HAZ hardness (1 kg load DPH)	Locus of Crack
492S1871	360	HAZ[1] - FL[2] - WM[3]
C10113	340	Mostly in HAZ
63843	350	HAZ - mostly FL
H471	330	HAZ - and mostly in WM
H473	380	HAZ - and mostly in WM
B319	344	WM - FL - HAZ - FL
88284	320	HAZ - FL - WM
A68-2	312	WM - and mostly in HAZ
A210	315	Mostly in HAZ - FL
IF5913	363	HAZ - WM
IF5914	288	No cracking
IF6221	328	HAZ - WM
2F1665	312	All in HAZ
NKK	273	No cracking
B229	316	WM - mostly in HAZ - finally in FL
B268	295	WM - mostly in HAZ
835	245	Mostly in WM or no cracking

1. HAZ - heat affected zone
2. FL - fusion line
3. WM - weld metal

Table 6. Modifications of the Slot Weld Test and Its Effect on the Extent of Cracking.

Specimen tested: Heat IF 5913. Lapse time - 24 hrs.

	Percent Cracking in break open test	Crack extent and locus in Metallographic Section	
1.	50	45%-30% HAZ, 15% W.M.	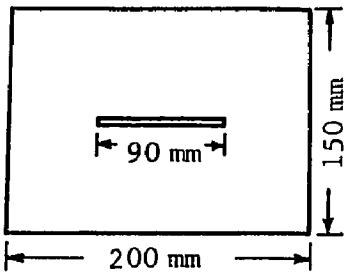
	Aside Hardness in coarse grain HAZ is about 363 H_V and in the weld metal it is 260 H_V.		
2.	Traces	Nil	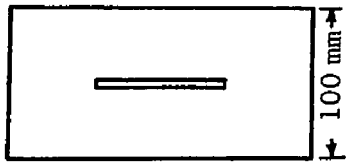
	Aside Hardness in coarse grain HAZ is about 360 H_V and in W.M. it is about 260 H_V.		
3.	30	40%-15% HAZ, 25% W.M.	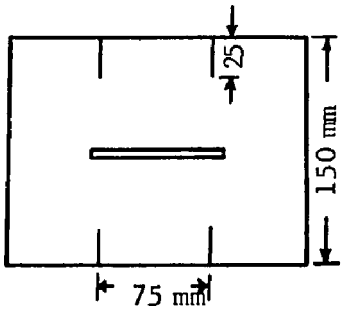
4.	~ 10	15%-10% HAZ, 5% W.M.	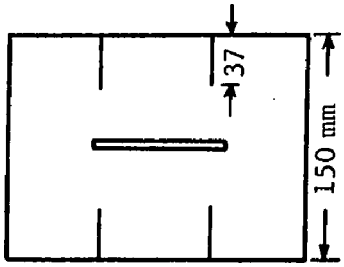

Table 7

Results of Metallographic Examination
of Shop Welded Pipes

Heat No. 492S1871

Welding Condition	Frequency of Crack per 12 Sections Examined	
1. No preheat. No hot pass	6	(50%)
2. No preheat. Hot pass deposited 20 minutes after the root pass	4	(33%)
3. No preheat. Hot pass deposited 5 minutes after the root pass.	1	(8%)
4. Preheat 66°C. No hot pass	3	(25%)
5. Preheat 66°C. Hot pass deposited 20 minutes after root pass.	Nil	--
6. Preheat 66°C. Hot pass deposited 10 minutes after root pass.	Nil	--

TABLE 8. Effect of Slot Width and Lapse Time on the Extent of Cracking

Heat	machined slot gap = 2.4 mm		fabricated slot gap < 1.6 mm		fabricated slot gap = 1.6 mm		fabricated slot gap = 2.4 mm	
	10 mins.	24 hrs.	10 mins.	24 hrs.	10 mins.	24 hrs.	10 mins.	24 hrs.
492S1871	50%	80%	70%	83%	70%	70%	5%	40%
B319	30%	40%	30%	50%			insufficient material	
88284	20%	20%	78%	95%			15%	25%
490S2441	2-3%	4-5%	18%	33%			1%	5-8%

TABLE 9. Effect of Plate Size on Extent of Cracking for Heat 492S1871
Plate Size = 200 mm x 125 mm

Test Condition	Cracking Percent (24 hrs.)
Machine Slot (2.4 mm gap)	15-20%
Fabricated Slot (1.6 mm gap)	80%
Fabricated Slot (2.4 mm gap)	About 20%

TABLE 10 Extent of Cracking in Slot Weld Test and Carbon Equivalence

Heat No.	Wall Thickness mm	% Crack 24 hrs.	Restraint Factor(A)	$CE_{(New)}$	CSF(1)	$CE_{(IB)}$	$CE_{(IIW)}$	P_{cm}	CSF(2)	CSF(3)
63843	14.3	50	1.55	0.630	0.977	0.315	0.467	0.839	0.784	0.347
B319	15.7	40	1.72	0.616	1.060	0.309	0.448	0.836	0.808	0.444
98173	14.3	25	1.55	0.578	1.900	0.276	0.427	0.801	0.720	0.318
88284	19.0	20	2.15	0.568	1.221	0.270	0.408	0.802	0.832	0.653
492S1871	14.6	80	1.60	0.656	1.050	0.335	0.487	0.860	0.830	0.394
C10113	18.3	20	2.04	0.346	0.706	0.205	0.522	0.736	0.494	0.359
H471	15.7	90	1.72	0.619	1.065	0.314	0.442	0.841	0.812	0.446
H473	25.4	100	3.15	0.568	1.789	0.245	0.436	0.787	1.008	1.221
W3134	10.3	2	1.15	0.492	0.566	0.232	0.431	0.750	0.528	0.074
H228	11.4	15	1.25	0.530	0.663	0.250	0.397	0.769	0.593	0.133
A210	15.7	10	1.72	0.518	0.891	0.239	0.375	0.766	0.680	0.373
59609	9.5	0	1.10	0.274	0.301	0.195	0.436	0.711	0.288	0.027
B259	15.7	0	1.72	0.350	0.602	0.145	0.272	0.672	0.460	0.252
Mobil	6.4	0	1.00	0.522	0.522	0.242	0.339	0.752	0.522	negligible
A69-2	11.4	3	1.25	0.558	0.700	0.262	0.420	0.781	0.624	0.140
A68-2	11.4	60	1.25	0.600	0.750	0.292	0.450	0.811	0.671	0.150
496S2211	14.6	2	1.60	0.570	0.912	0.272	0.430	0.801	0.721	0.342
496S1871	14.6	1	1.60	0.573	0.917	0.275	0.419	0.801	0.725	0.344
490S2441	14.6	4-5	1.60	0.553	0.885	0.260	0.416	0.785	0.701	0.332
492S2681	14.6	8	1.60	0.552	0.883	0.259	0.412	0.784	0.708	0.331
490S2391	14.6	2-3	1.60	0.540	0.864	0.251	0.408	0.776	0.683	0.324
493S2761	14.6	1	1.60	0.535	0.856	0.249	0.399	0.772	0.677	0.321
493S2791	14.6	0	1.60	0.521	0.834	0.240	0.371	0.764	0.660	0.313
1F5913	19.0	50	2.15	0.472	1.015	0.224	0.431	0.756	0.692	0.543
1F5914	19.0	0	2.15	0.366	0.787	0.181	0.404	0.713	0.537	0.421
1F6221	20.3	0-10	2.32	0.408	0.947	0.199	0.437	0.733	0.621	0.539
2F1665	20.3	5	2.32	0.381	0.884	0.201	0.495	0.744	0.580	0.503
N.K.K.	25.4	0	3.15	0.270	0.850	0.153	0.343	0.700	0.480	0.581

$$CE_{(New)} = C^{\frac{1}{4}}\left(1+\frac{Mn+Cr+Mo+V}{5}+\frac{Ni+Cu+Si}{25}\right)$$

$$CE_{(IB)} = C+\frac{Mn}{20}+\frac{Si}{30}+\frac{Cu}{20}+\frac{Ni}{60}+\frac{Cr}{20}+\frac{Mo}{15}+\frac{V}{10}+5B \quad \text{- Ito and Bessyo}$$

$$P_{cm} = CE_{(IB)}+\frac{H}{60}+\frac{t}{600}$$

$$CSF(1) = CE_{(New)}\,(A)\,(H/30)$$

$$CSF(2) = CE_{(New)}\,(A)^{\frac{1}{2}}\,(H/30)$$

$$CSF(3) = CE_{(New)}\,(A-1)\,(H/30)$$

where H = diffusible hydrogen - assumed to be 30 ppm for E7010 electrode

and t = plate thickness in mm.

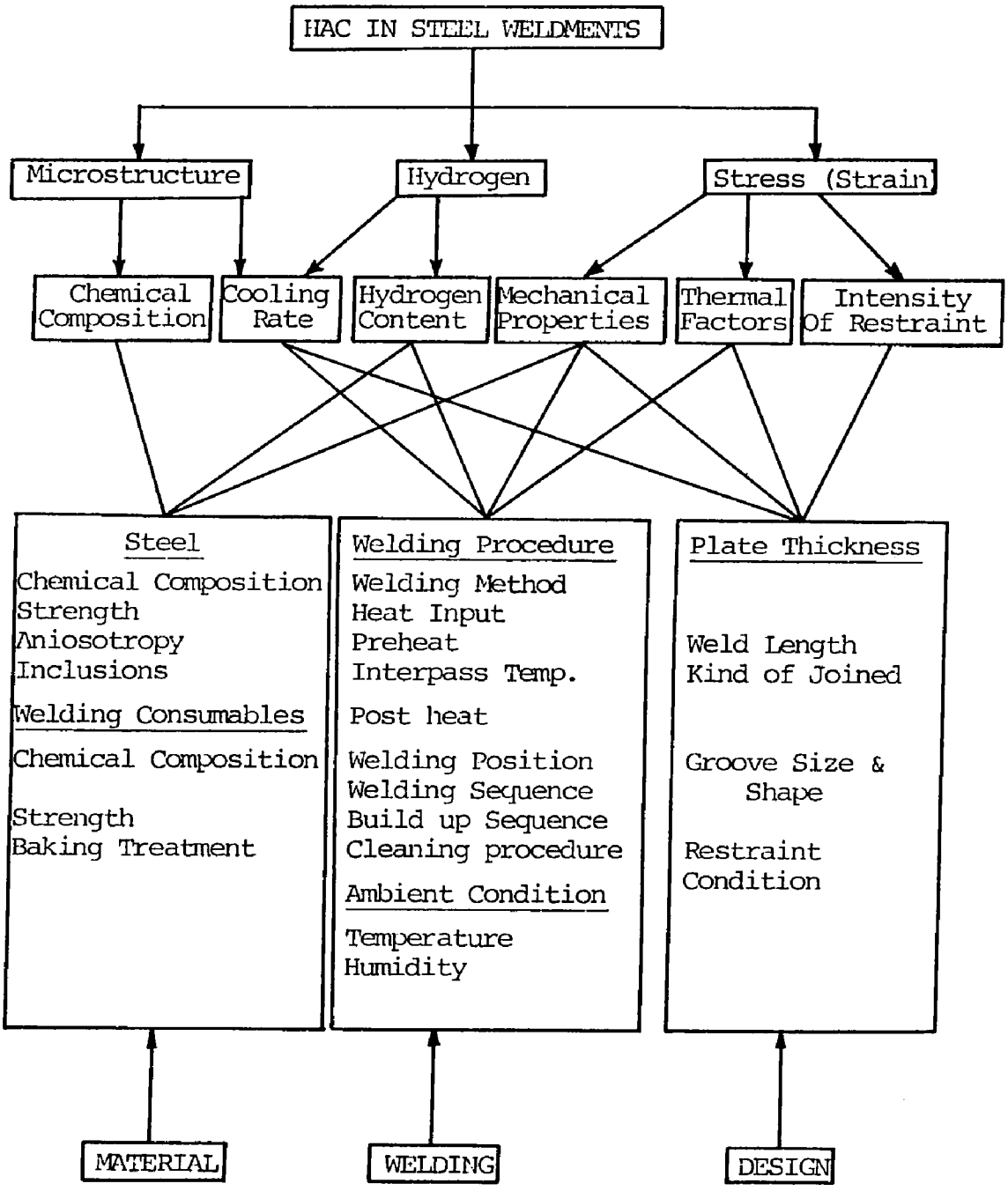

Fig. 1 Various Factors Contributing to Hydrogen Assisted Cracking in Steel Weldments

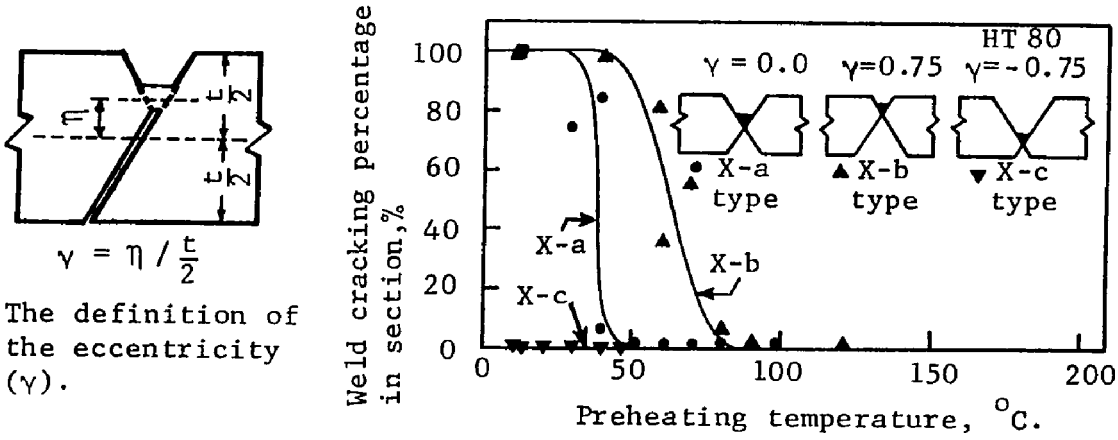

Fig. 2. Relation Between Weld Cracking Percentage and Preheating Temperature for Steel HT 80 for Various Eccentricities of Weld Bead (Ref. 65).

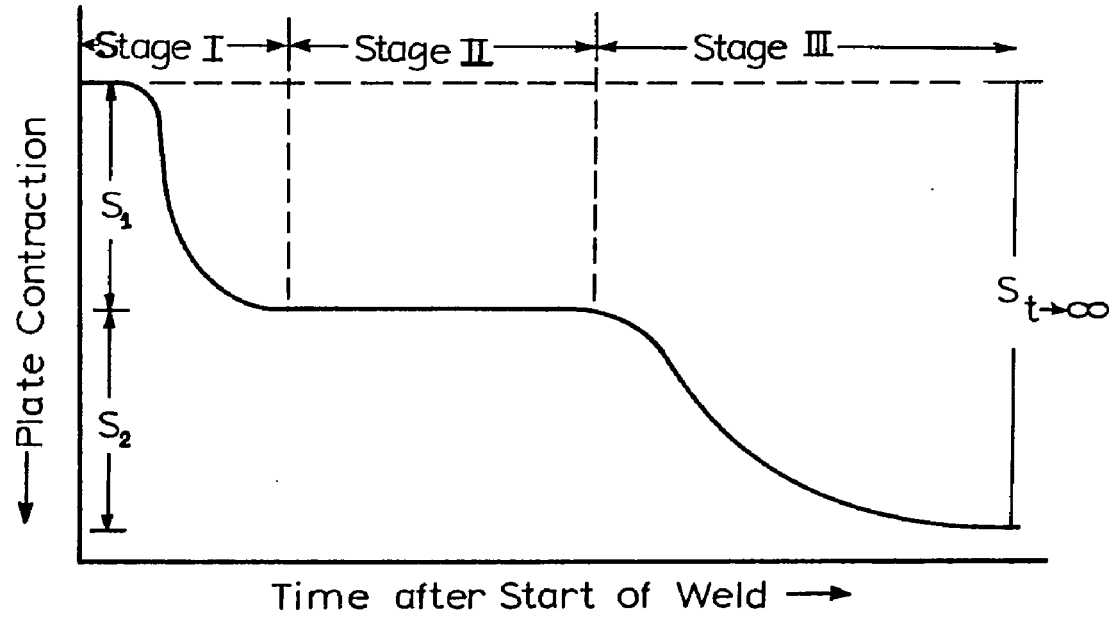

Fig.3 Typical Contraction Curve of a Butt Weld Joint During Cooling (70).

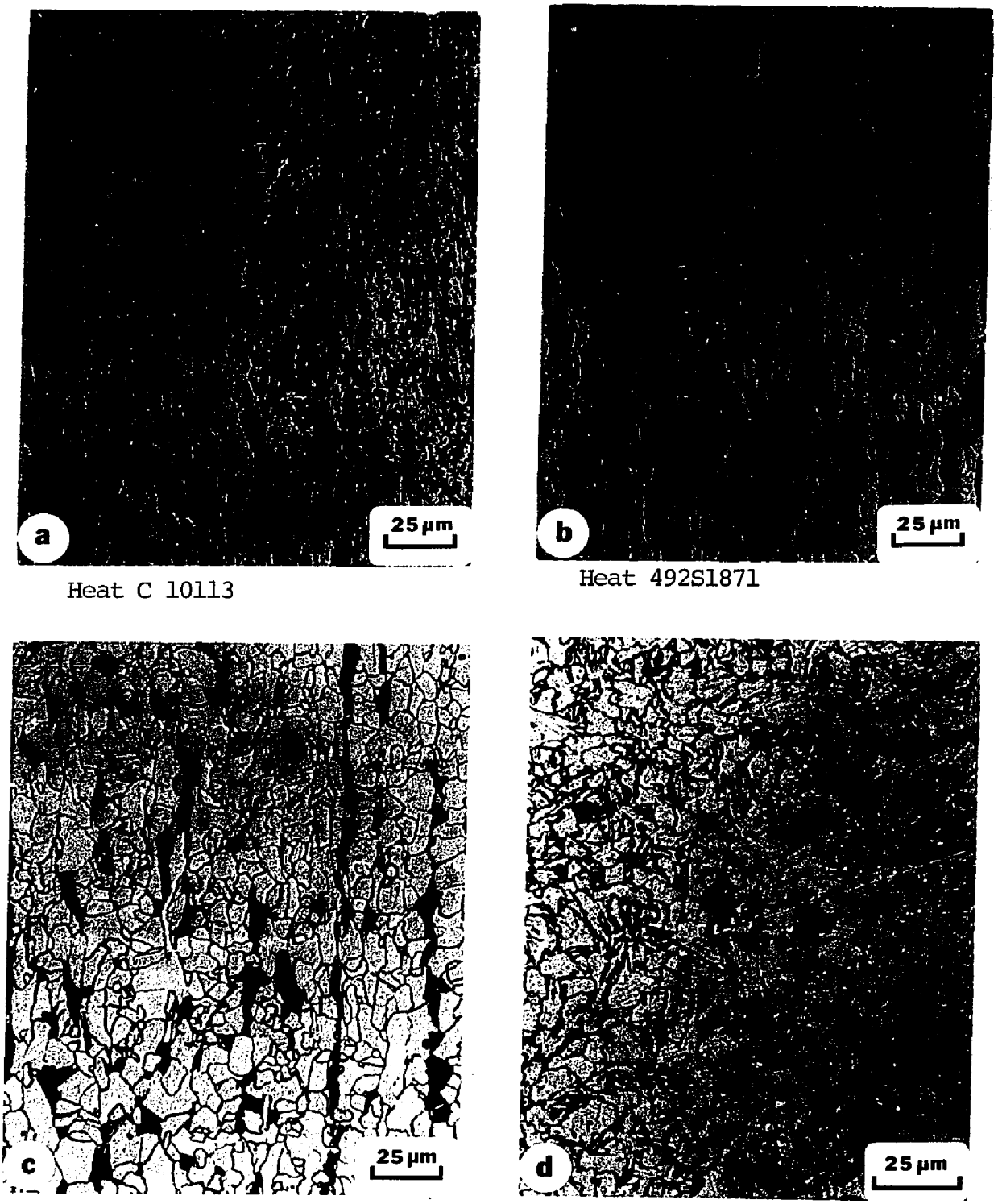

Heat C 10113

Heat 492S1871

Heat B 259

Heat NKK

Fig. 4. Representative base metal microstructures. Nital etch

Heat 63843

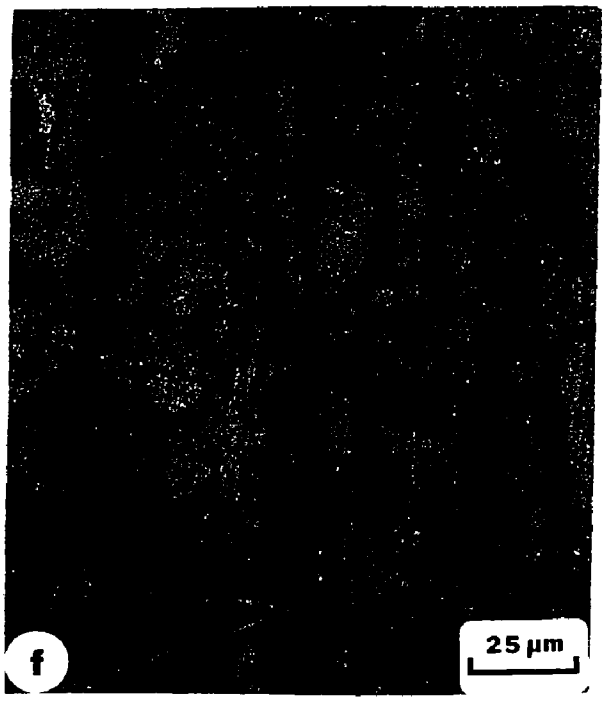

Heat IF 5913

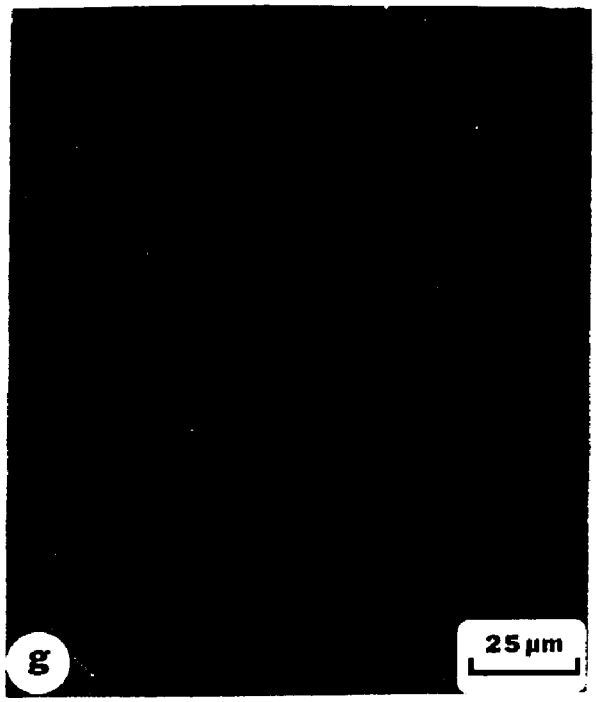

Heat 835

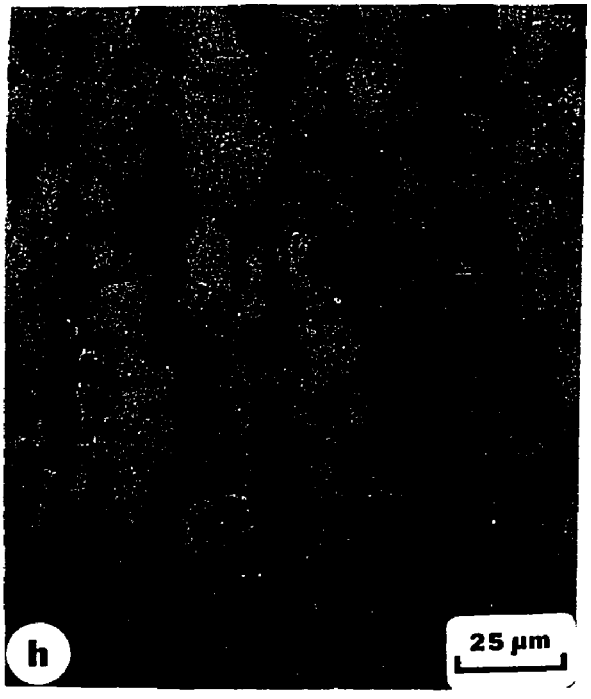

Heat B 229

Fig. 4. (cont.) Representative base metal microstructures. Nital etch

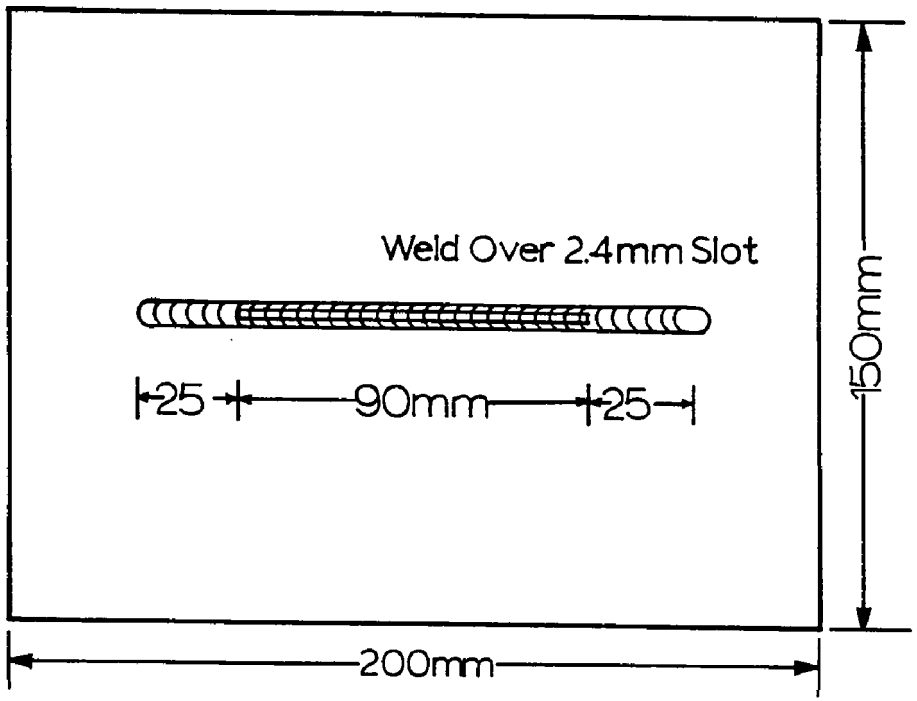

Fig.5 Slot Weld Test Specimen Design

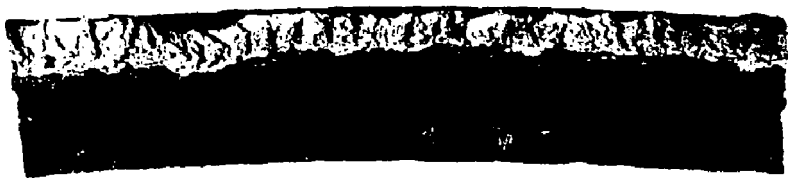

Fig. 6 Fracture surface of Heat 63843. Extent of cracking shown by darkened fracture surface.

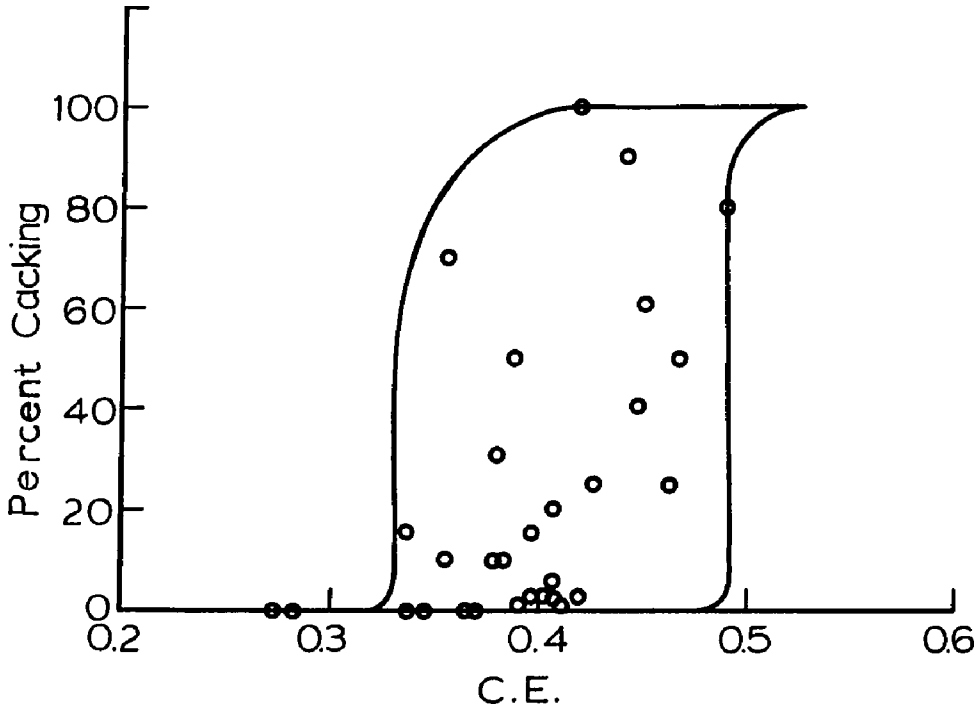

Fig. 7 Relation between Carbon Equivalent and the Extent of Hydrogen Induced Cracking.
C.E.=C+Mn/6+Ni/20+(Cr+Mo)/10+Cu/40

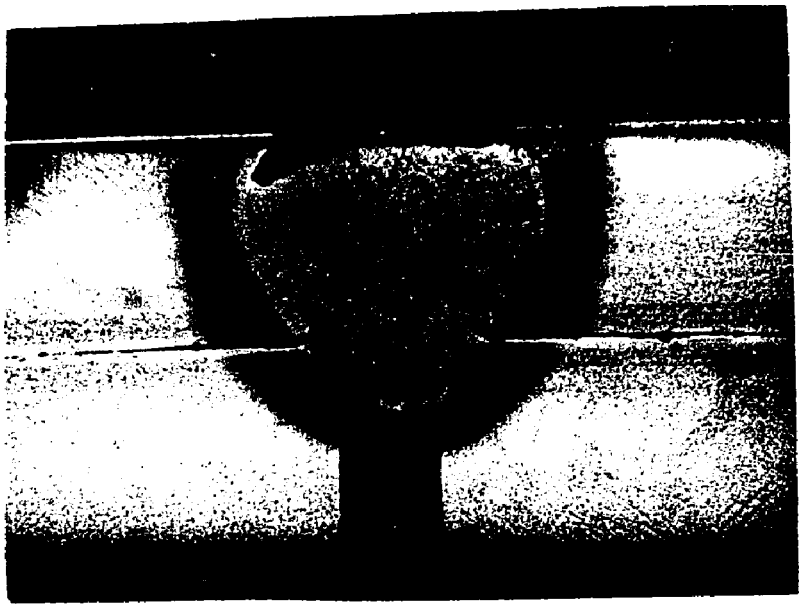

Laminated

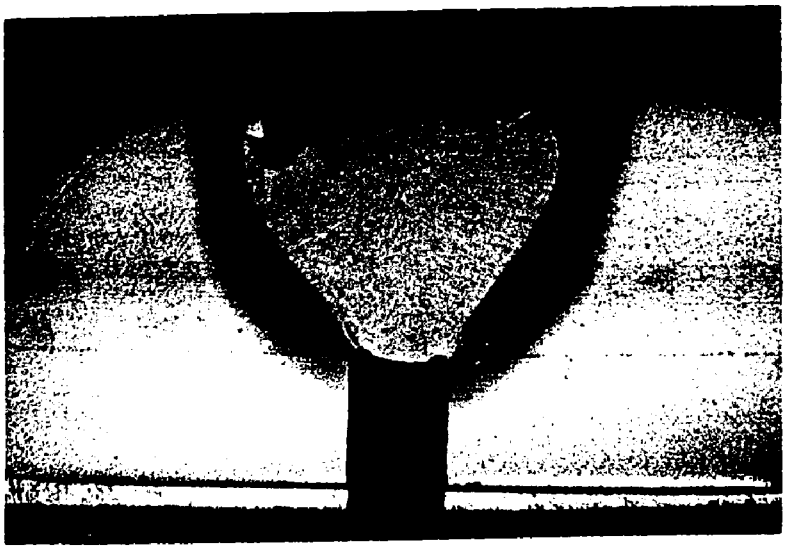

Not Laminated

Fig. 8. Cross sections of the welded Heat A68-2 showing the elimination of hydrogen cracking in the laminated region of the pipe. Nital etch

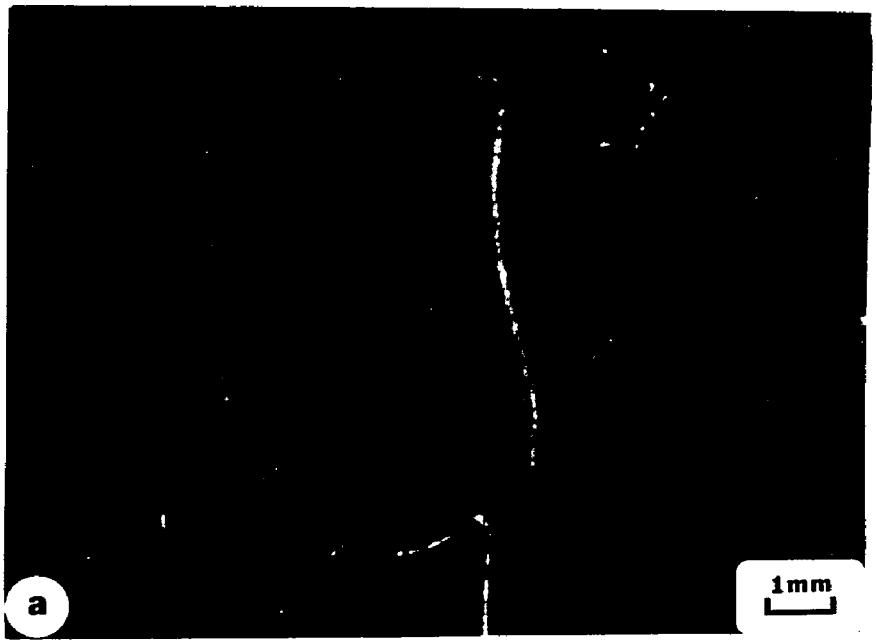

Locus of crack in heat Nos. H471 and 473. Nital etch

Heat No. 63863. Nital etch

Fig. 9. Transverse sections showing the locus of crack initiation and growth in different steels.

Fig. 9. (cont.) Heat B 319 Nital etch

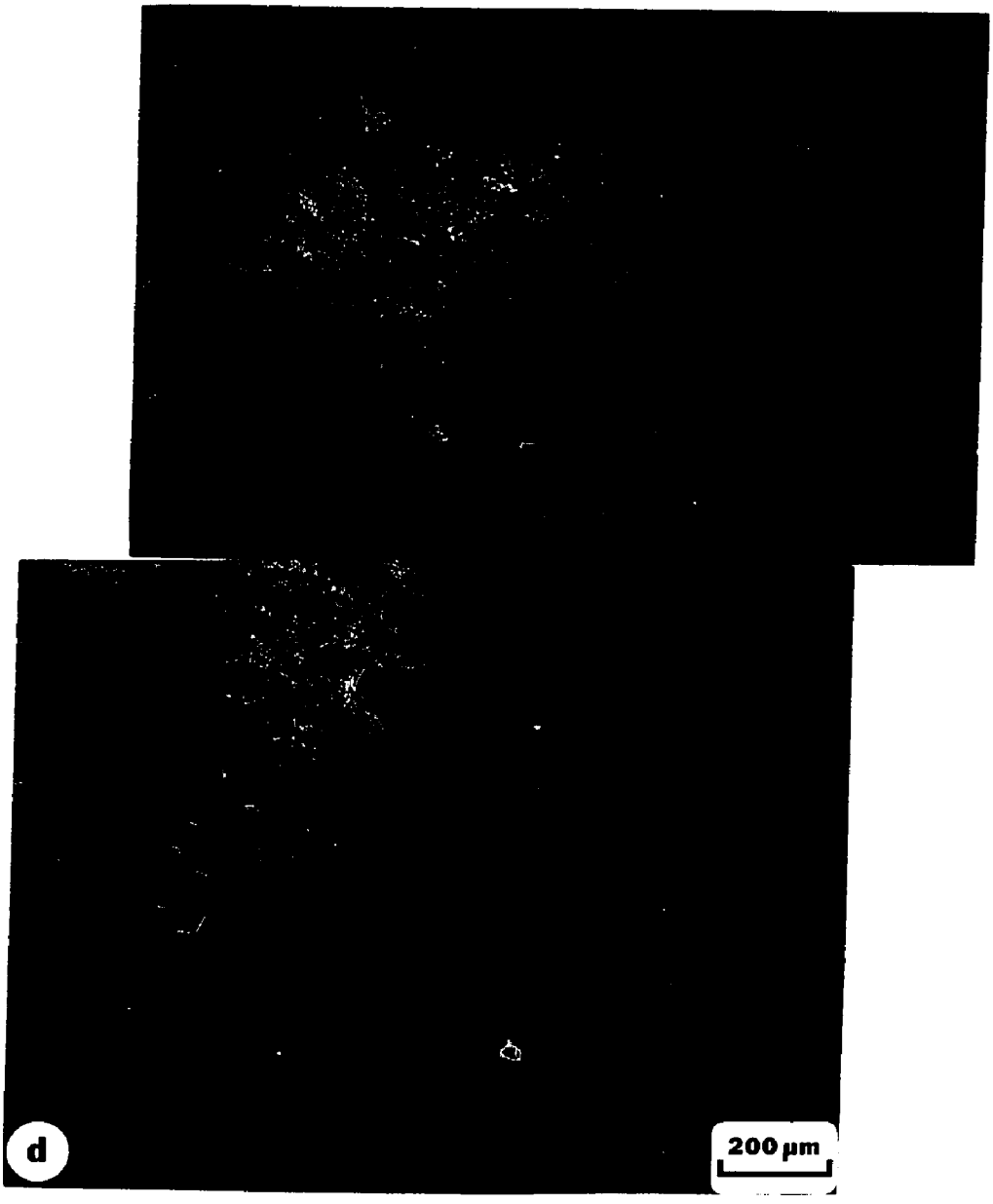

Fig. 9 Heat 88284 and 492S1871. Nital etch

Fig. 9. (cont.) Heat A68-2 and C 10113. Nital etch

Fig. 9. (cont.) Heat A210 Nital etch

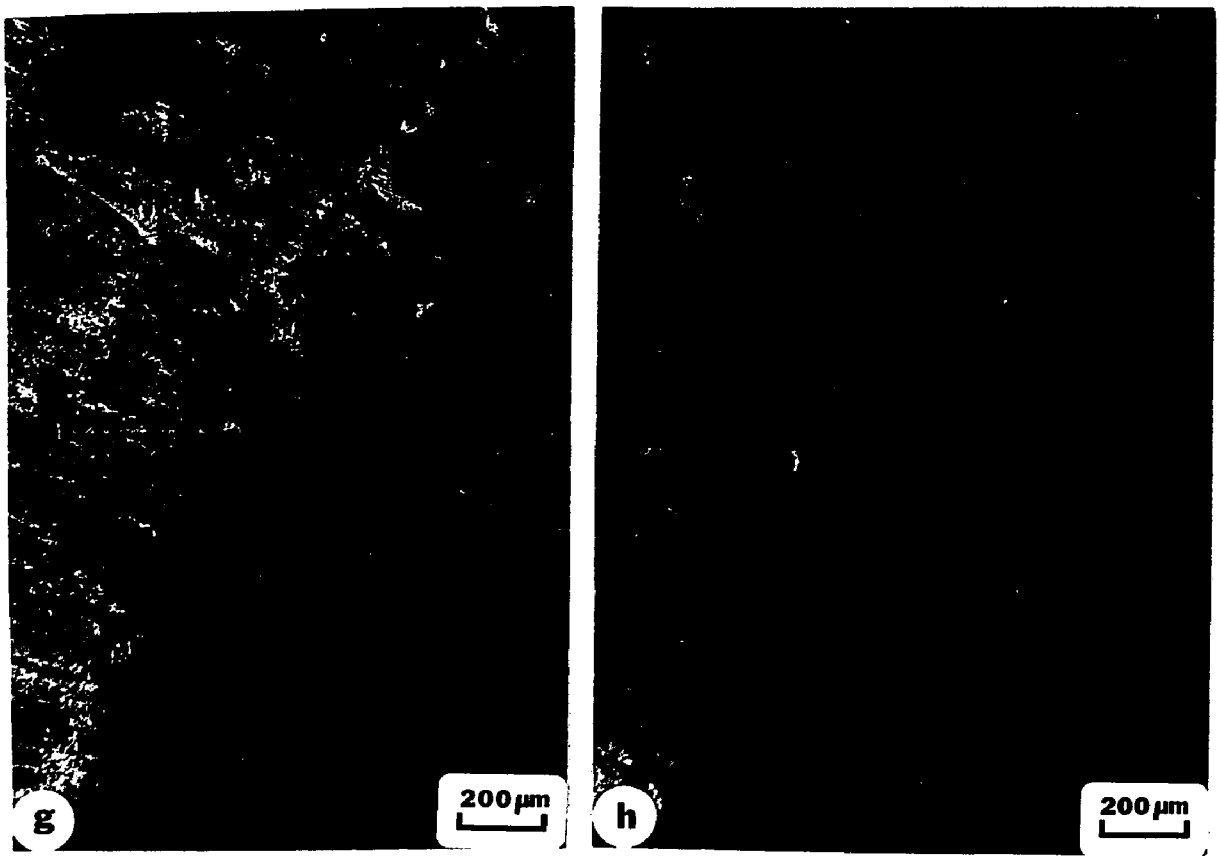

Heat IF 5913 Heat B 229

Fig. 9. (cont.) Cracking paths produced at the weld root in the Lehigh Slot Test

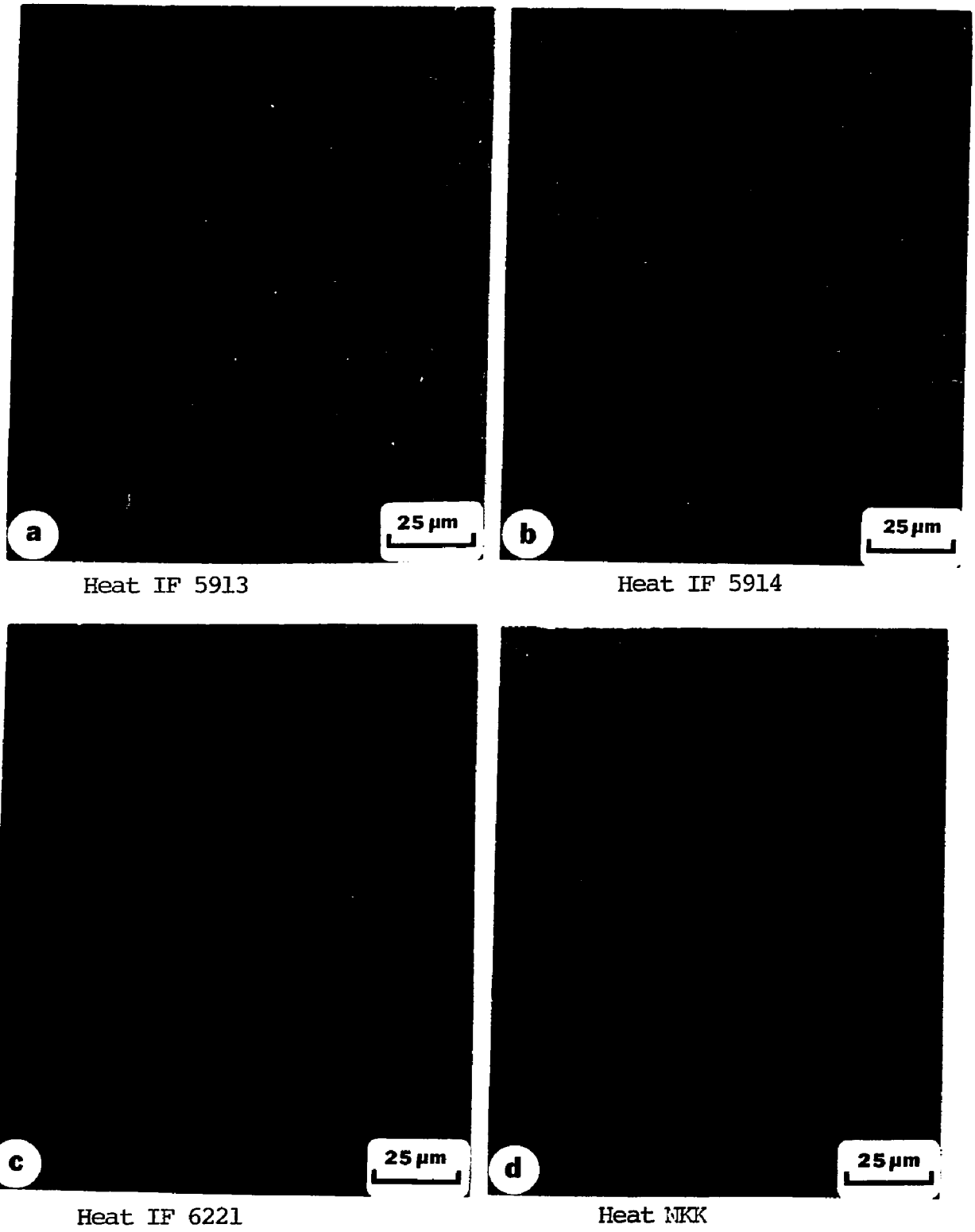

Heat IF 5913 Heat IF 5914

Heat IF 6221 Heat NKK

Fig. 10. Microcracks observed in weld metal of root passes in the slot test. Nital etch

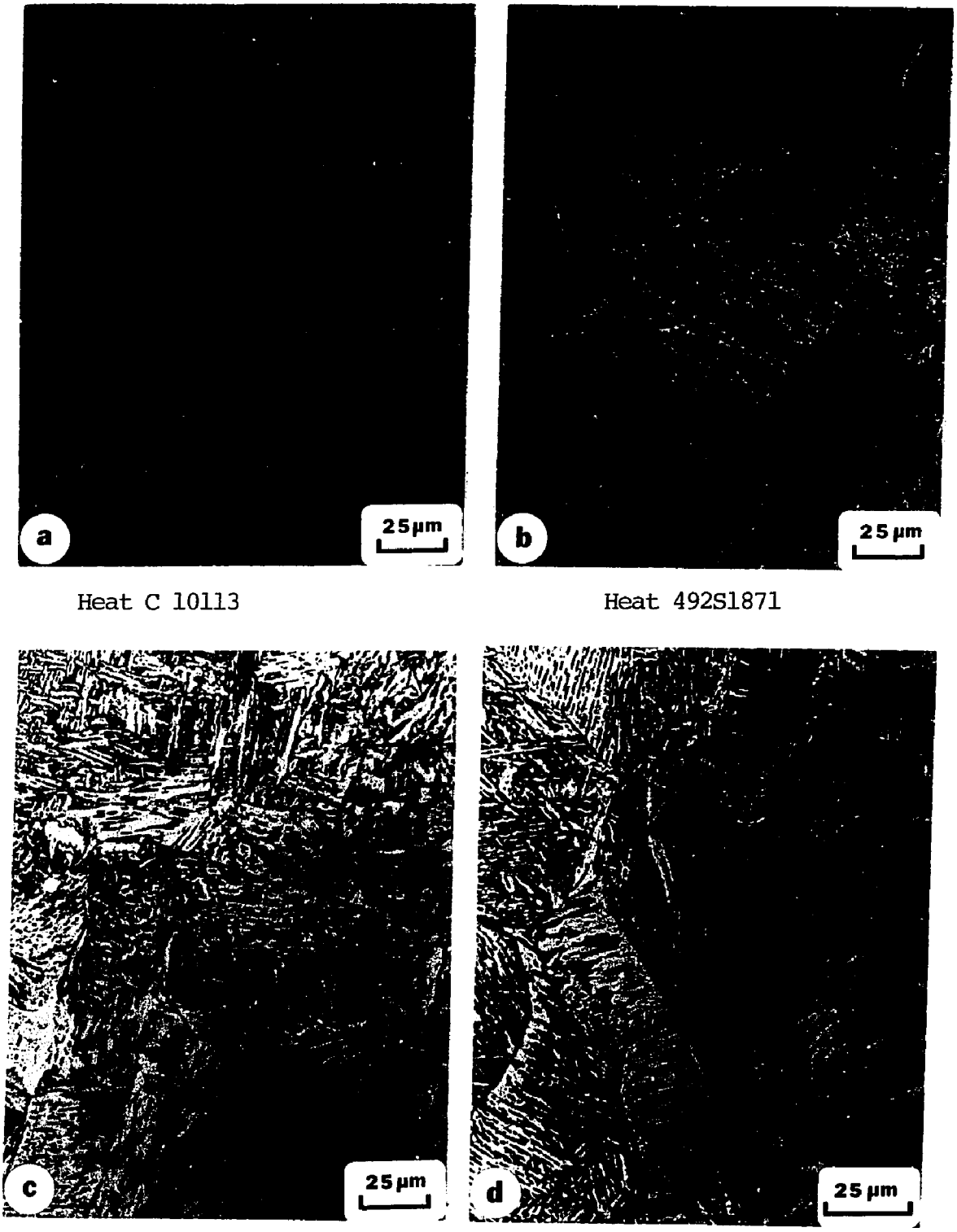

Heat C 10113 Heat 492S1871

Heat B 259 Heat NKK

Fig. 11. Representative microstructures of coarse grain heat-affected zones of root passes in slot wled test Nital etch

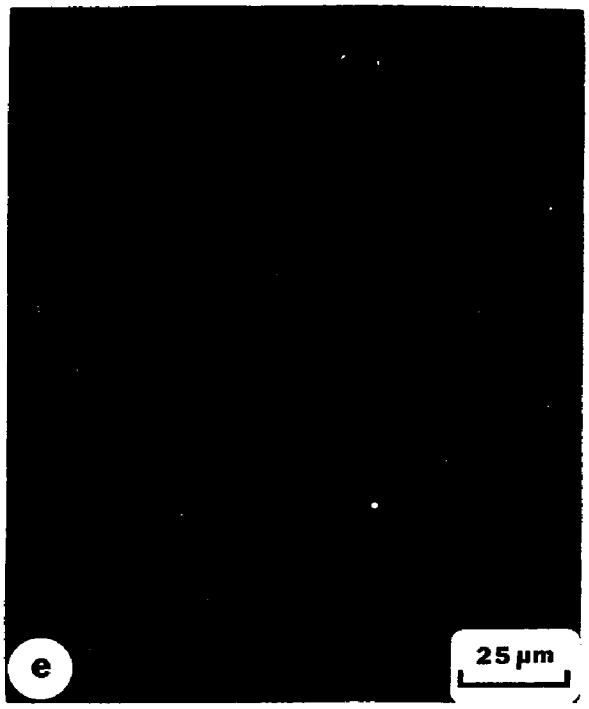

Heat IF 5913

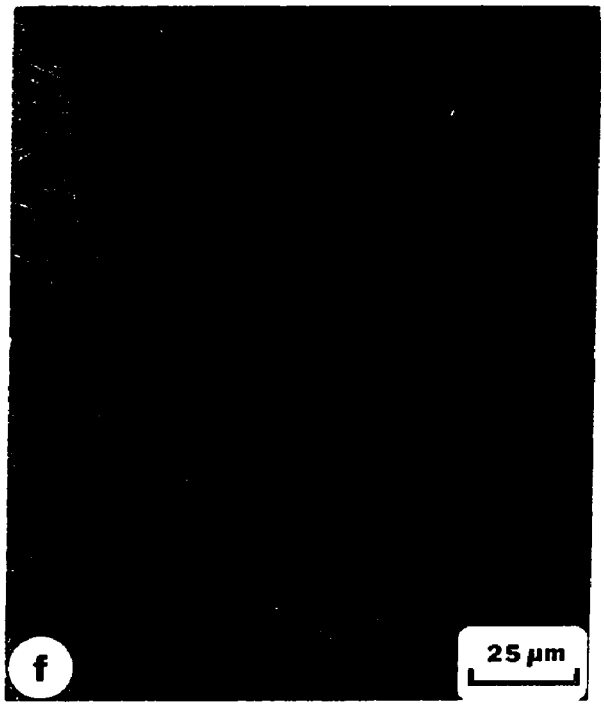

Heat IF 5914

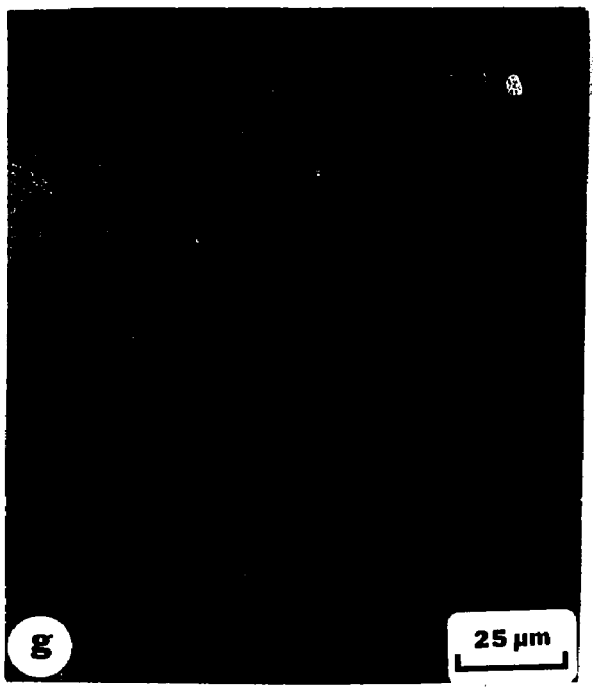

Heat B 229

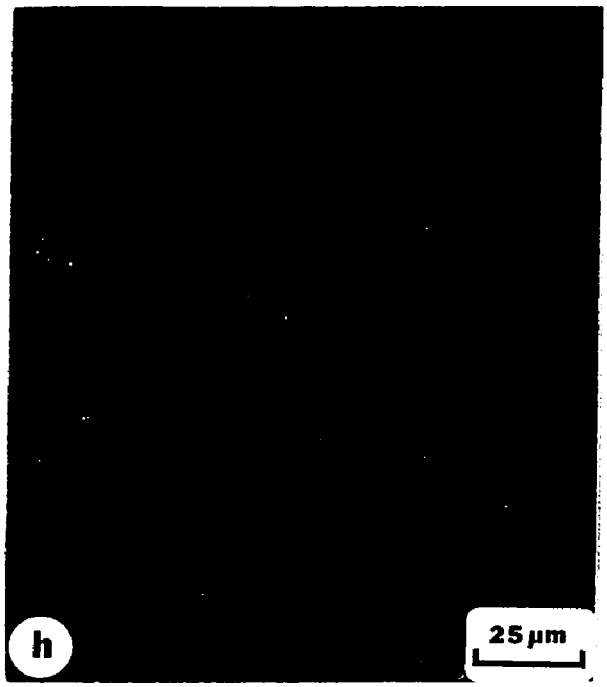

Heat 835

Fig. 11. (cont.) Microstructures of heat-affected zones of root passes Nital etch

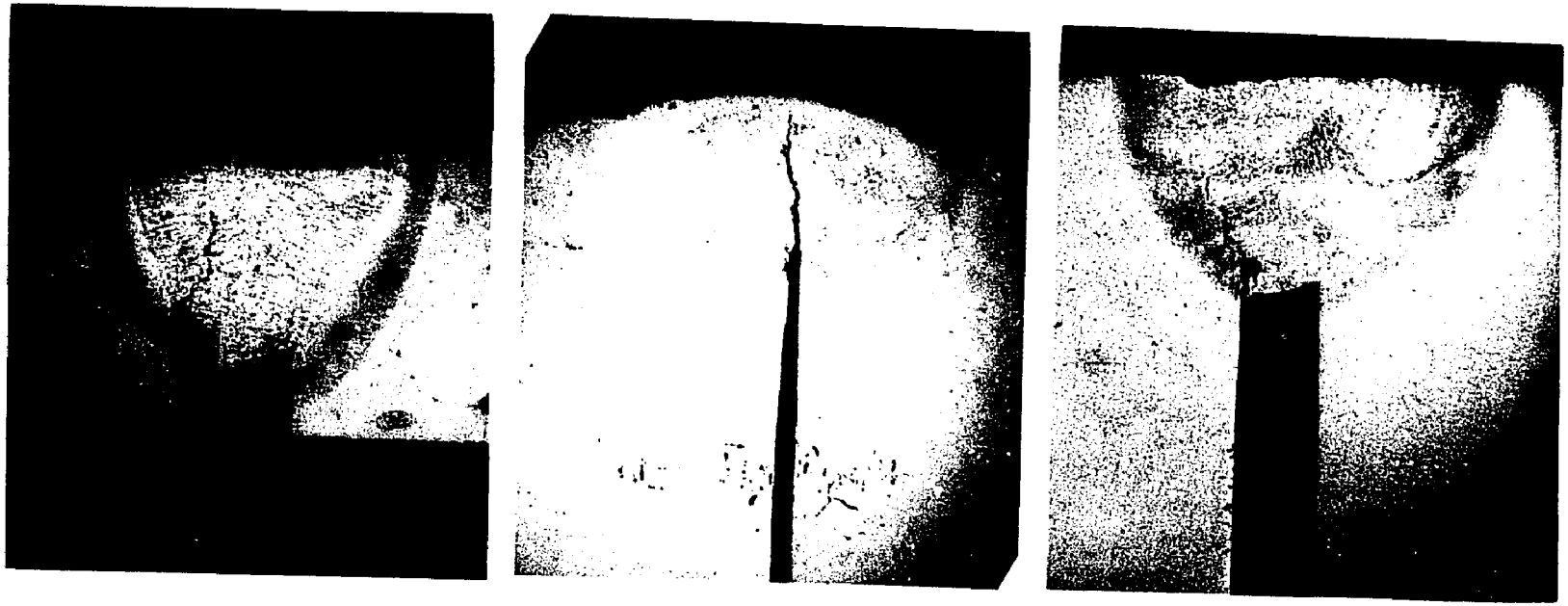

Fig. 12 Effect of slot width on crack locus

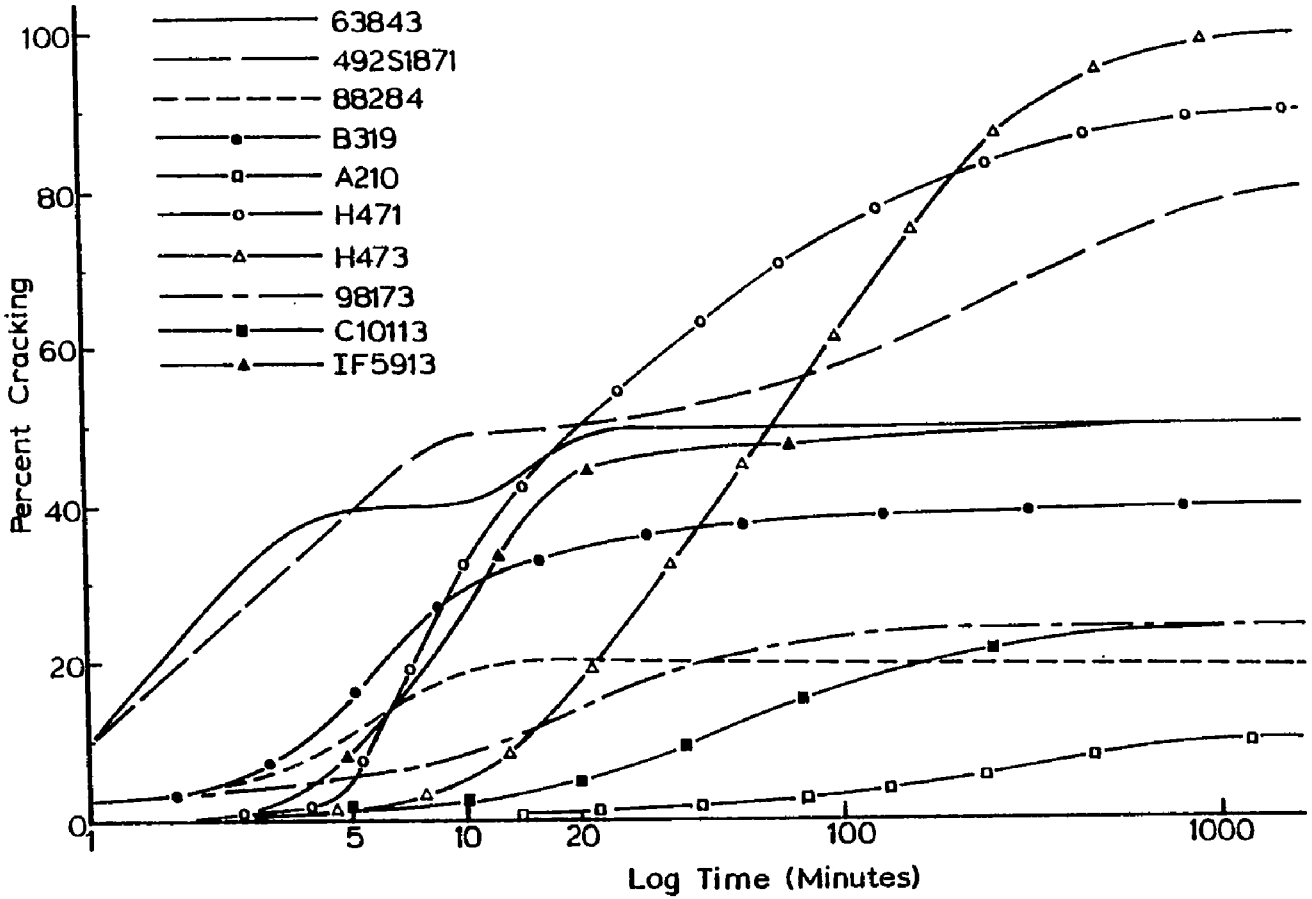

Fig.13 Plot of Percentage Cracking vs. Log Time Indicating Effect of Time Elapse After Welding on Percent Crack. (No Preheat)

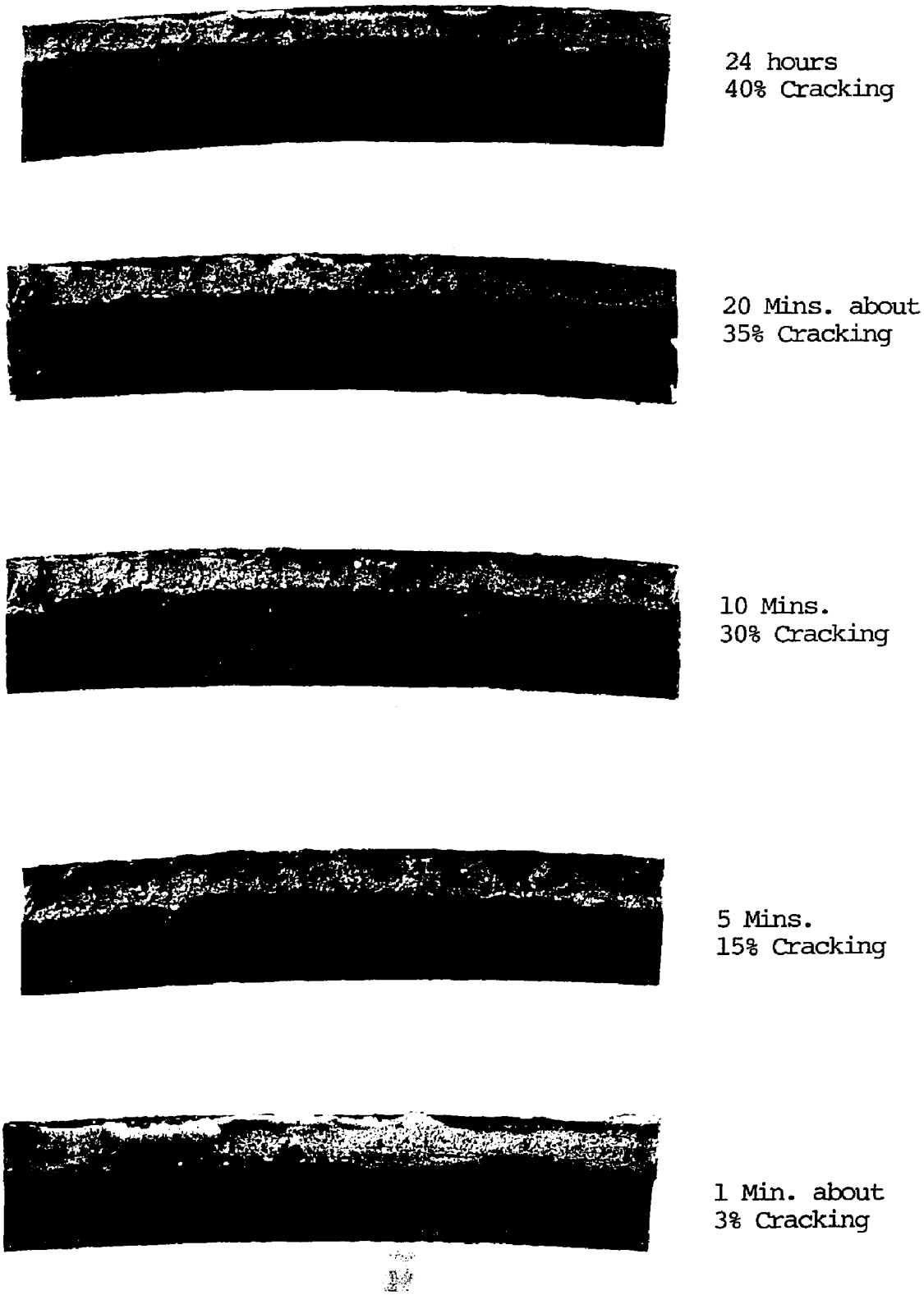

Fig. 14. Fracture surfaces showing the effect of time lapse in the extent of cracking in Heat No. B319.

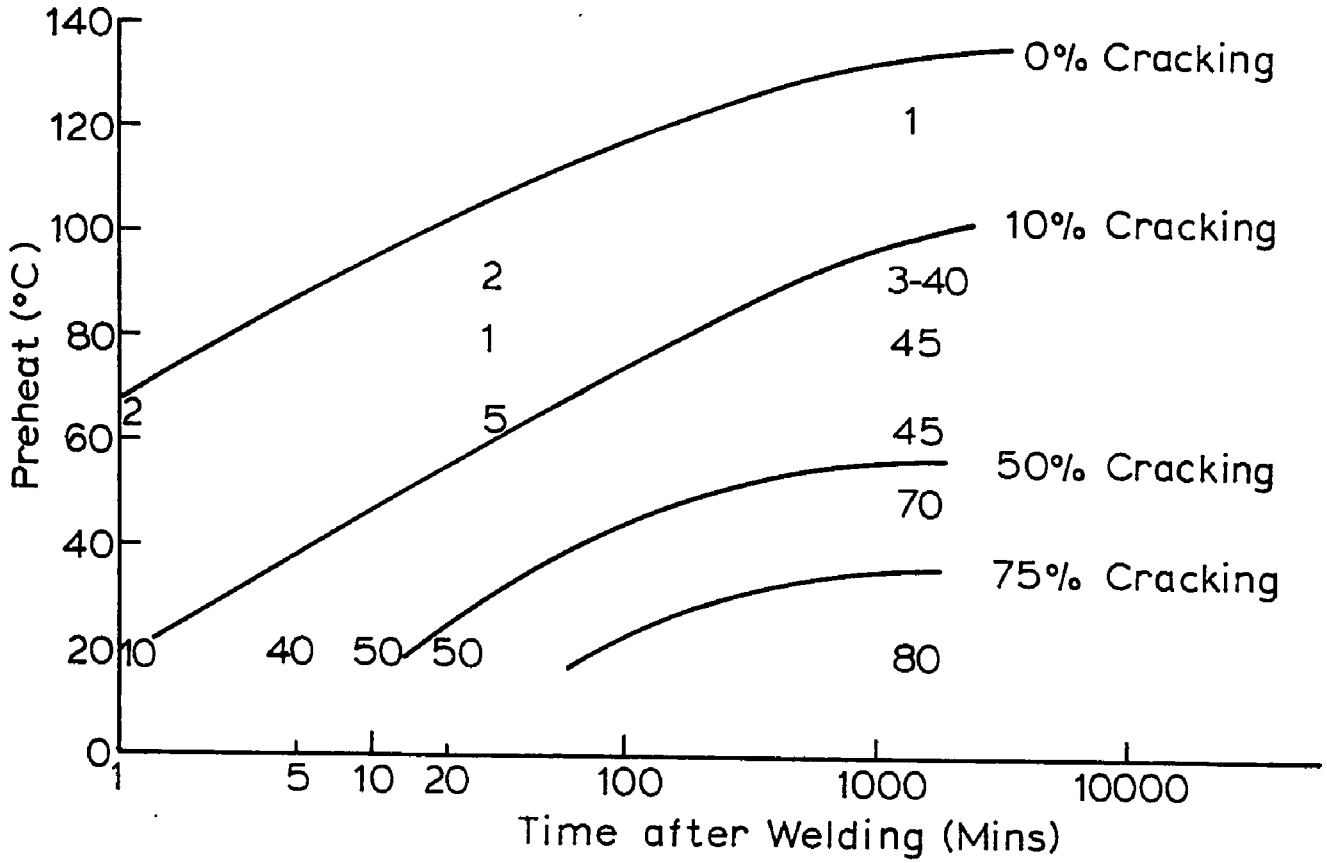

Fig.15 Isocracking Curves for Heat492S1871.

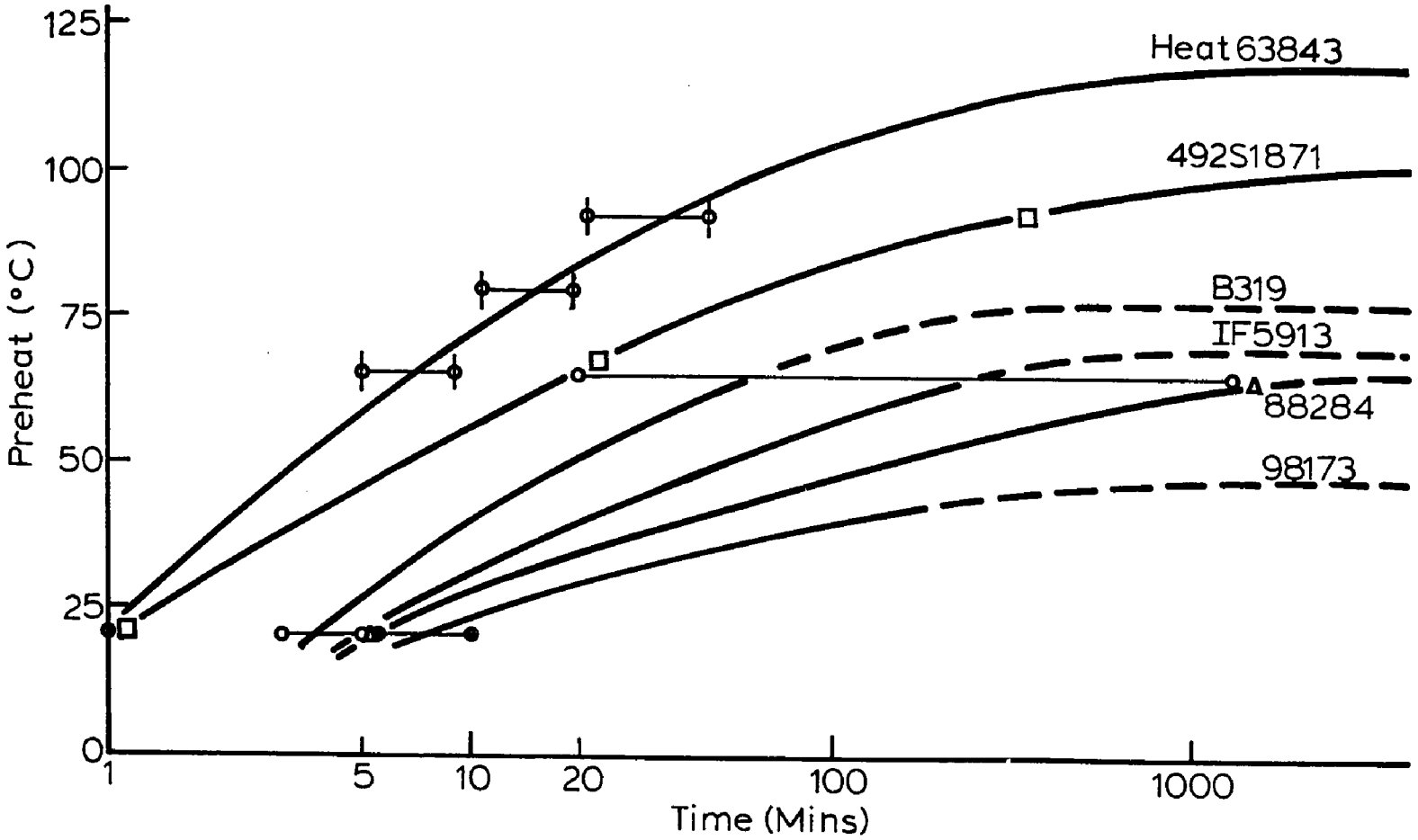

Fig.16 Effect of Preheat on the Time Interval after Welding for 10% Cracking.

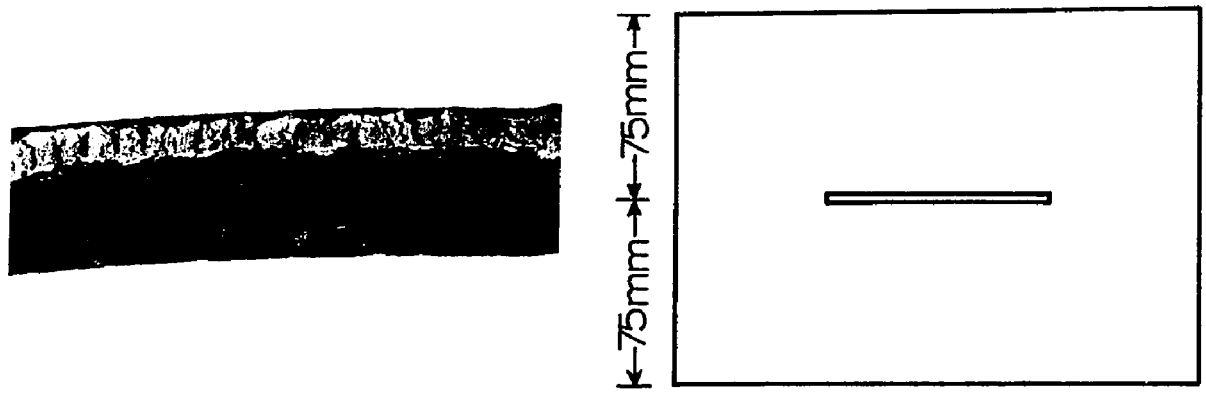

50% Cracking

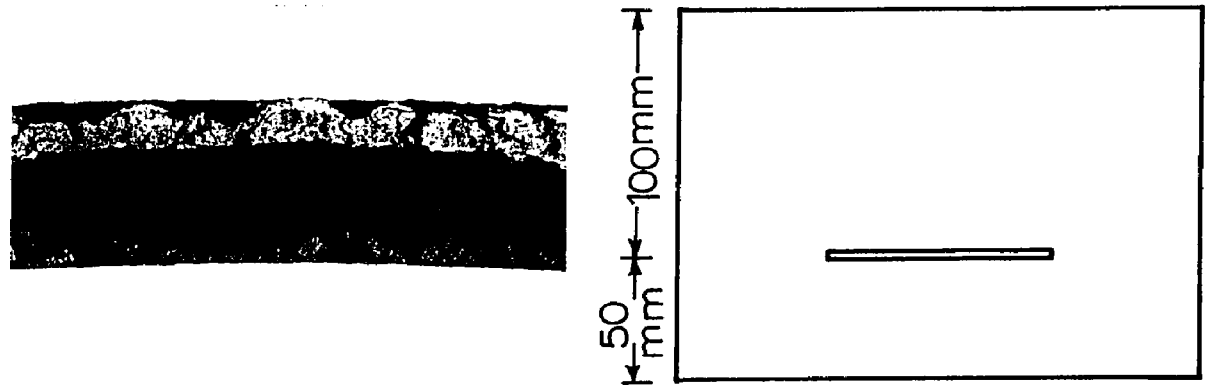

30% Cracking

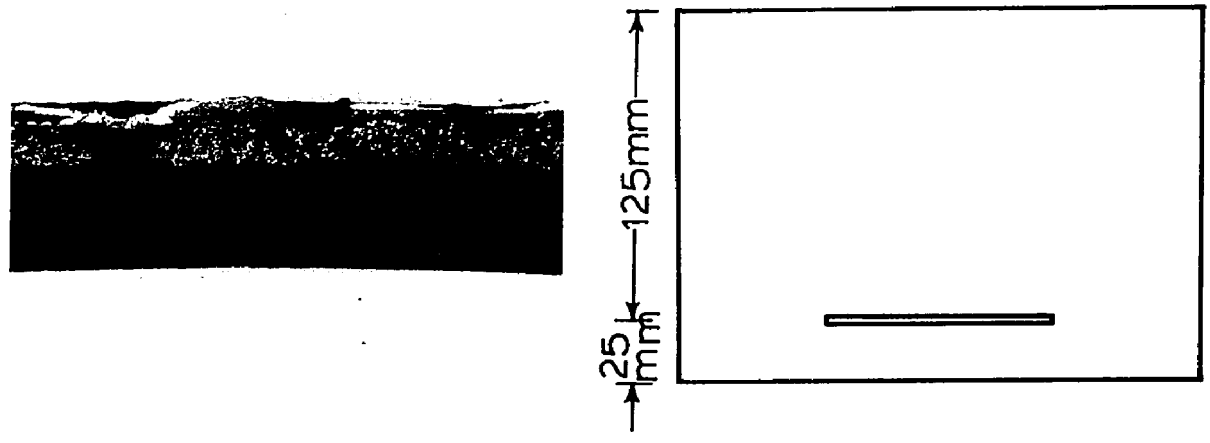

No Cracking

Fig. 17. Variation of restraint in the slot specimen by moving the slot toward one side and its effect on hydrogen cracking in Heat 63843.

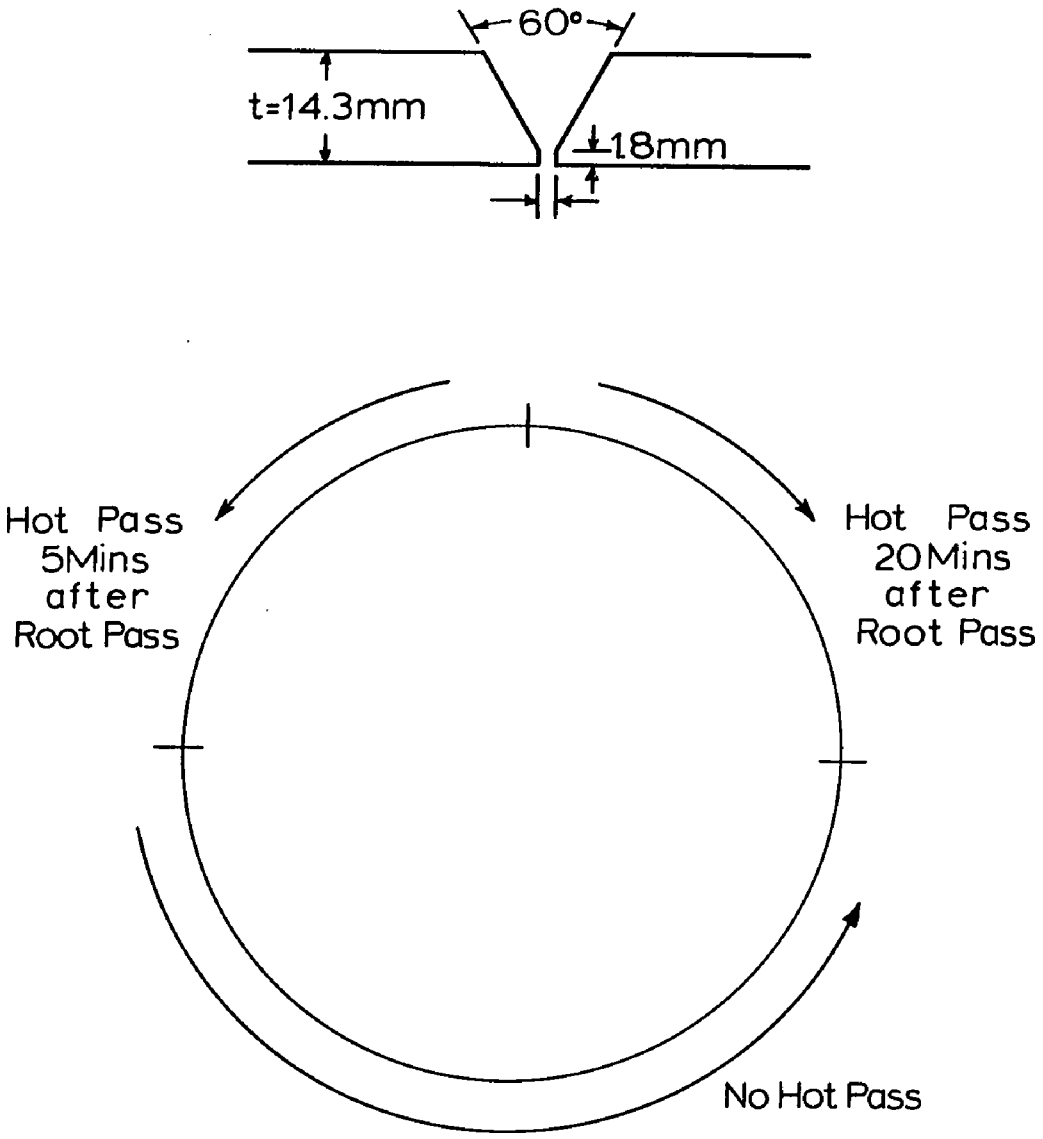

Pipe 1 — No Preheat

Pipe 2 — 66°C Preheat

Fig.18 Weld Joint Design and Procedure for Shop Girth Welded Pipes on Heat 492S1871.

No preheat. Infinite time interval after welding. No hot pass. Etch - 4% Picral.

No preheat. Hot pass laid 20 minutes after the root pass. Etch - 4% Picral.

Fig. 19. Effect of Welding Condition on the Severity of Cracking on Shop Welded 492S1871 Steel

No preheat. Hot pass laid 5 minutes after the root pass. Etch - 4% Picral

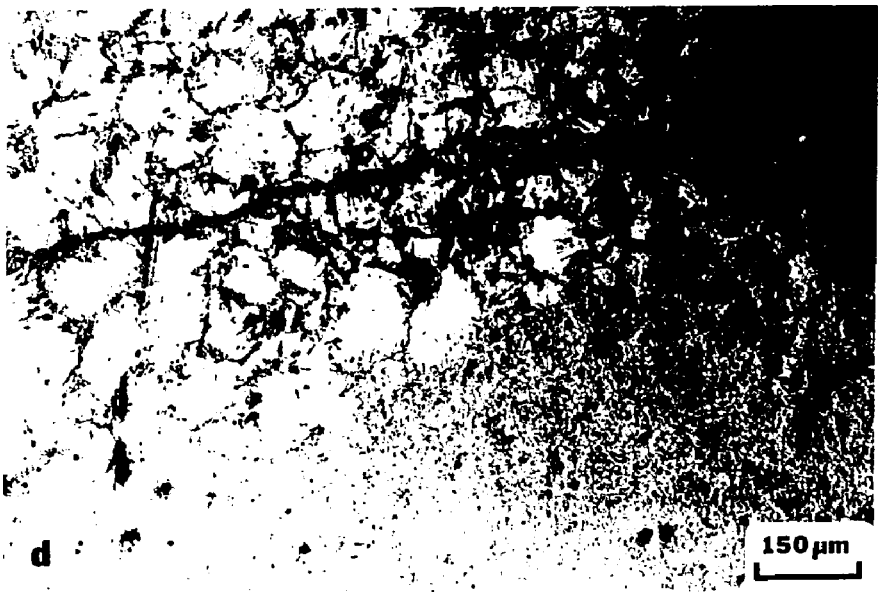

Preheat 66°C Infinite time interval after welding. No hot pass. Etch - 4% Picral

Fig. 19. (cont.) Effect of Welding Condition on the Severity of Cracking on Shop Welded 492S1871 Steel

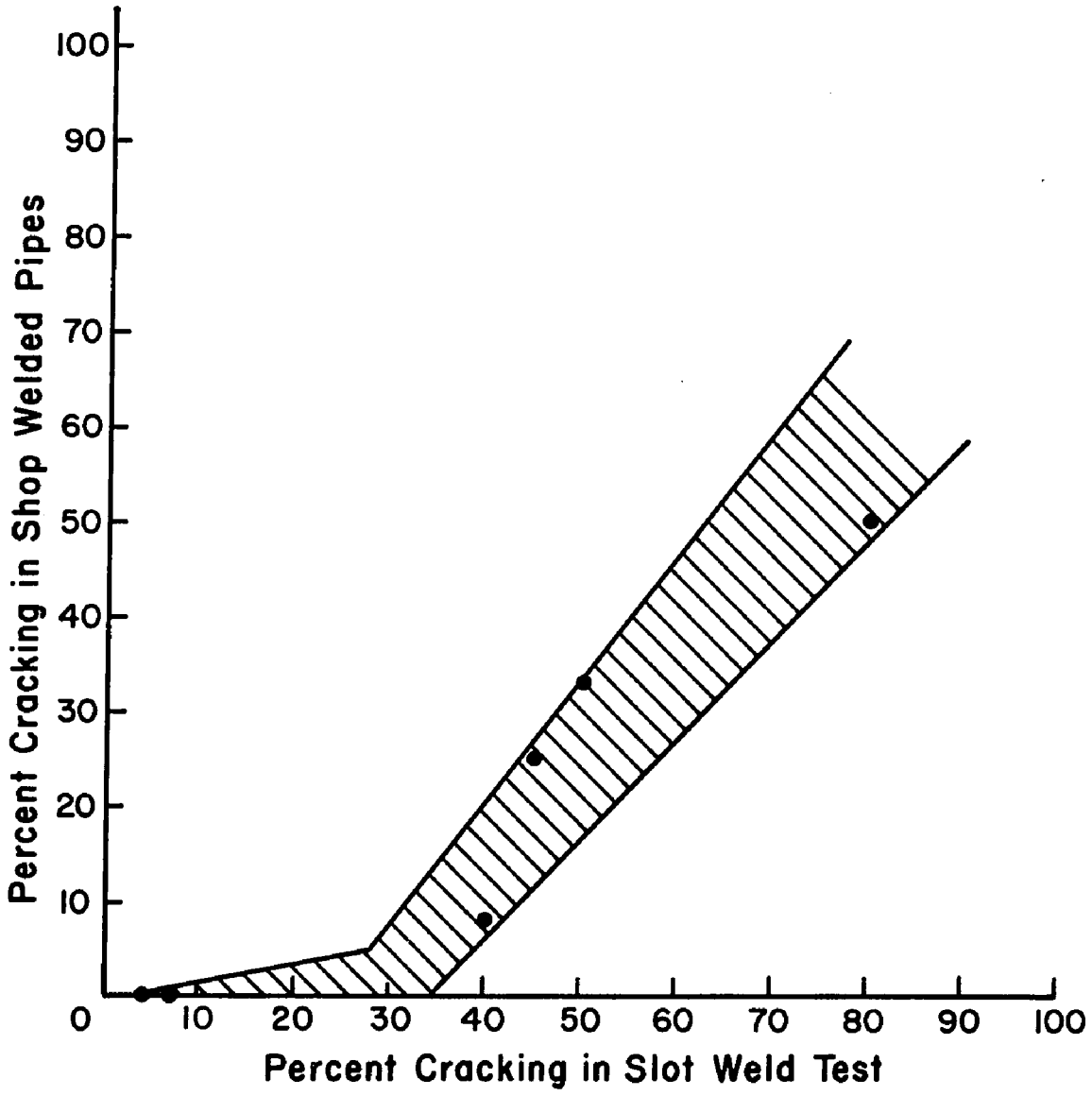

Fig. 20 Correlation between the actual girth welded pipes in the shop and the laboratory Slot Weld Test. (Heat No. 492 S 1871)

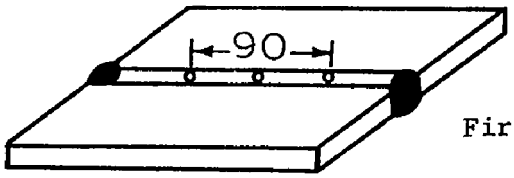

Tack Weld -
First Fabrication Step

Tack weld with spacers in place.

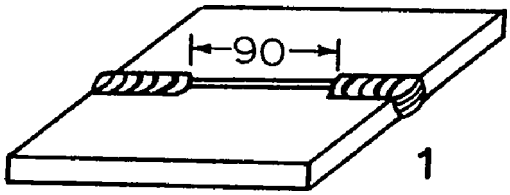

Tack weld with 2.4 mm spacers. Remove spacers before restraint weld. Final slot width <1.66mm before test weld was made.

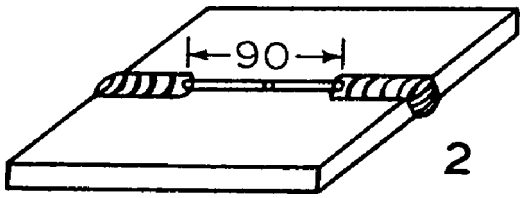

Tack weld with 2.4 mm spacers. Restraint weld with the three 2.4 mm spacers in position. Center spacer removed before test weld. Final slot width 1.6 mm before test weld was made.

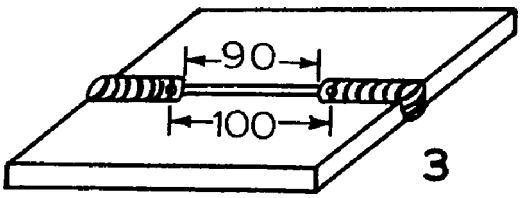

Tack weld with 3.2 mm spacers. Restraint weld over the spacers. No center spacer used. Final slot width 2.4 mm before test weld was made.

Fig. 21. Slot Weld Specimen Fabrication Sequence.

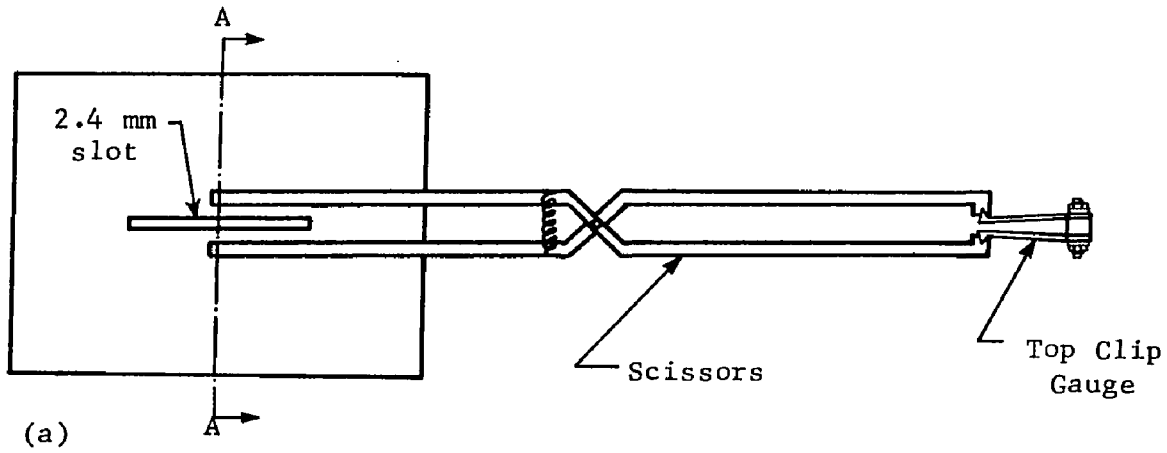

(a)

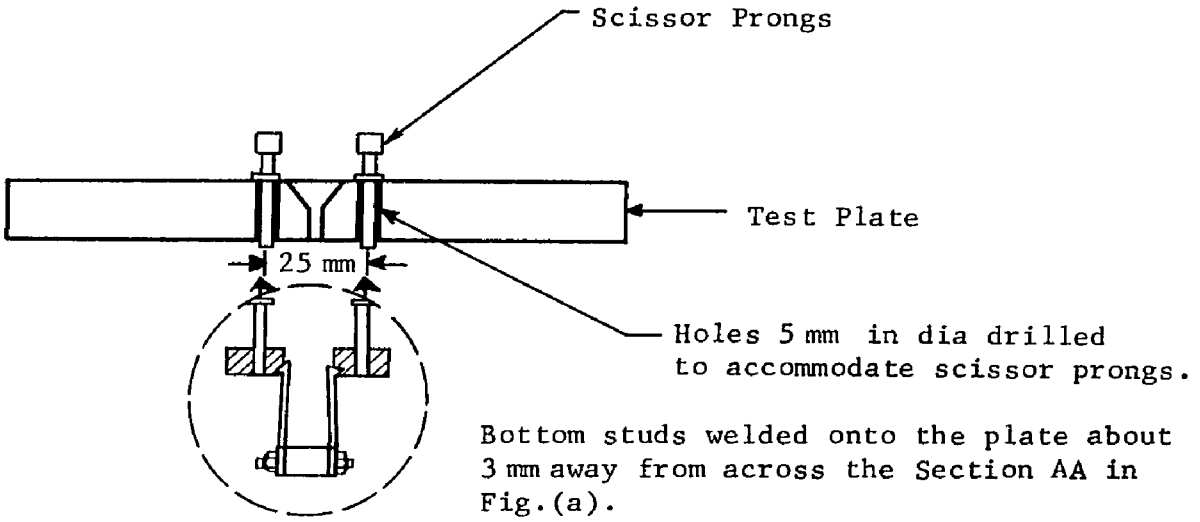

(b) Design 1.

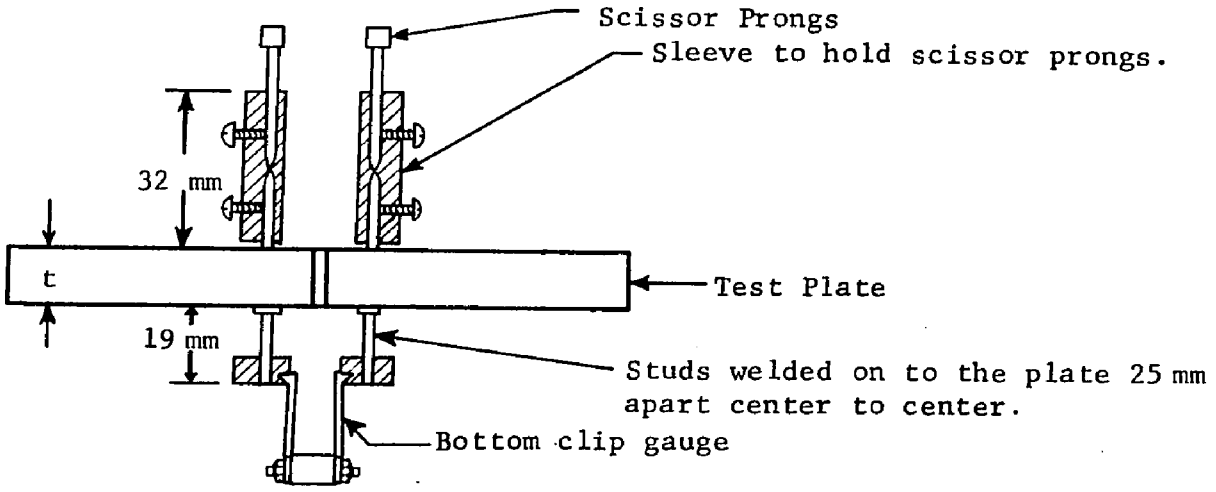

(c) Design 2.

Fig. 22. Experimental Set-up for Dilation Measurements.

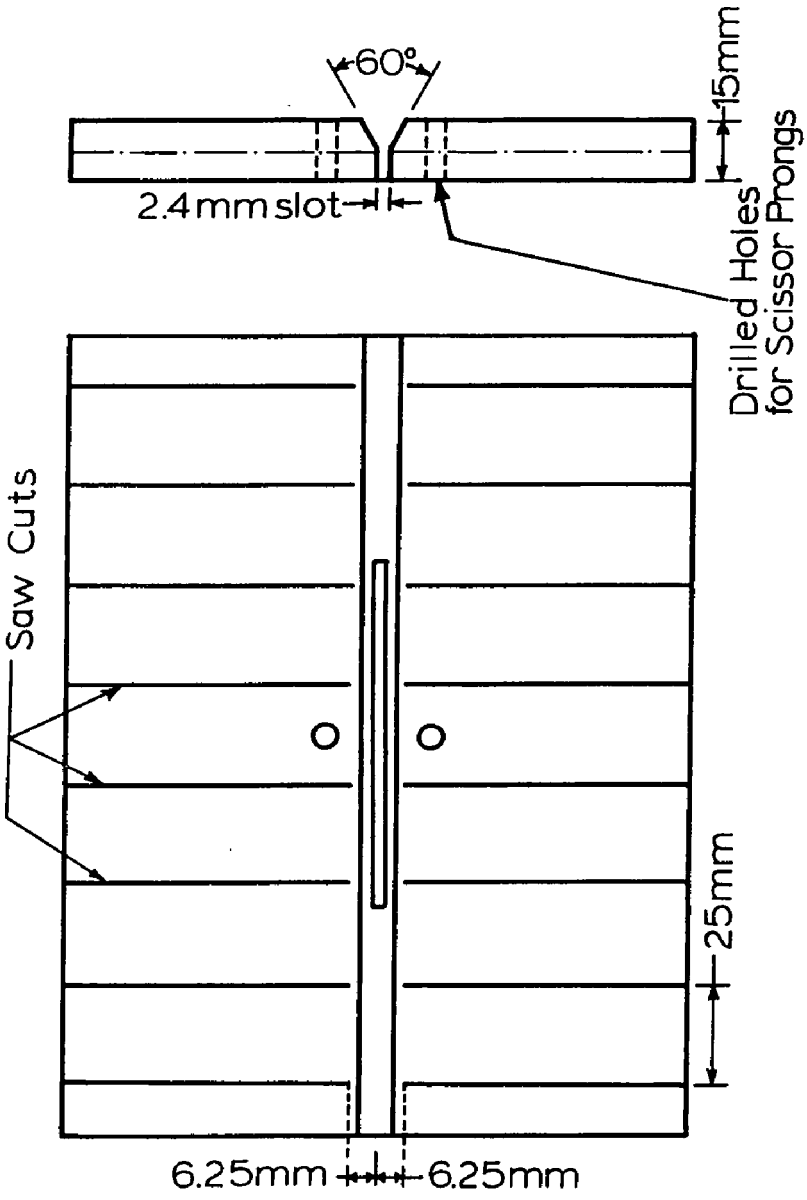

Fig.23 Specimen Design for Free Contraction Measurement.

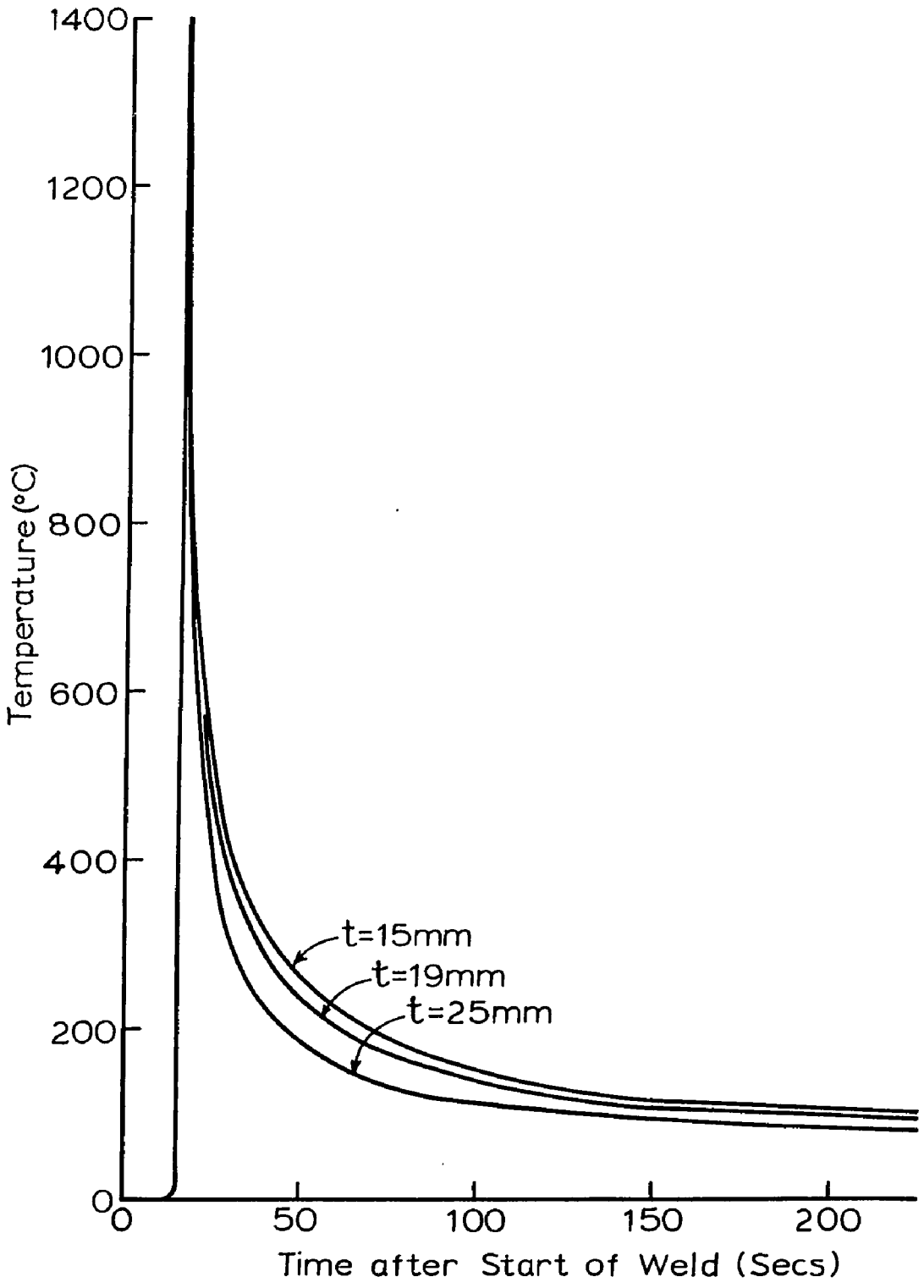

Fig.24 Temperature-Time Profile at the Center of the Weld for Various Plate Thicknesses (H·I = 9KJ/Cm)

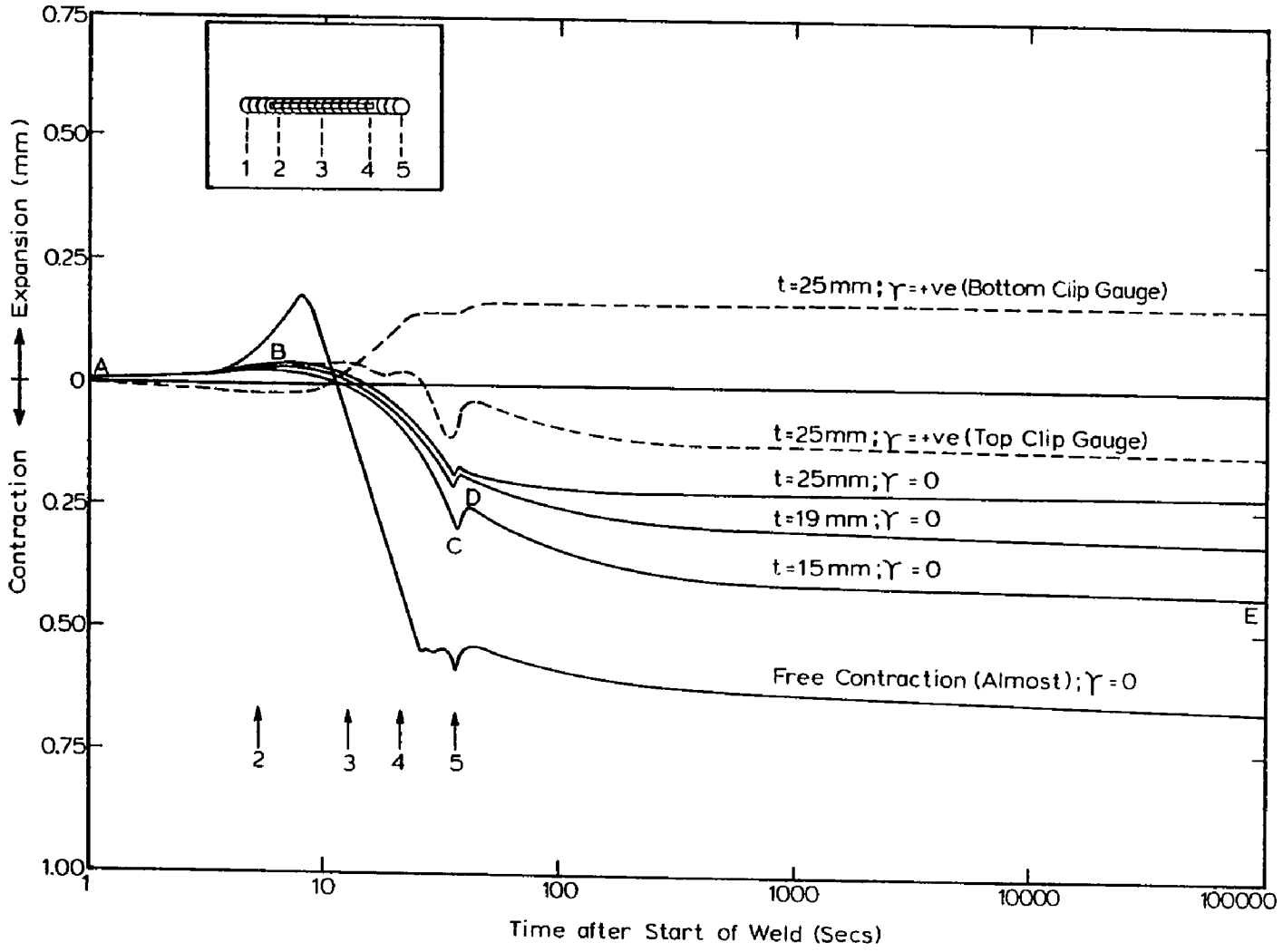

Fig.25 Effect of Plate Thickness on Dilation Measurement in Heat N.K.K. Using Design 1.

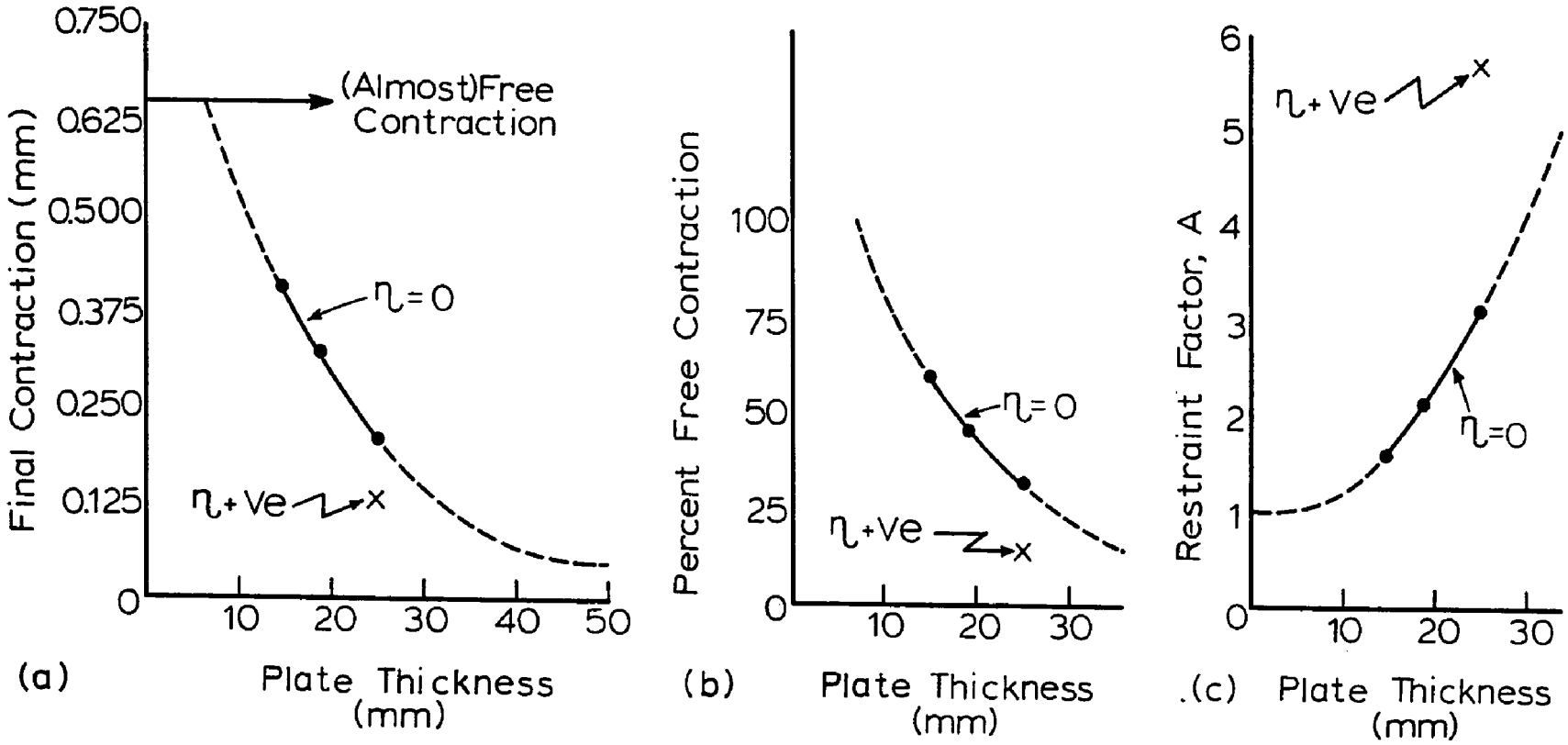

Fig. 26 Effect of Plate Thickness on Final Contraction, Percent Free Contraction and Restraint in Heat NKK (H.I. = 9KJ/Cm).

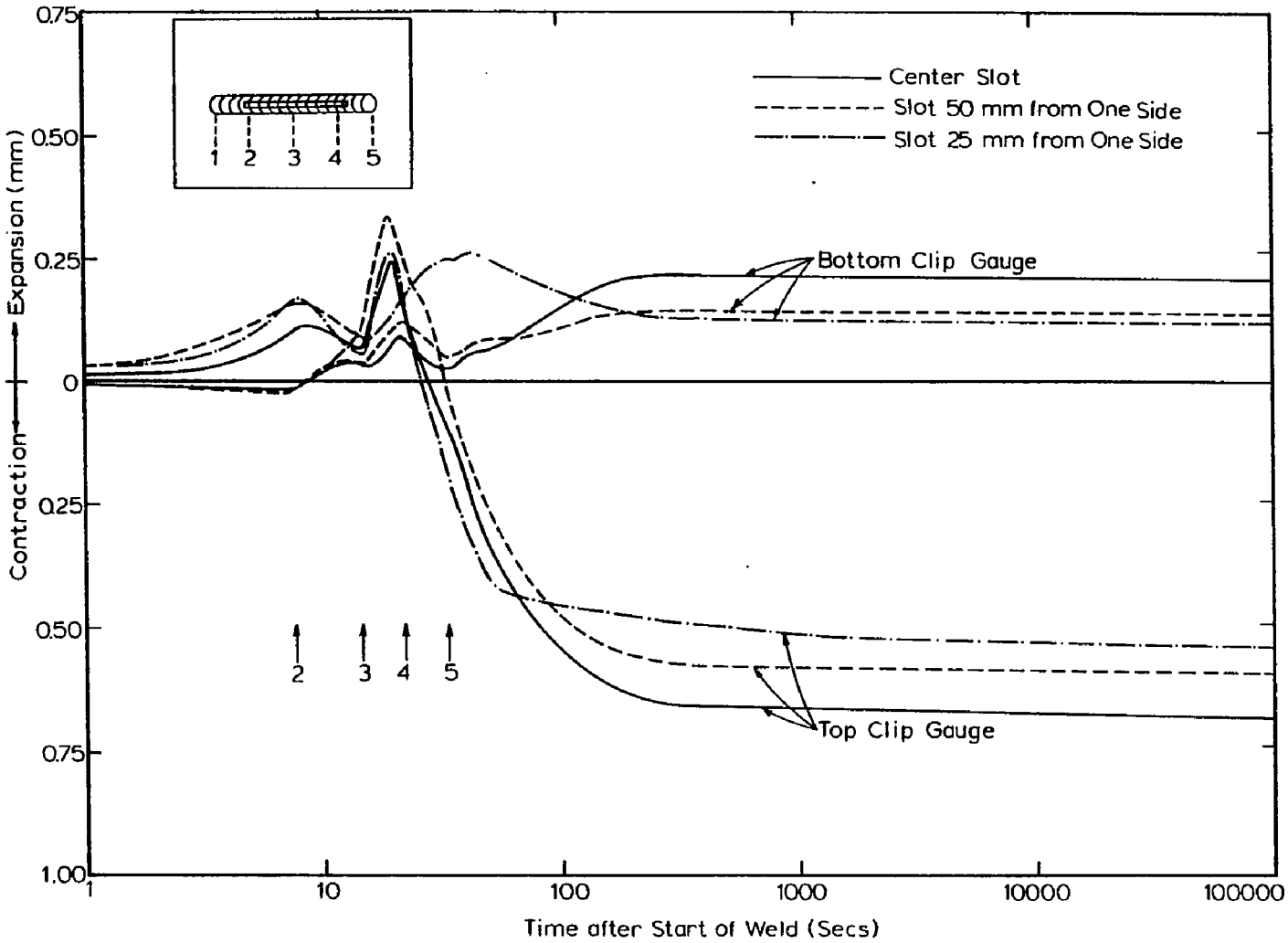

Fig.27(a) Effect of Off-Center Slot on Dilation Measurement in Heat B259 Using Design 2.

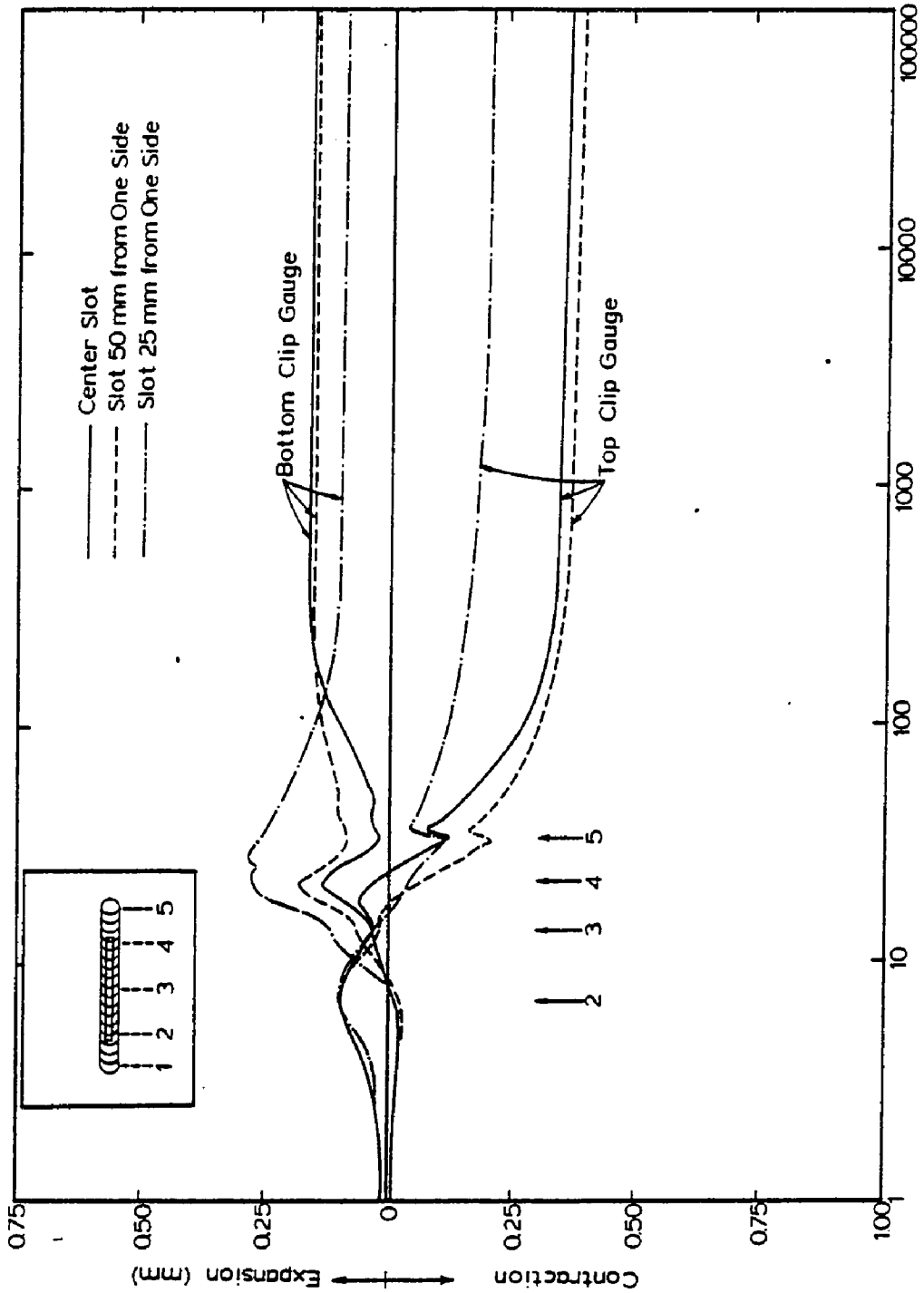

Fig.27(b) Effect of Off-Center Slot on Dilation Measurement in Heat B259 Using Design 1.

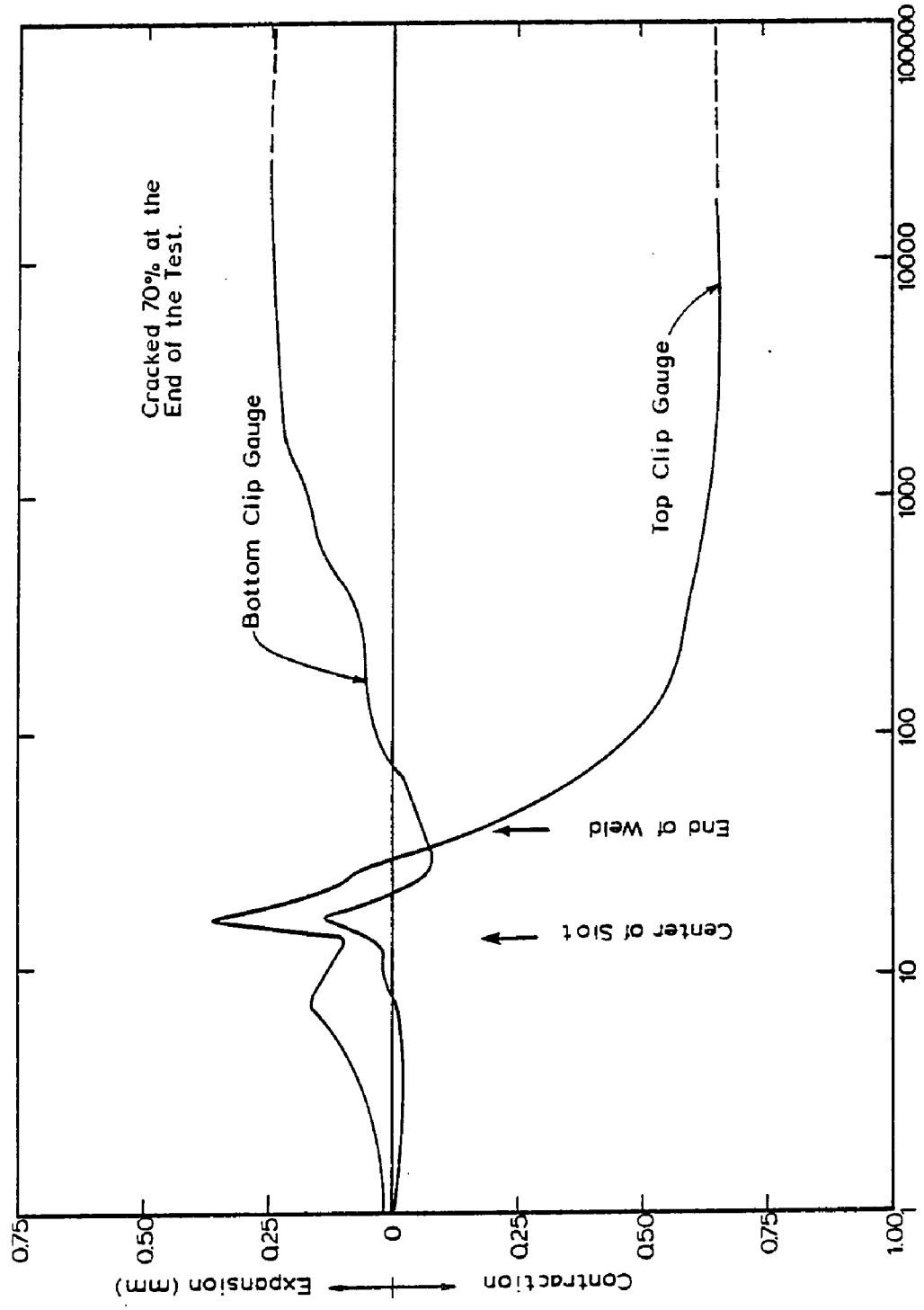

Fig.28 Hindered Dilation Measurement on Heat 492S1871.

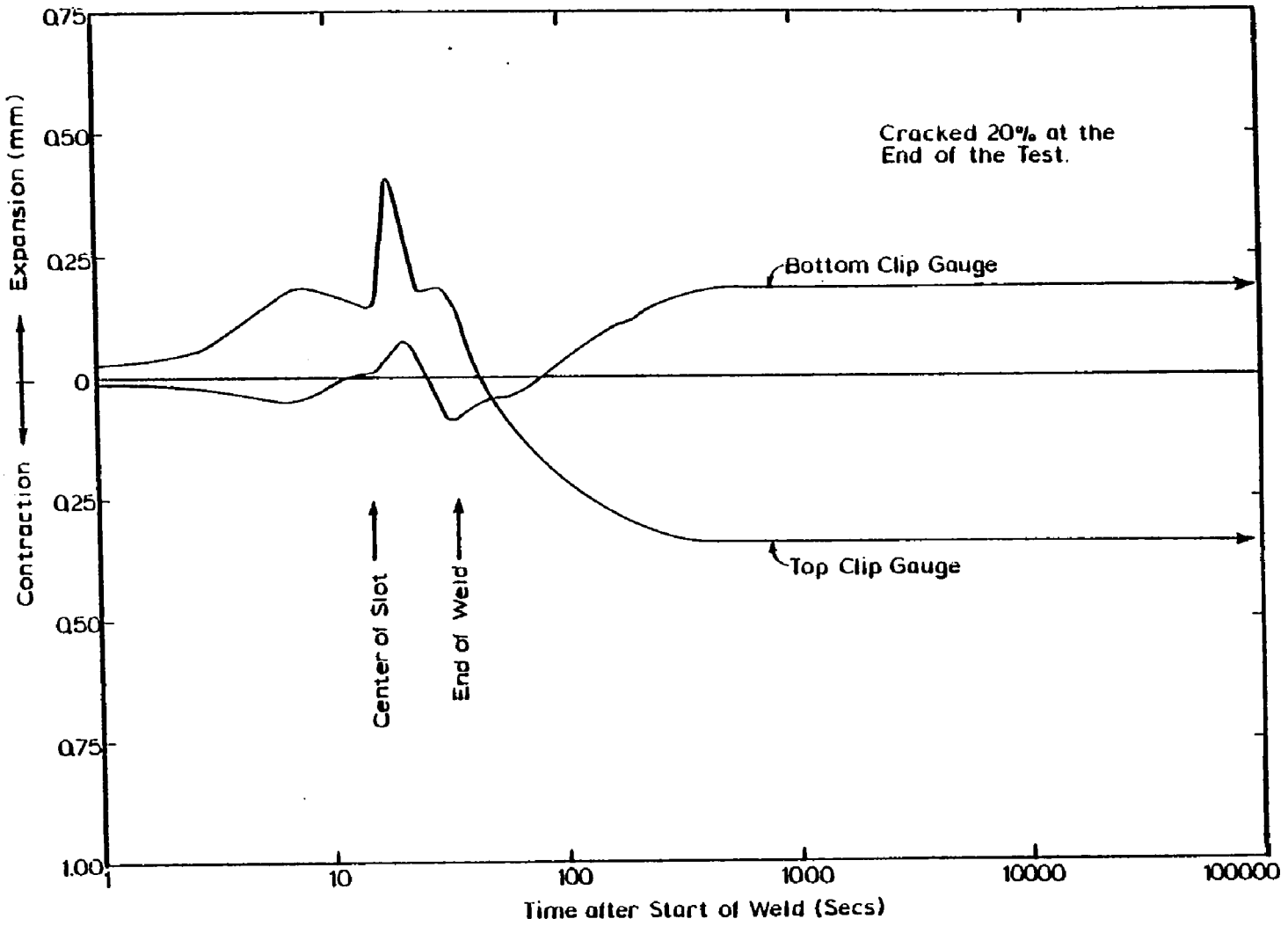

Fig.29 Hindered Dilation Measurements on Heat C10113.

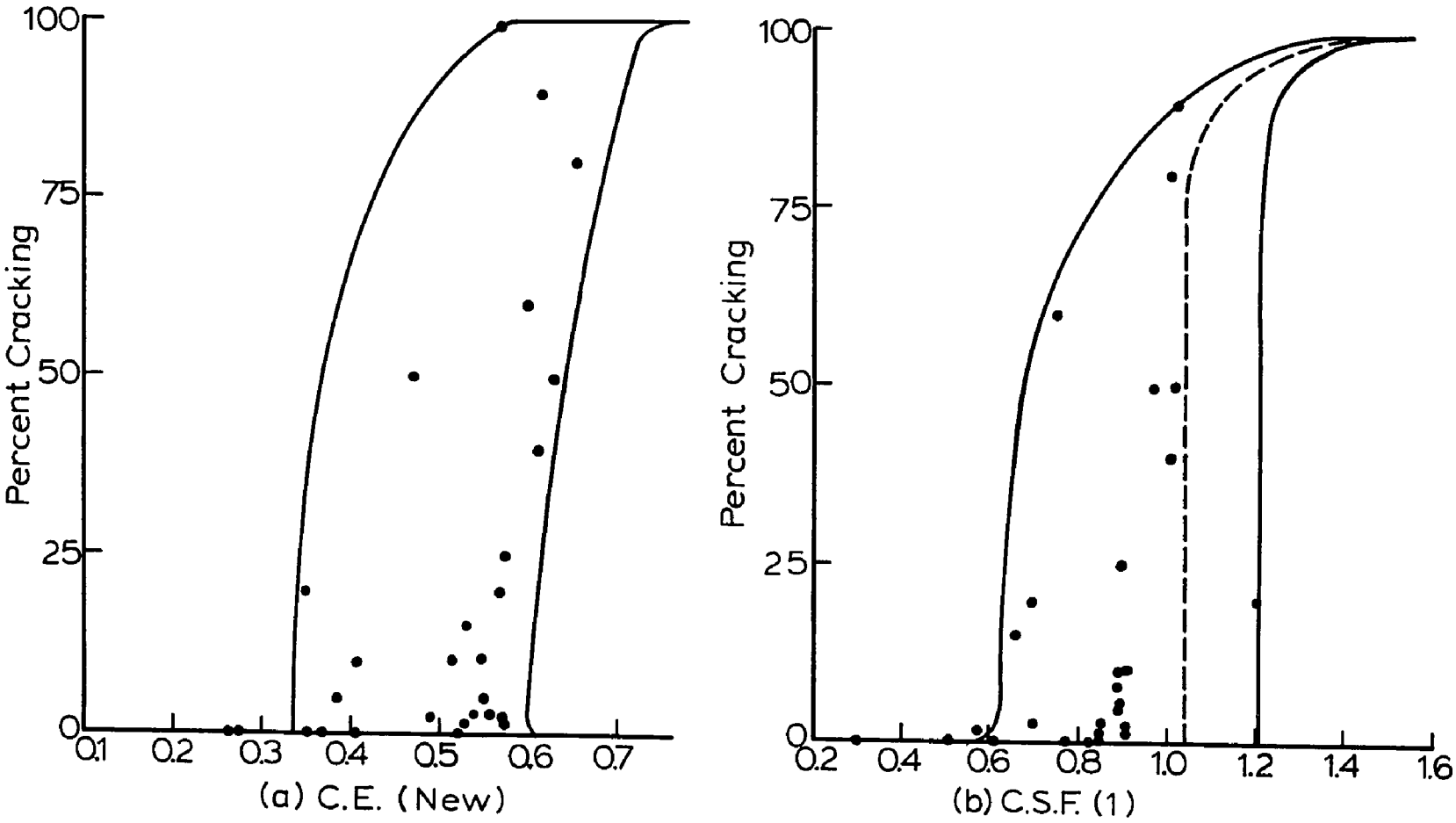

Fig. 30 Correlation between Extent of Cracking and Carbon Equivalence.

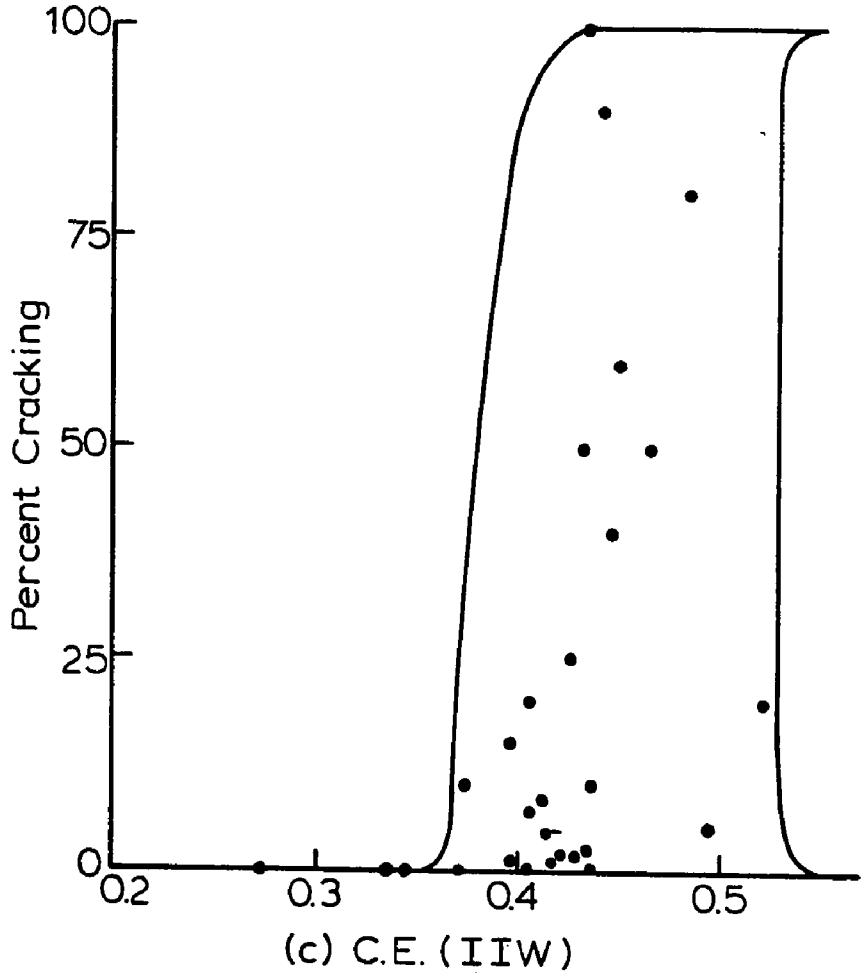
100
75
50
25
0
Percent Cracking
0.2
0.3
0.4
0.5
(c) C.E. (IIW)

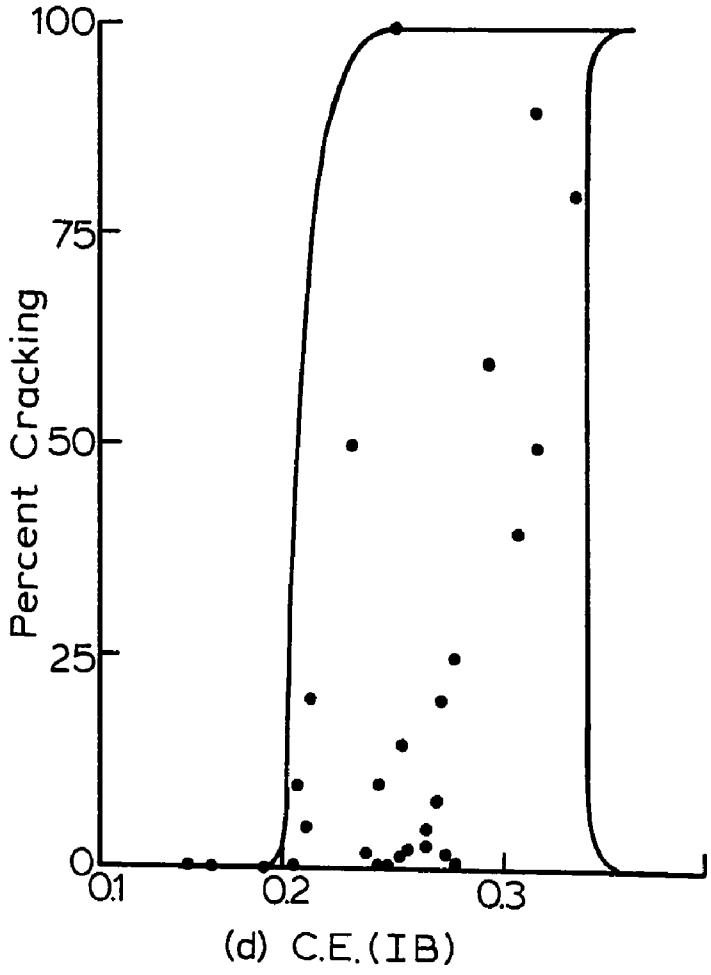
100
75
50
25
0
Percent Cracking
0.1
0.2
0.3
(d) C.E. (IB)

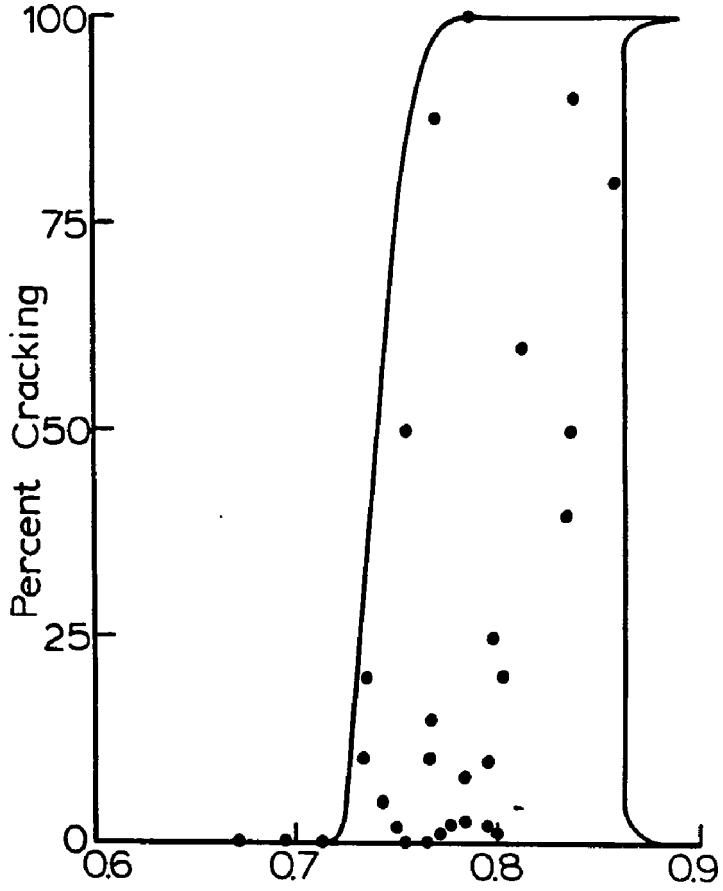
100
75
50
25
0
Percent Cracking
0.6
0.7
0.8
0.9

(e) Pcm

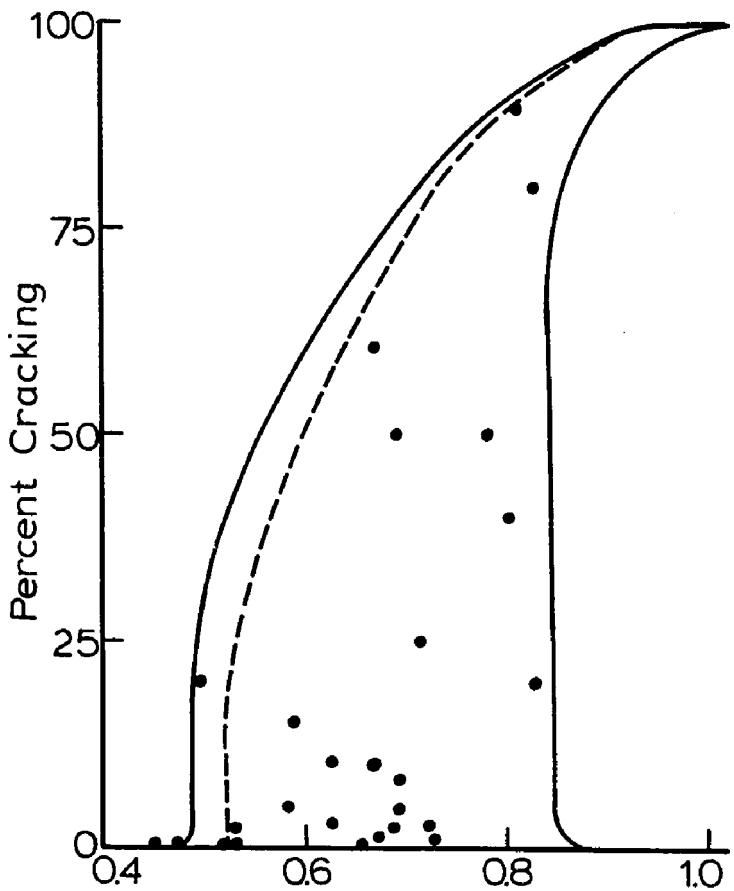
100
75
50
25
0
Percent Cracking
0.4
0.6
0.8
1.0

(f) C.S.F. (2)

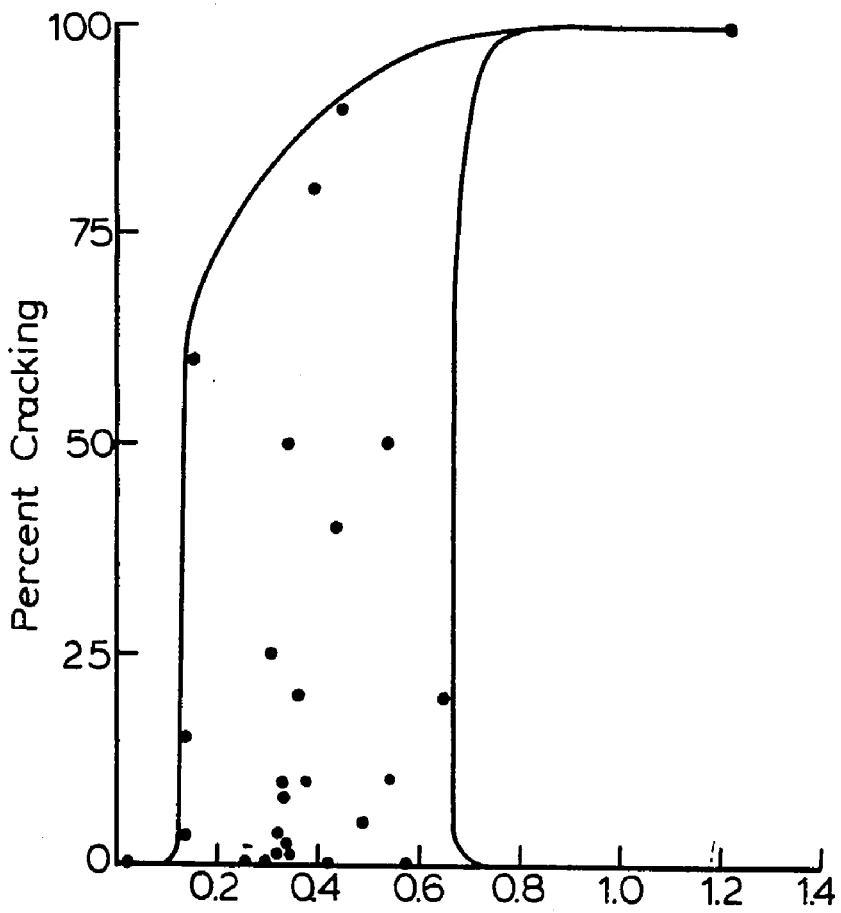

(g) C.S.F. (3)

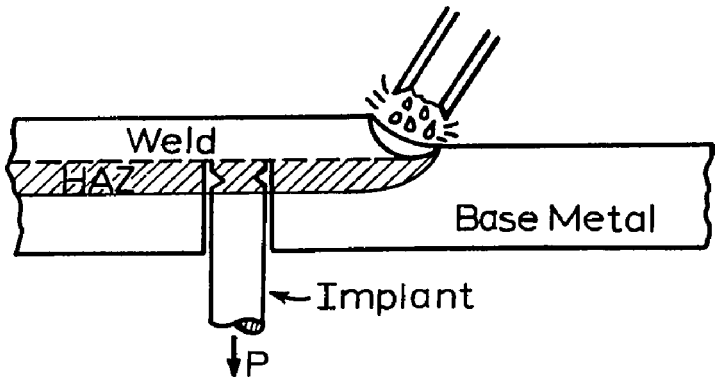

Fig.31 Original Implant Test.

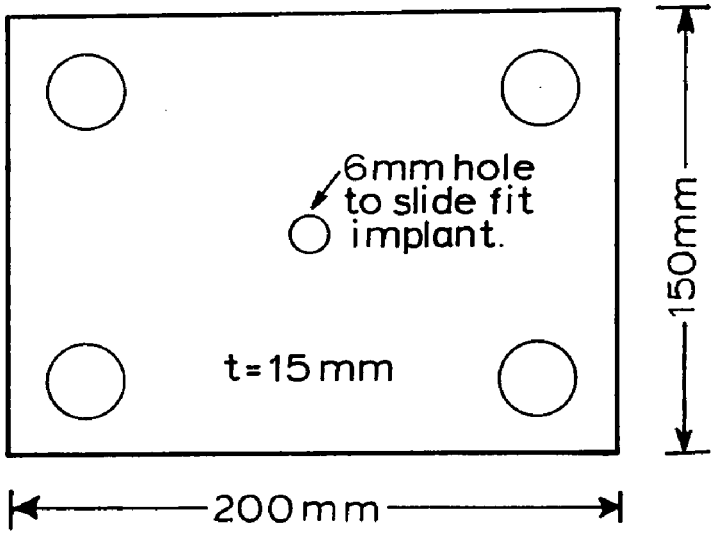

Implant Base Plate.

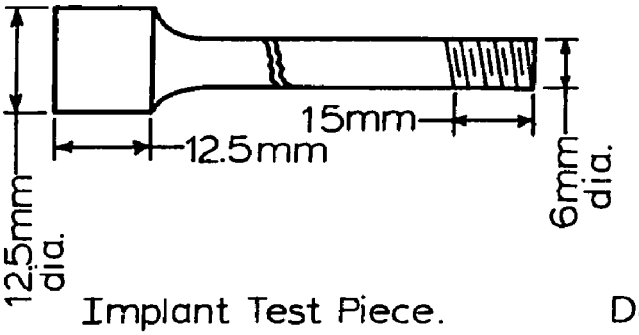

Implant Test Piece.

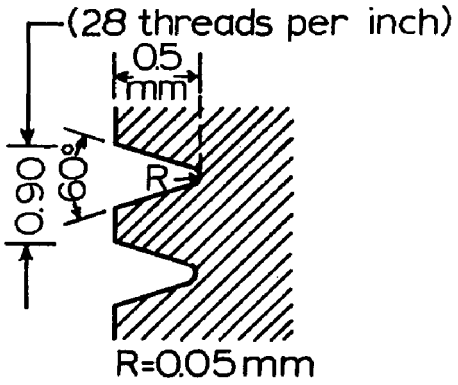

Details of Helical Notch.

Fig.32 Details of Implant Specimen and Backing Plate.

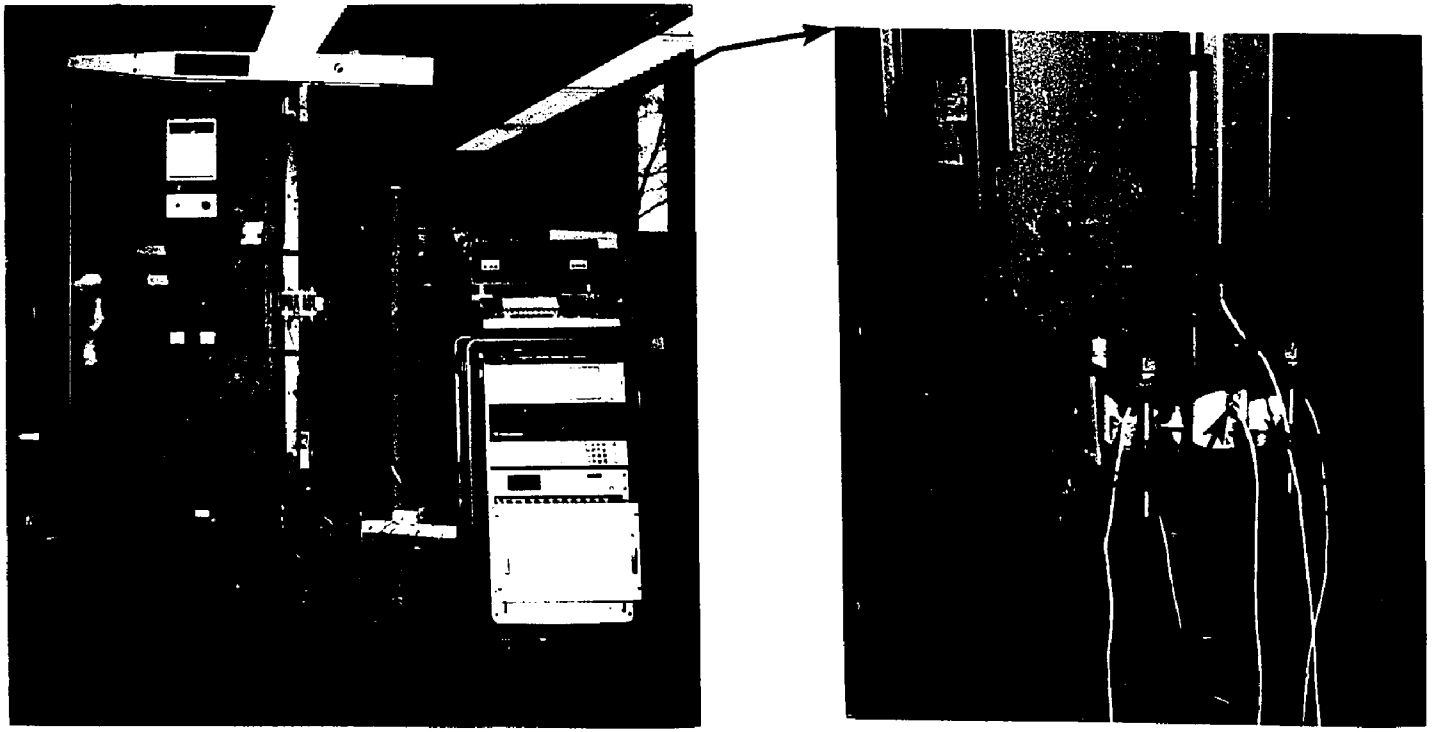

1. Implant Testing M/C
2. Loading quill-with micro-switch
3. Load
4. Wheel for loading
5. Preamplifier
6. A.E. System
7. Teleprinter
8. Implant Specimen
9. Implant base plate
10. Sensor
11. Magnet to hold Sensor in position
12. Positioners for alignment
13. Back-up plate

Fig. 33. Details of the Implant Testing machine and Acoustic Monitoring System

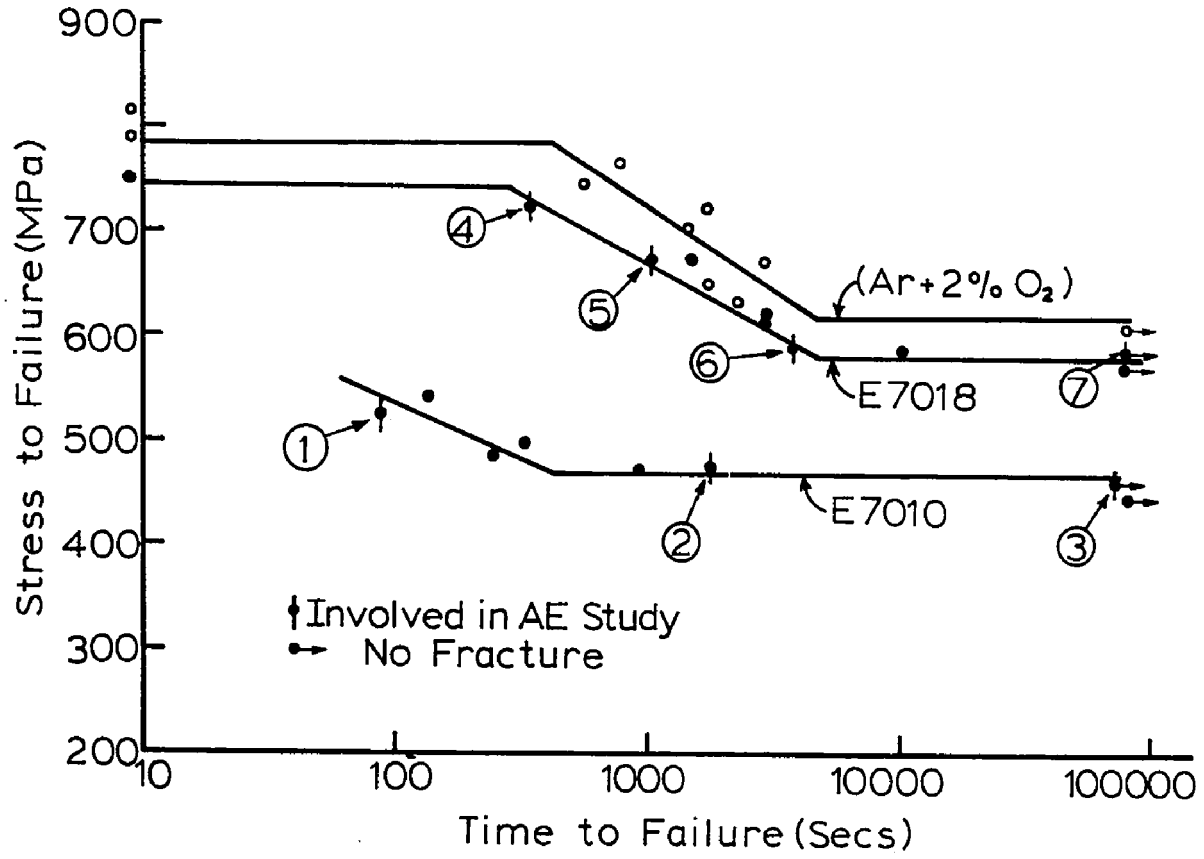

Fig.34 Stress-Time to Rupture Curve for Heat 492S1871.

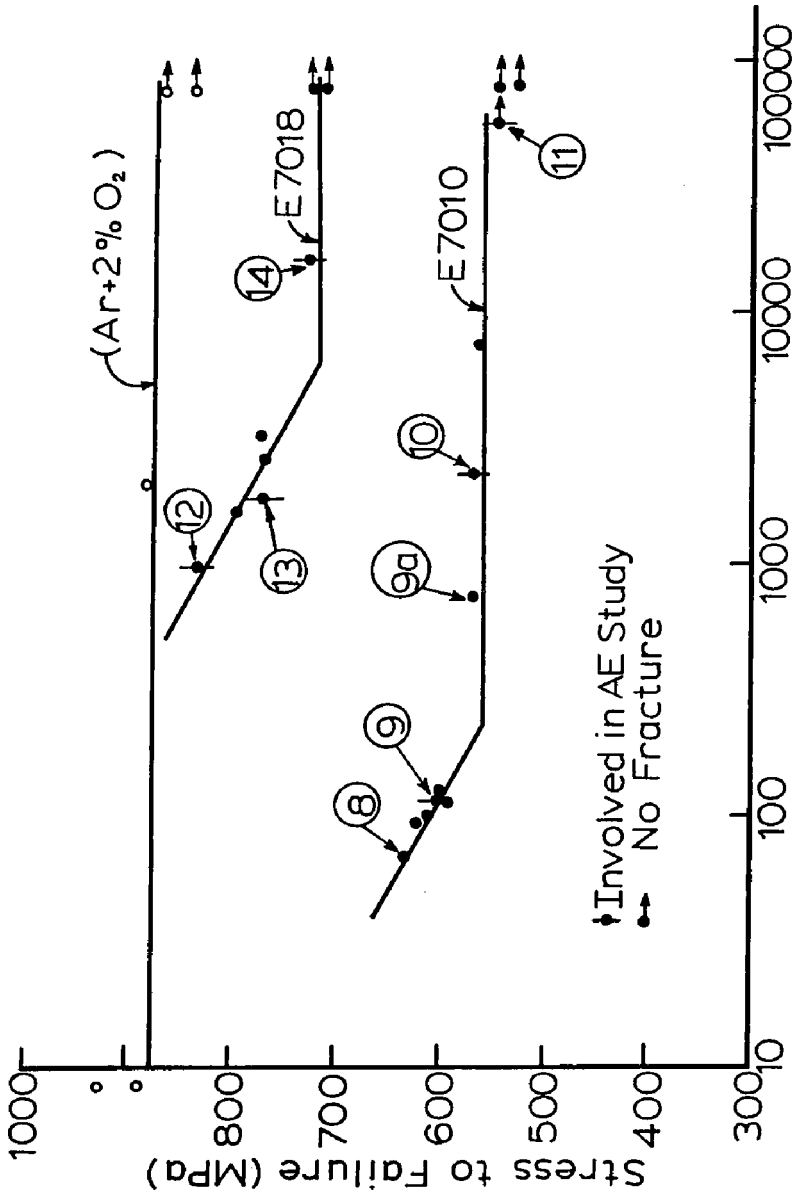

Fig.35 Stress-Time to Rupture Curve for Heat C1011 3.

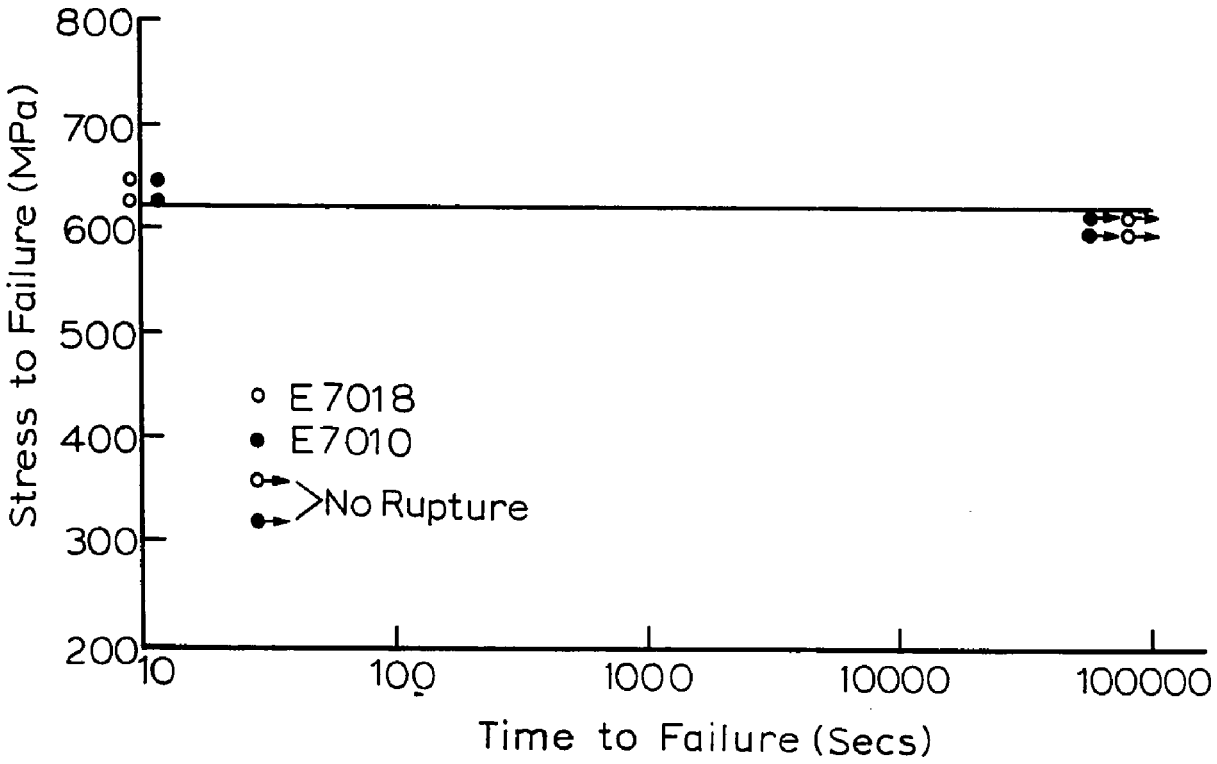

Fig.36 Stress-Time to Rupture Curve for Heat B259.

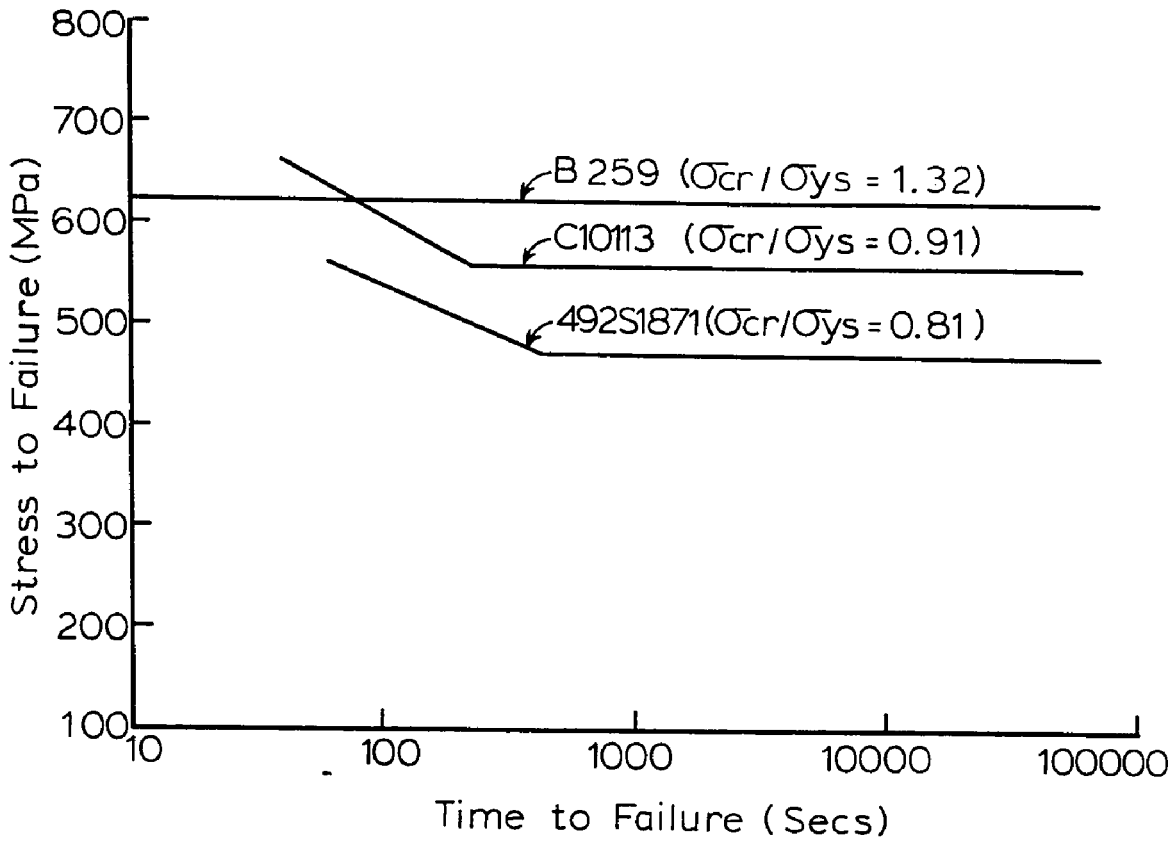

Fig.37 Stress-Time to Rupture Curve for Various Heats Welded with E 7010.

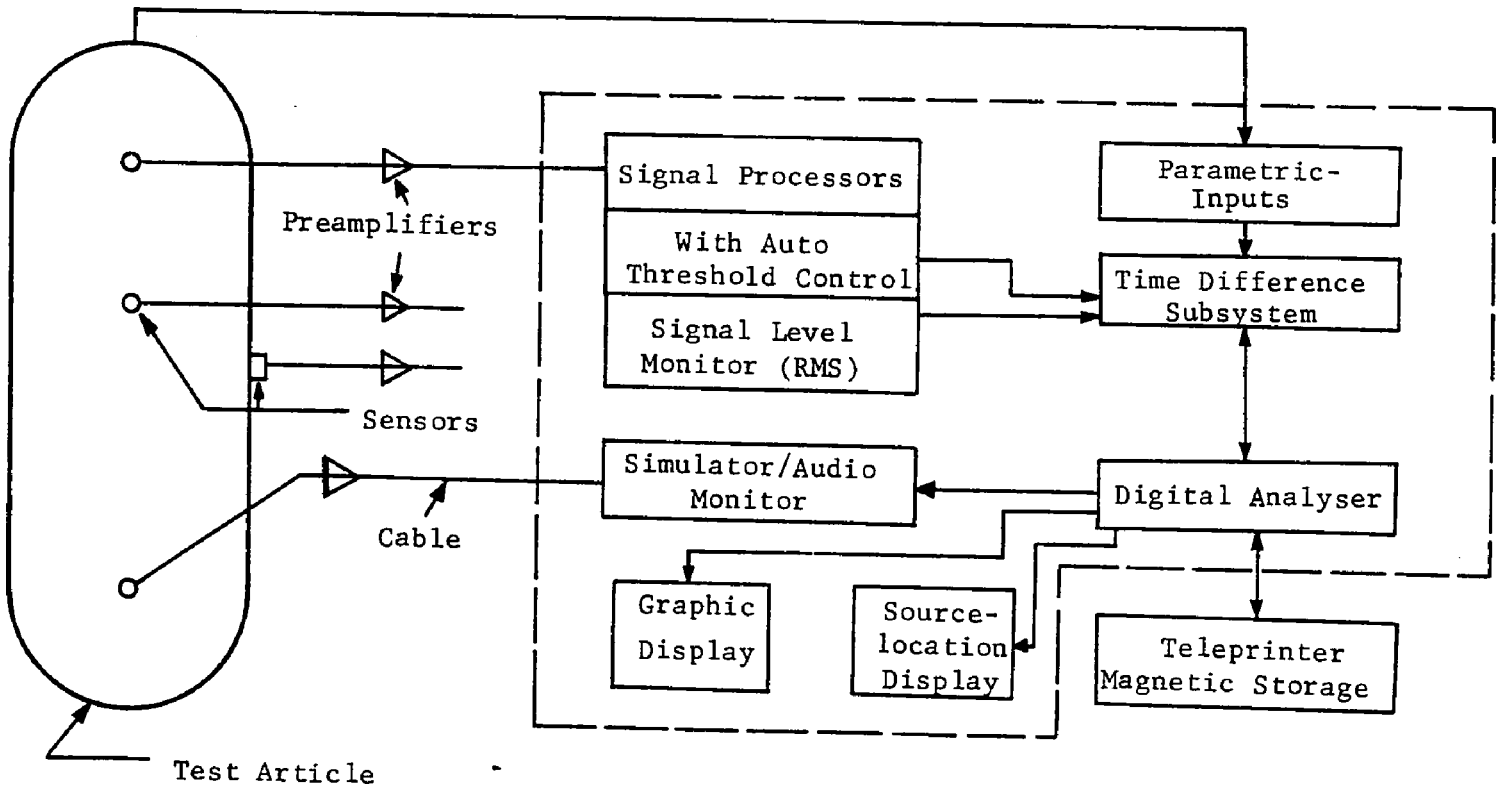

Fig. 38 Block Diagram of the Acoustic Monitoring System.

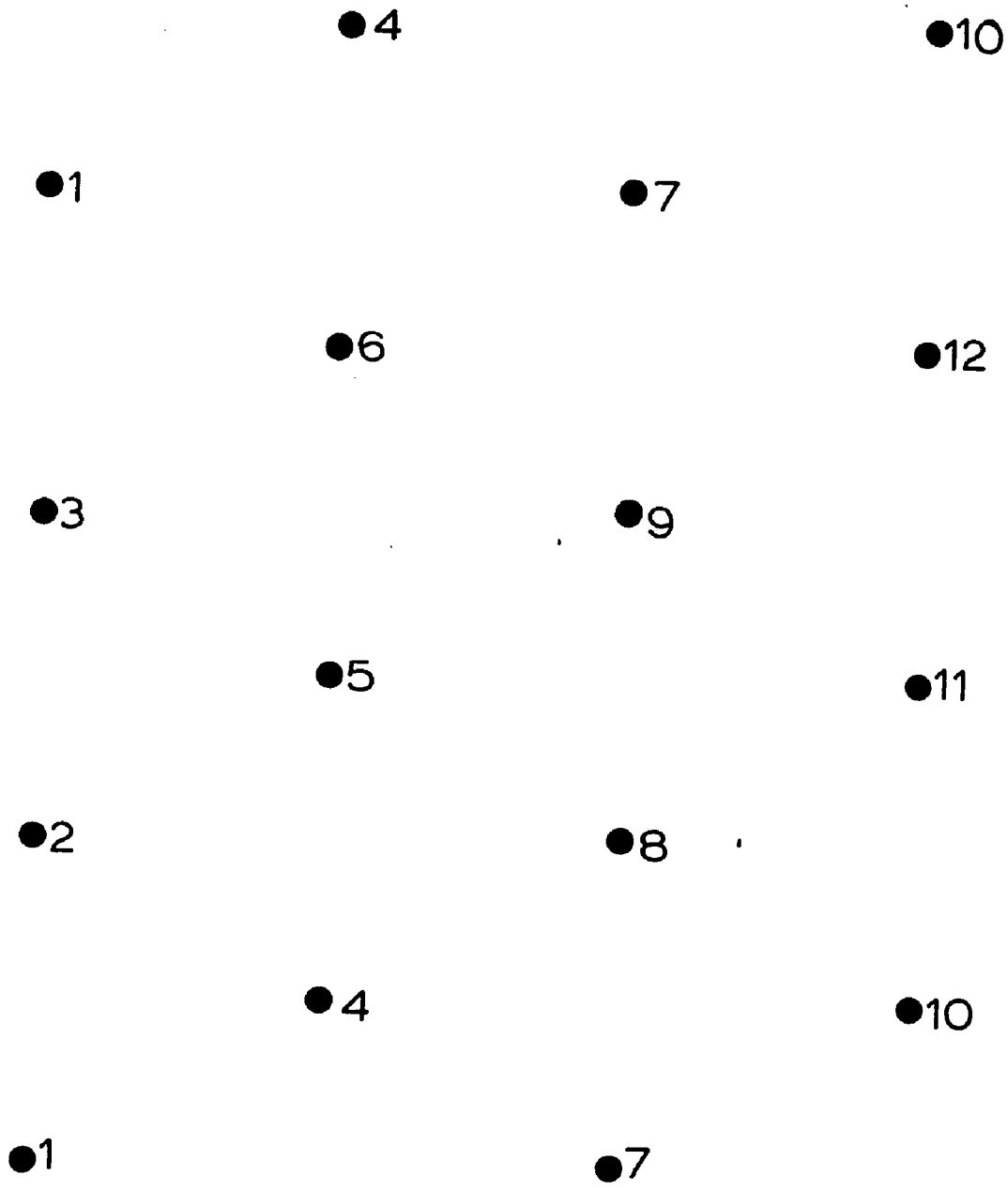

Fig. 39 A Hard Copy from CRT Display Showing the Sensor Layout on Cylindrical Portion of a Pressure Vessel.

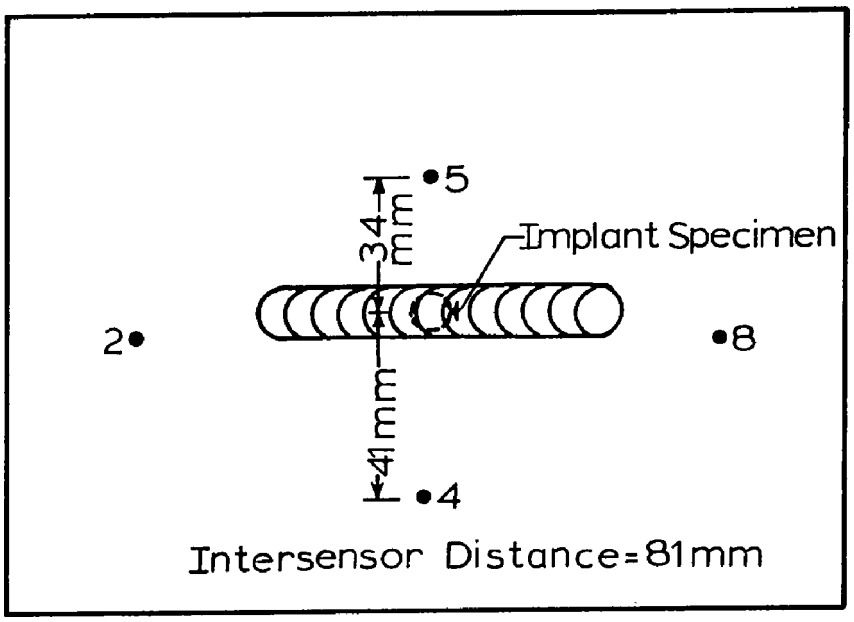

Fig.40 AE Sensor Position on the Base Plate with Respect to Weld and Implant Specimen.

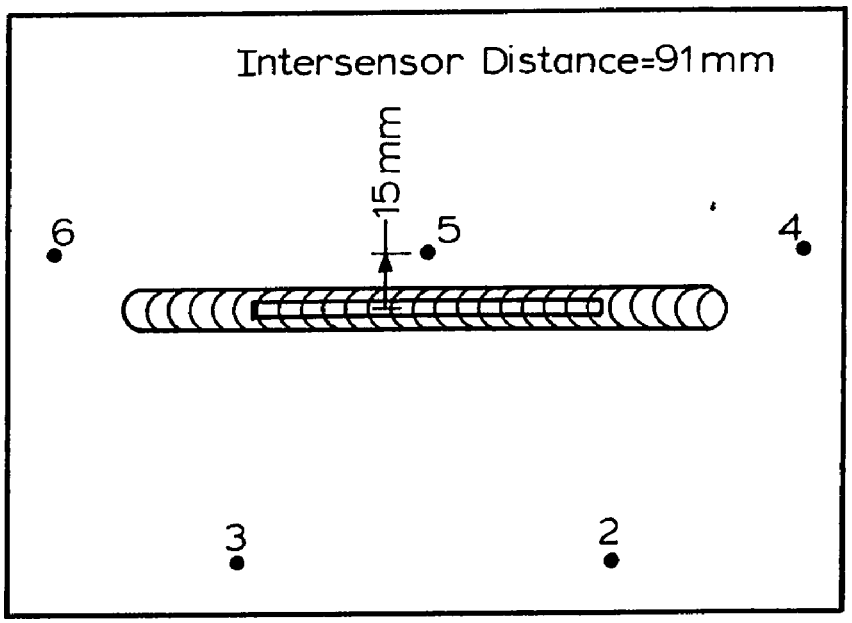

Fig.41 AE Sensor Positions on Slot Weld Test Specimen.

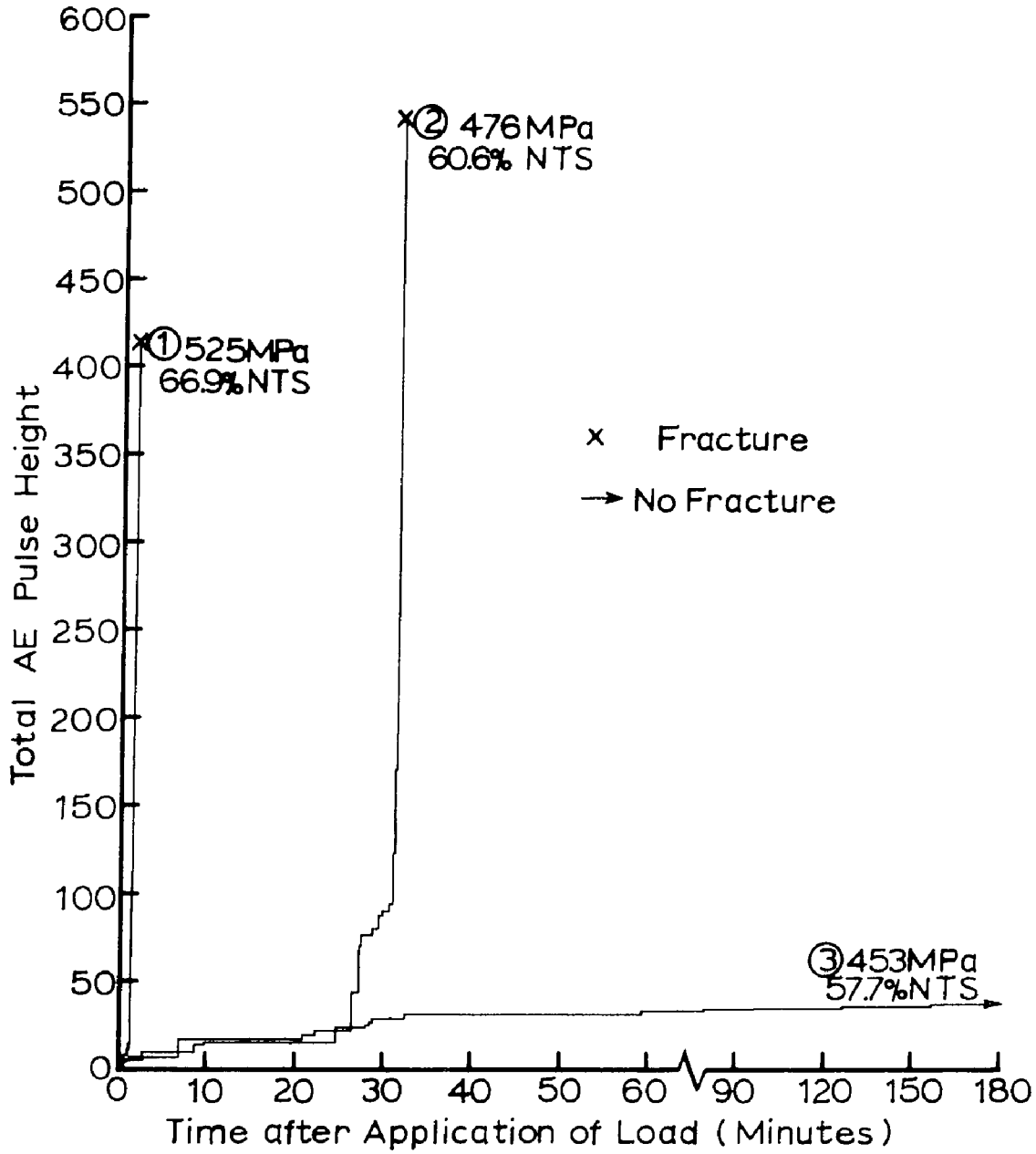

Fig.42 Acoustic Emission Responses for Implant Tests in Heat 492S1871 Welded with E7010 at Various Stress Levels.

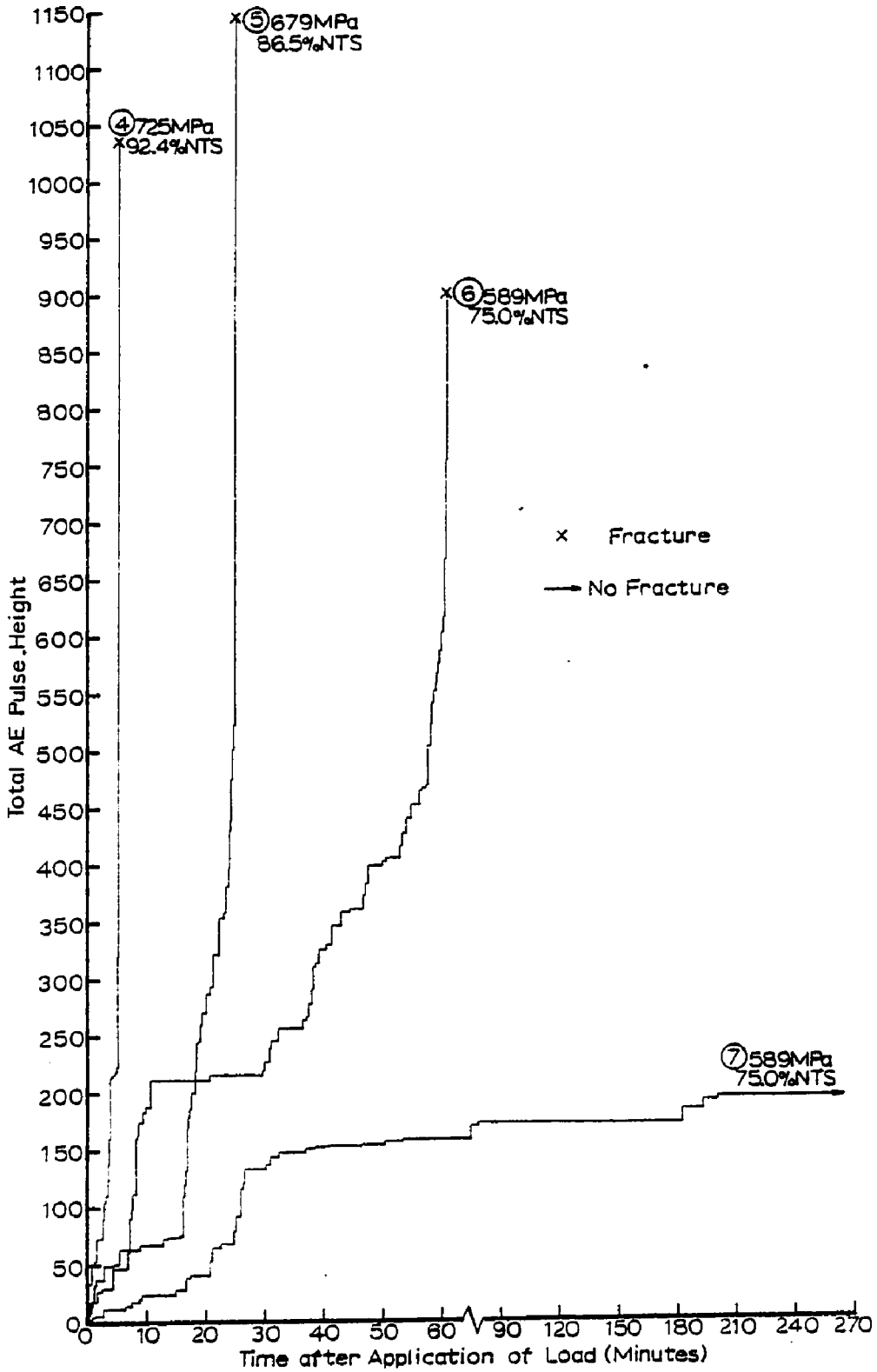

Fig. 43 Acoustic Emission Responses for Implant Tests in Heat 492S1871 Welded with E7018 at Various Stress Levels

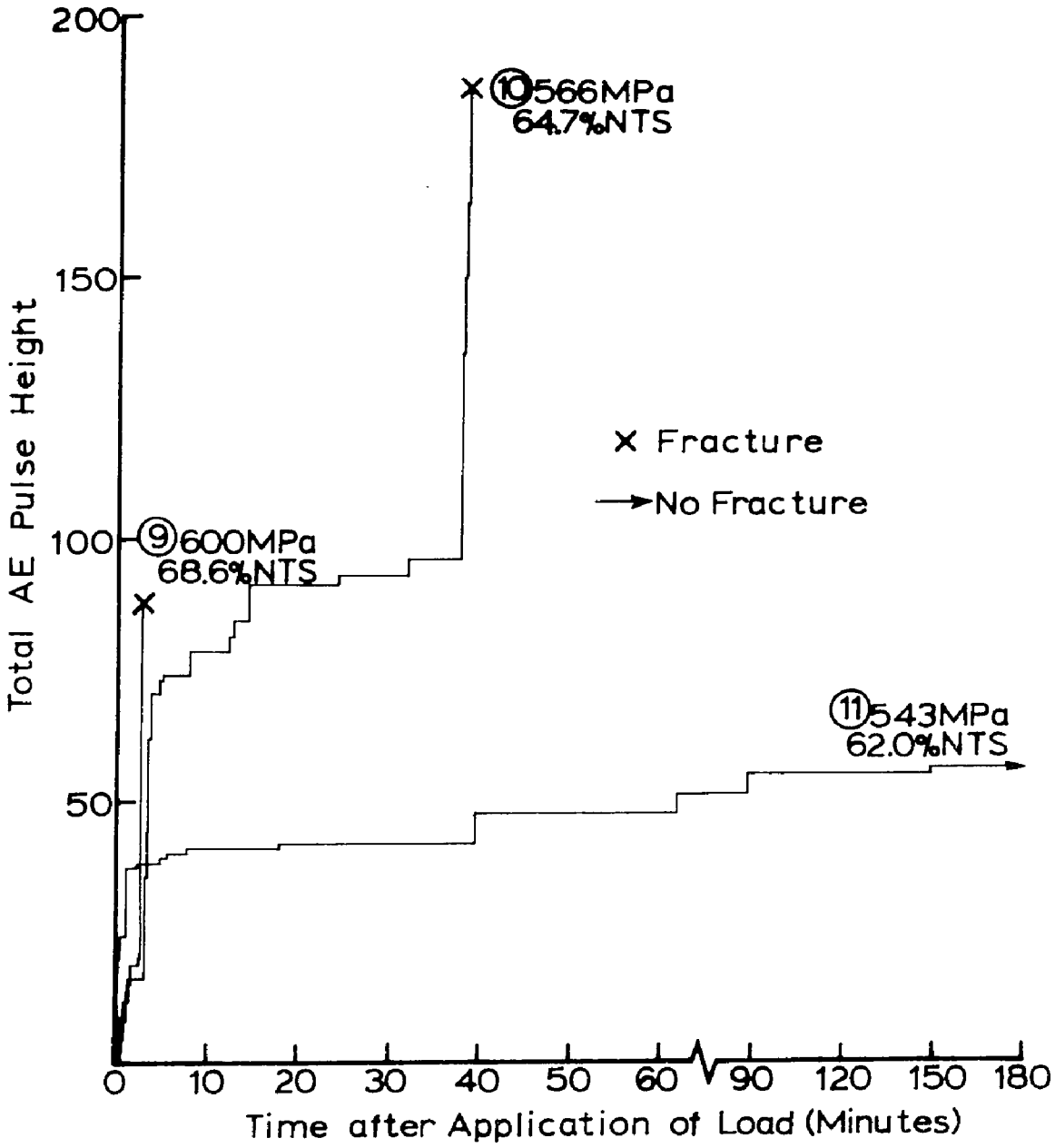

Fig.44 Acoustic Emission Responses for Implant Tests in Heat C10113 Welded with E7010 at Various Stress Levels.

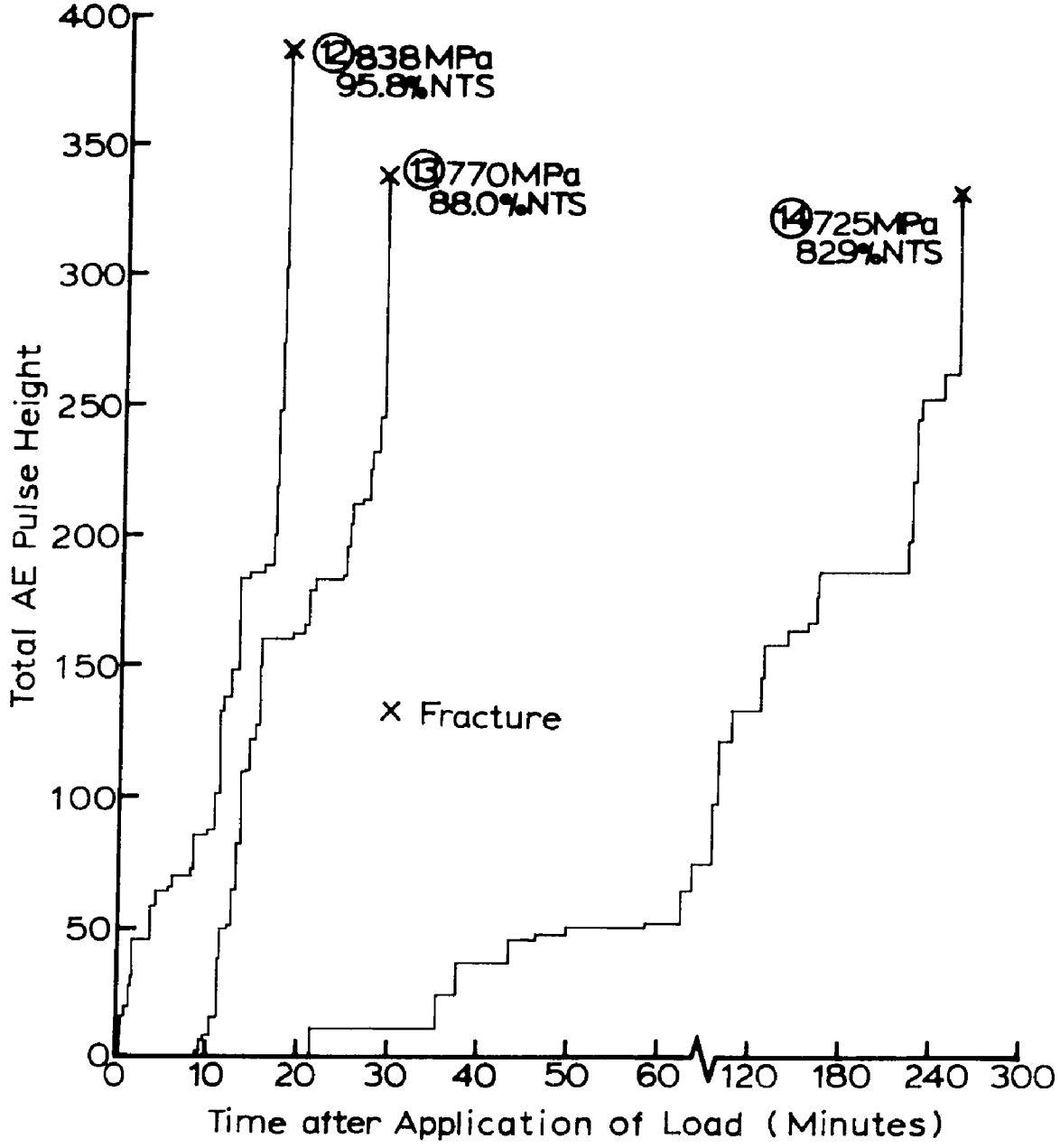

Fig.45 Acoustic Emission Responses for Implant Tests in Heat C10113 Welded with E7018 at Various Stress Levels.

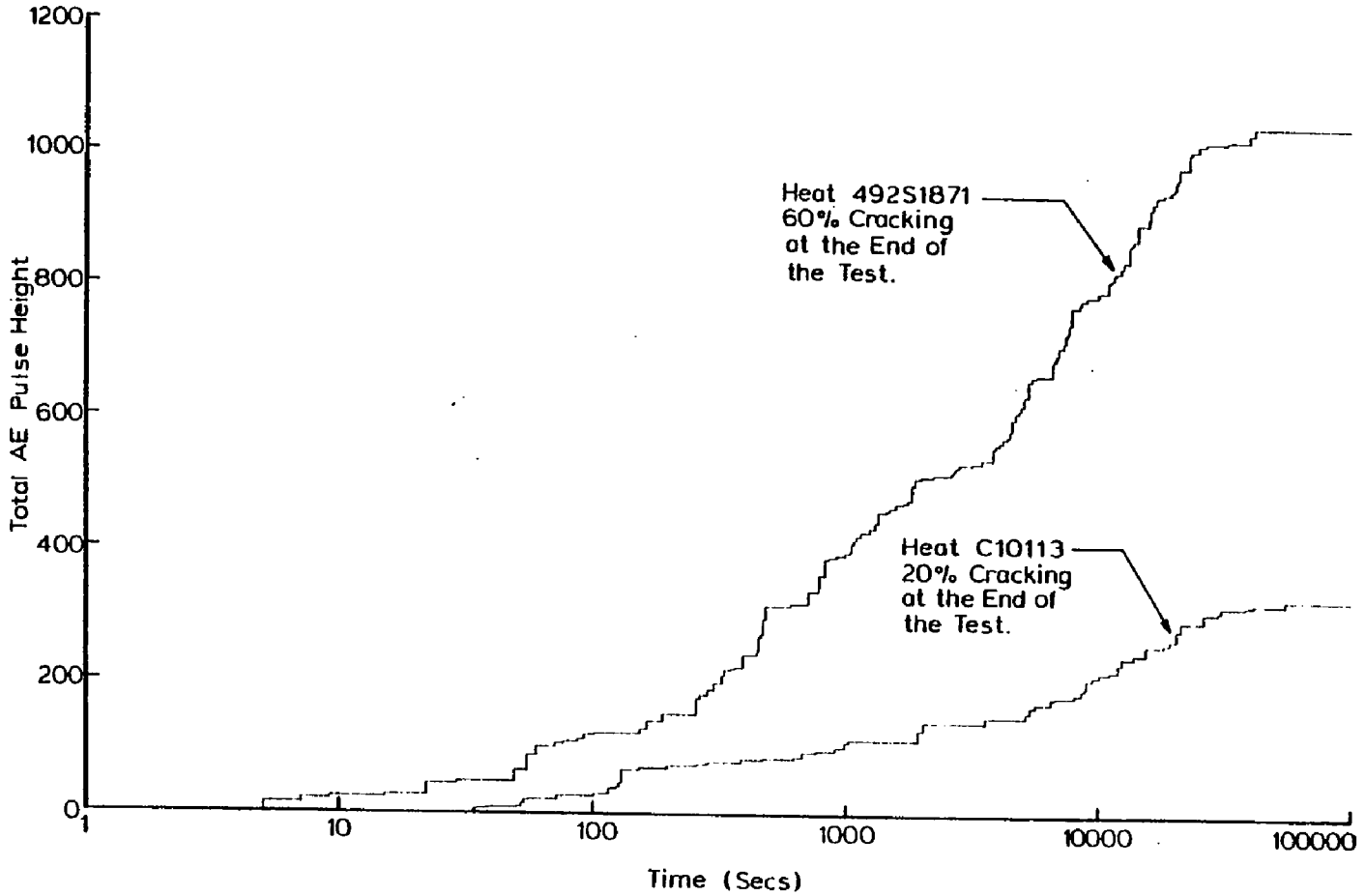

Fig.46 Acoustic Emission Response in Slot Weld Test for Heats 492S1871 and C10113 Welded with E7010 Electrode.

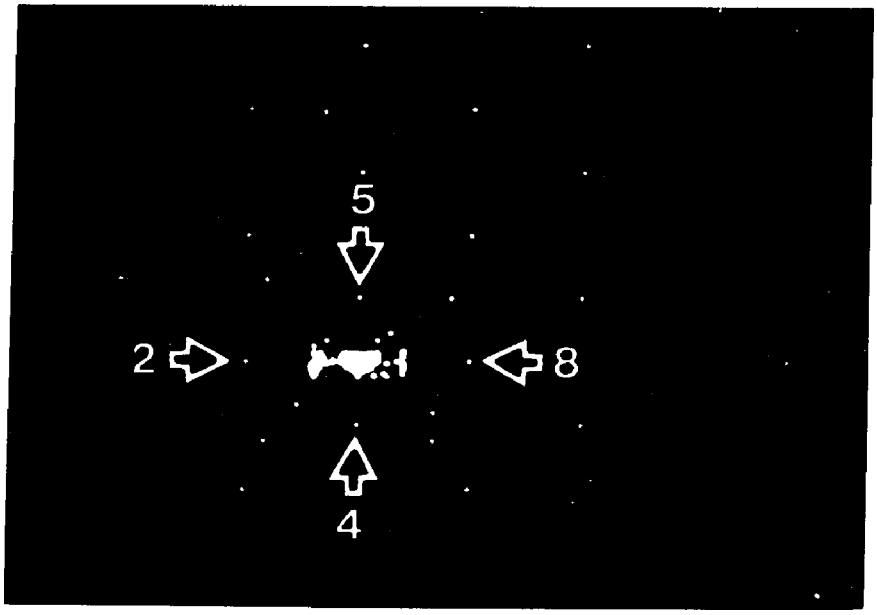

Fig. 47. Typical Source location produced on CRT during Implant test

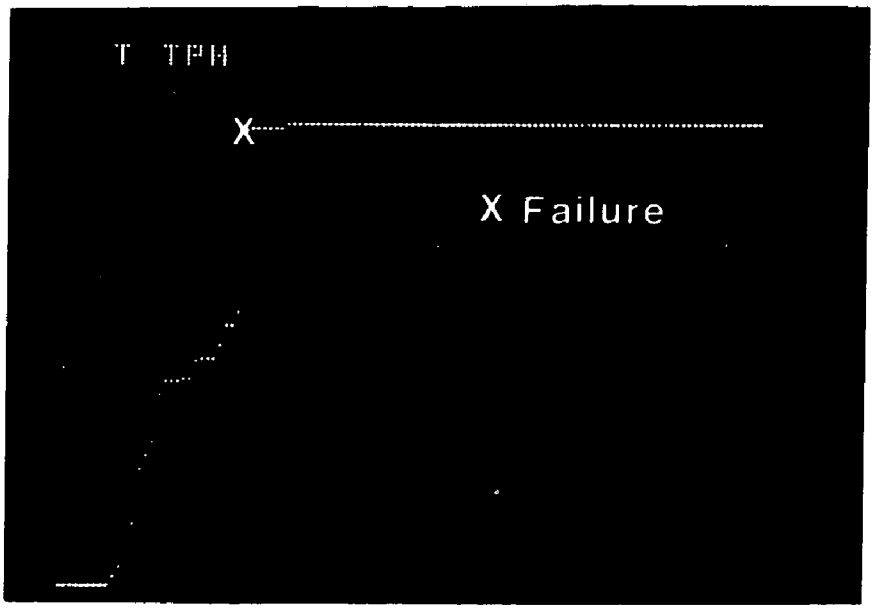

Fig. 48. Typical Time vs Total pulse height plot on CRT Screen during Implant test
Full scale = 2 hours

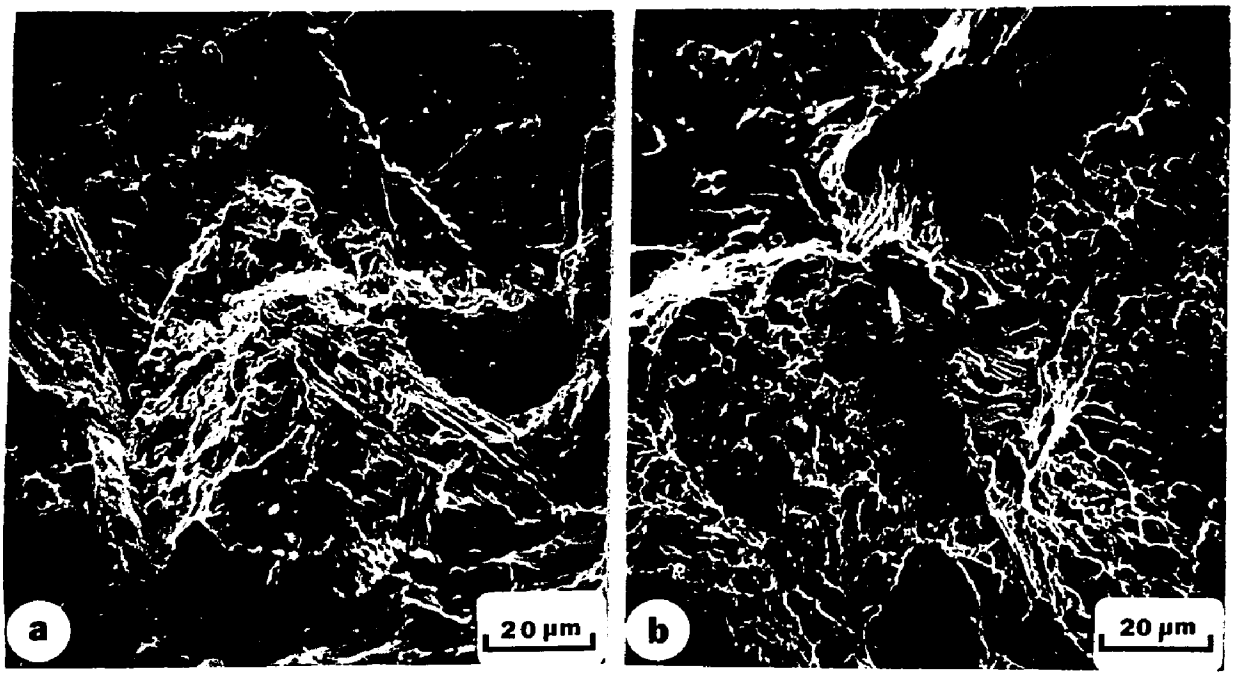

High Stress. Initiation Site

High Stress. Near final failure

Corresponds to point 1 in Fig. 34

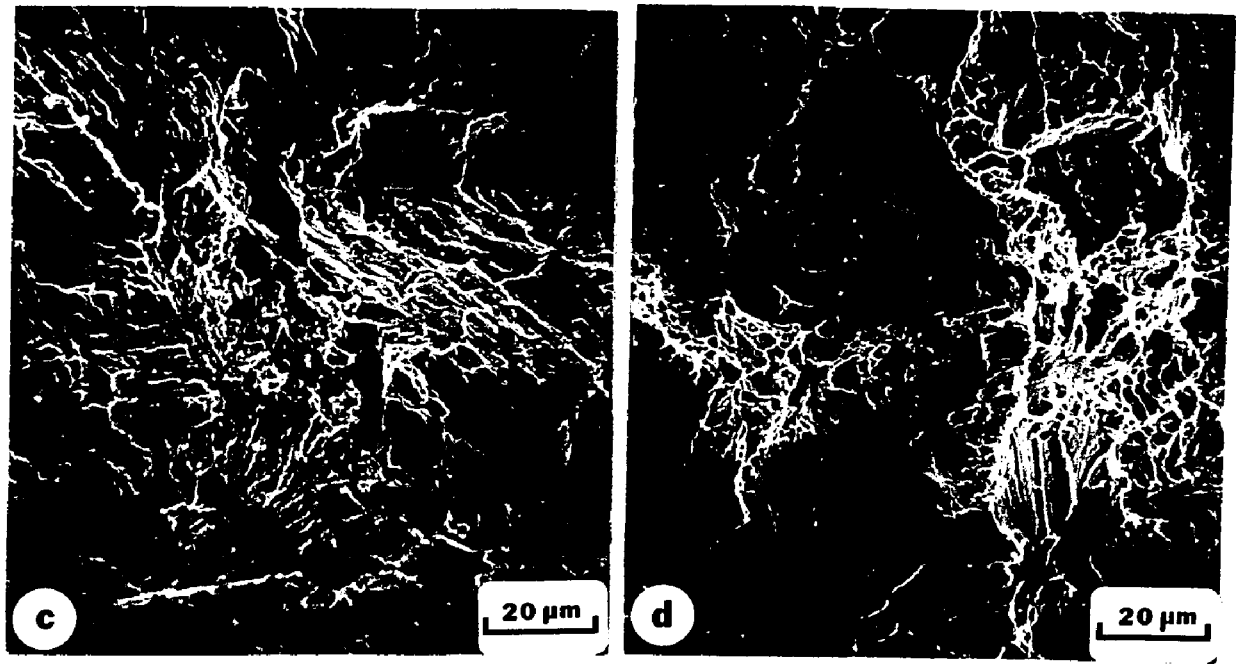

Low Stress. Initiation Site

Near final failure

Corresponds to point 2 in Fig. 34

Fig. 49. Fracture Morphology in Implant test in Heat 492S1871 welded with E7010 electrode

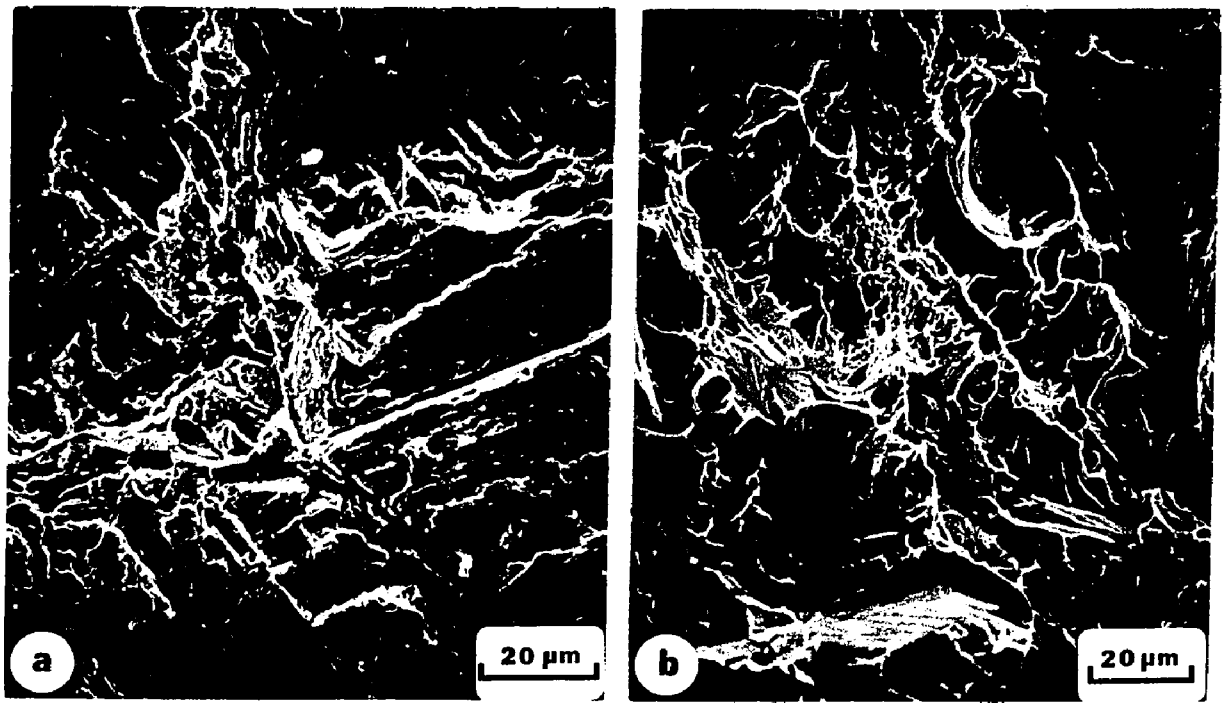

High Stress. Initiation Site — Close to failure

Corresponds to point 4 in Fig. 34

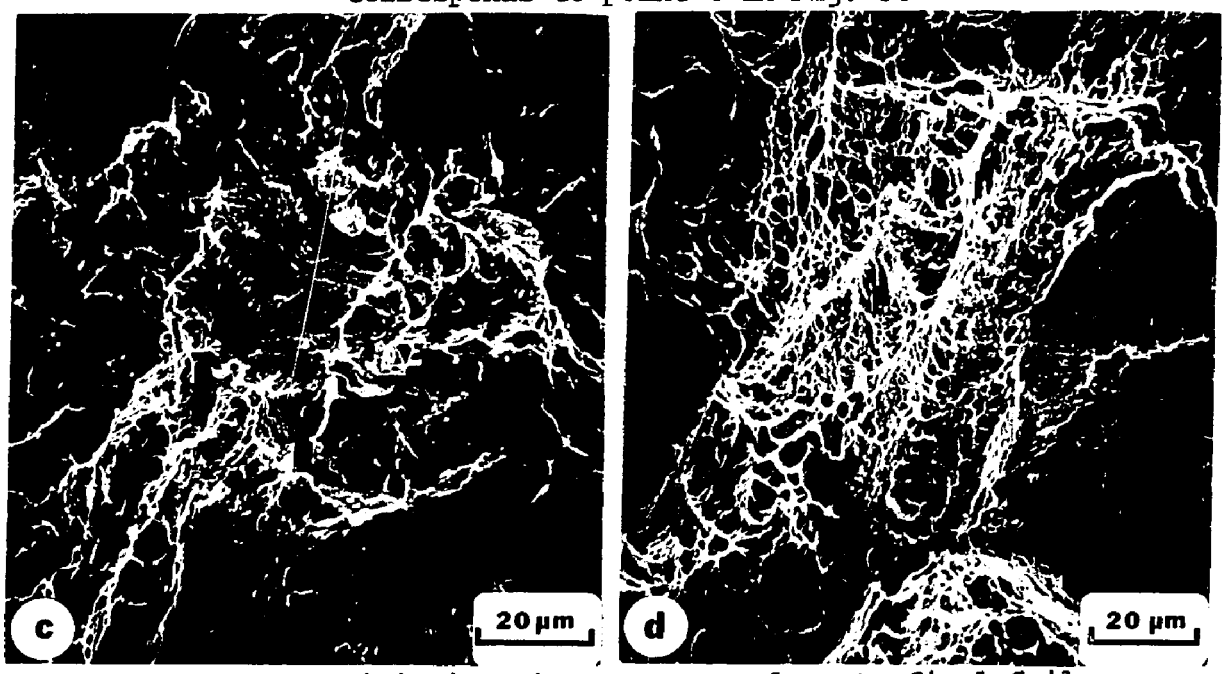

Low Stress. Initiation Site — Close to final failure

Corresponds to point 6 in Fig. 34

Fig. 50. Fracture Morphology in Implant test in Heat 492S1871. Welded with E7018 electrode

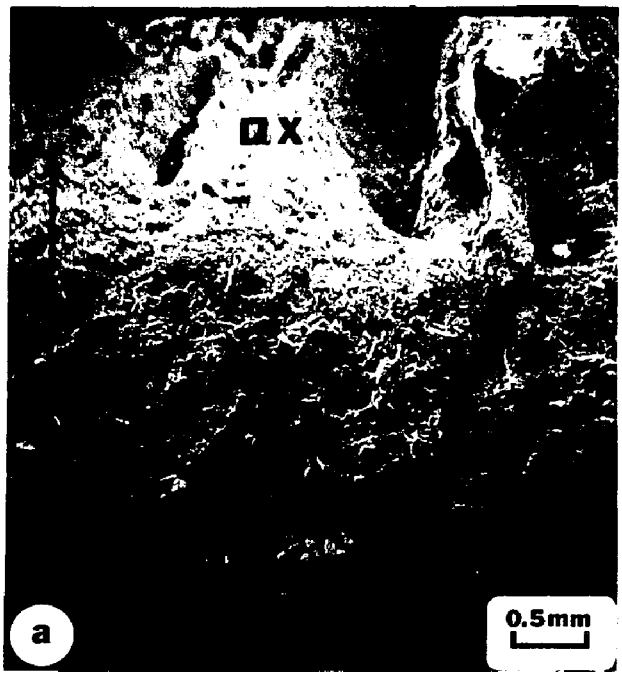

Center of the weld in slot.
General Fracture Appearance

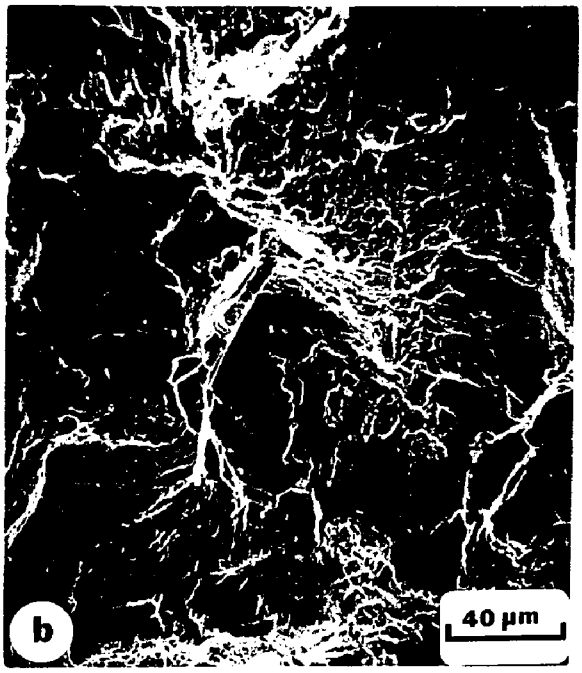

Position Z in figure (a)

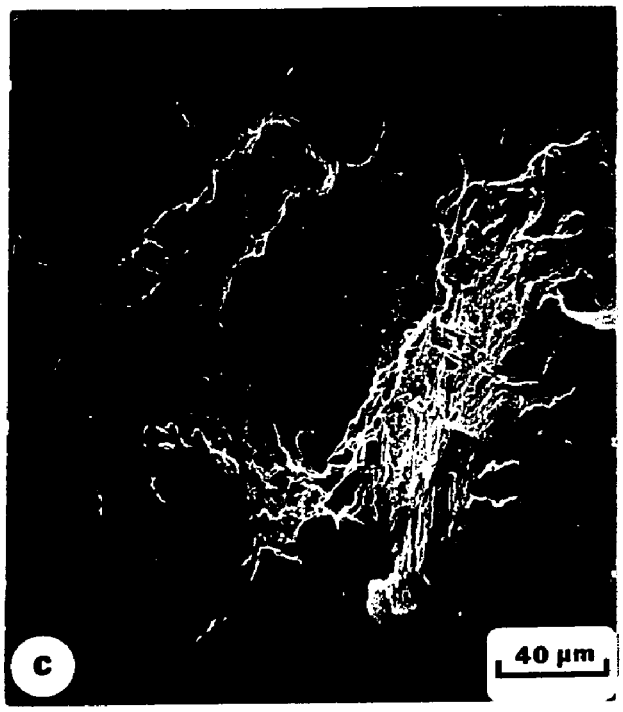

Region Y in figure (a)

Position X on figure (a)

Fig. 51 Fracture morphology in Slot Weldability test in Heat 492S1871. Welded with E 7010 electrode.
Note: Arrow indicates direction of crack growth

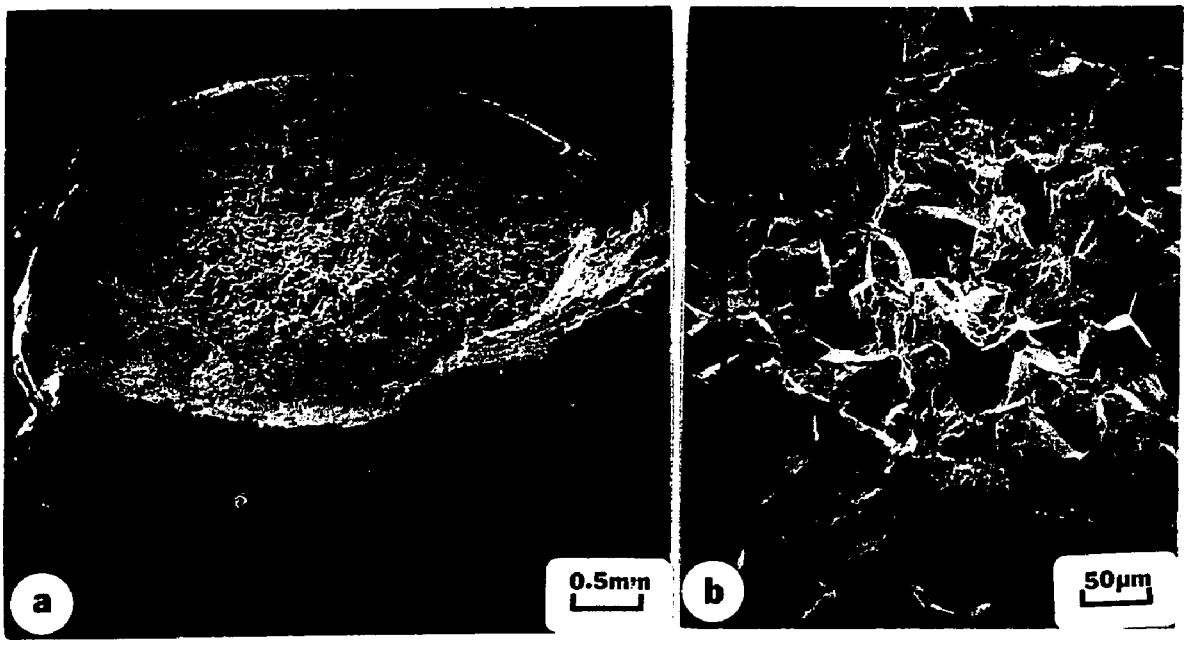

General fracture surface in Implant specimen

Region X in Fig. (a)

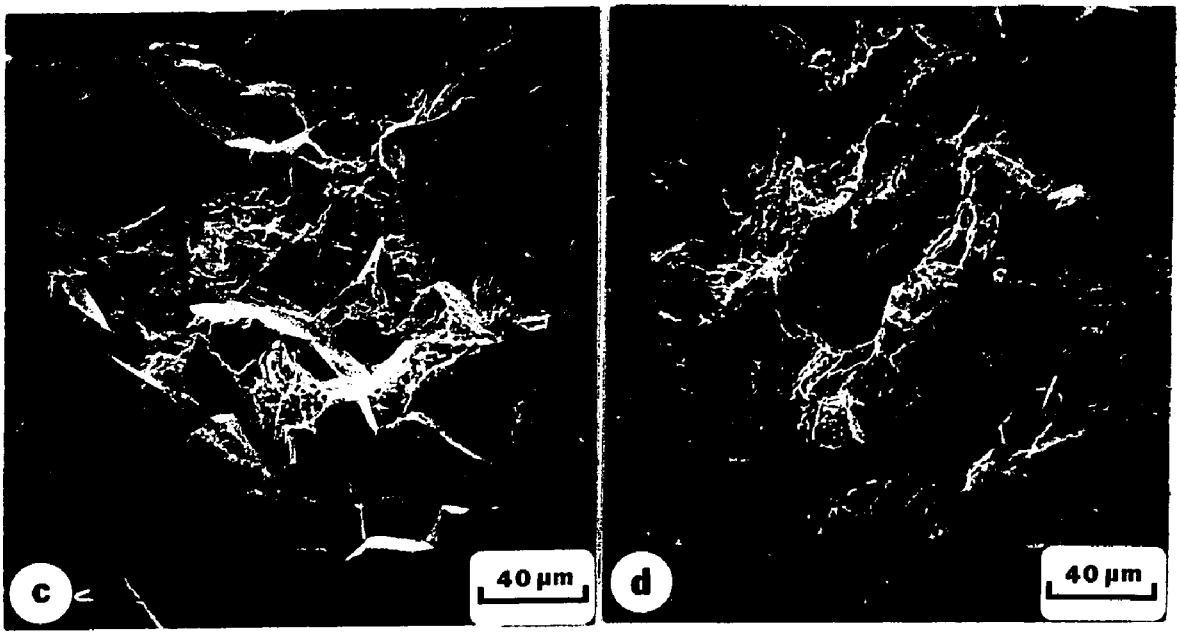

Region Y in Fig. (a) Crack initiation site

Region Z in Fig. (a) near final failure

Fig. 52. General fracture surface and morphology in Implant test in Heat C10113 welded with E 7010 electrode at low stress (Point 10 in Fig. 35)
Note: Arrow indicates direction of crack growth

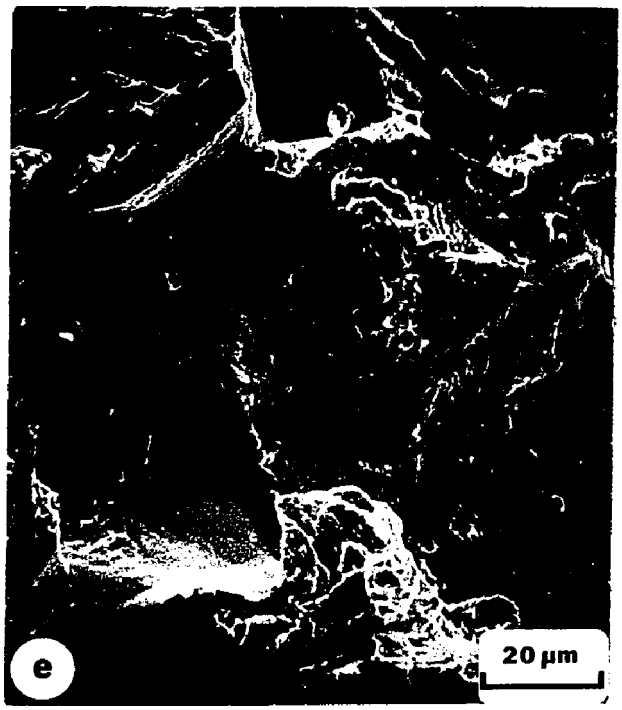

High Stress. Initiation Site

High Stress. Near final failute

Corresponds to point 8 in Fig. 35

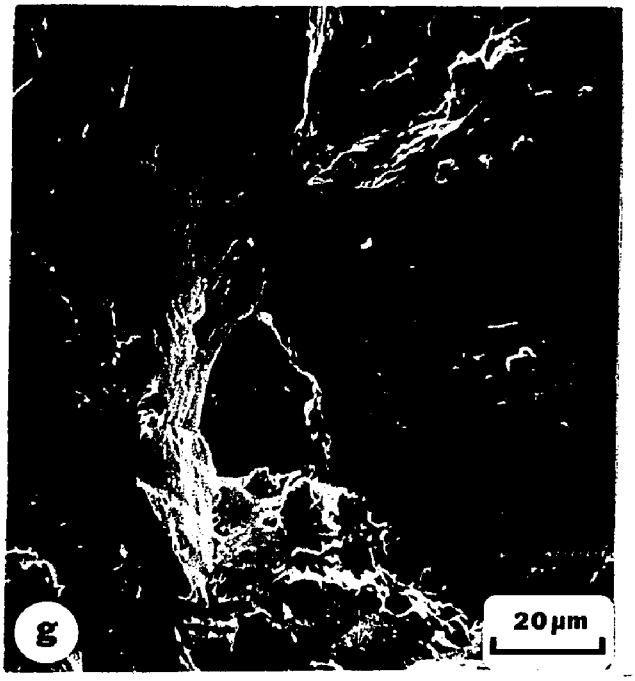

Low Stress. Initiation Site

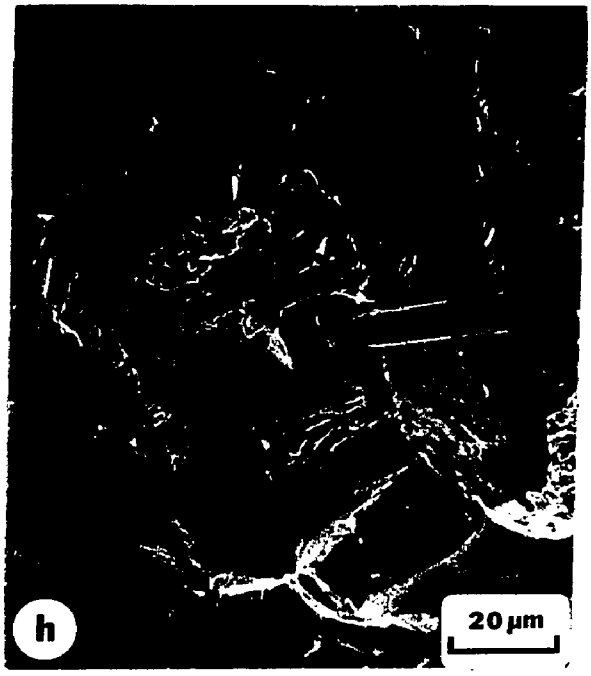

Low Stress. Near final failure

Corresponds to point 9A in Fig. 35

Fig. 52. (cont.) Fracture morphology in Implant test in Heat C10113 welded with E7010 electrode

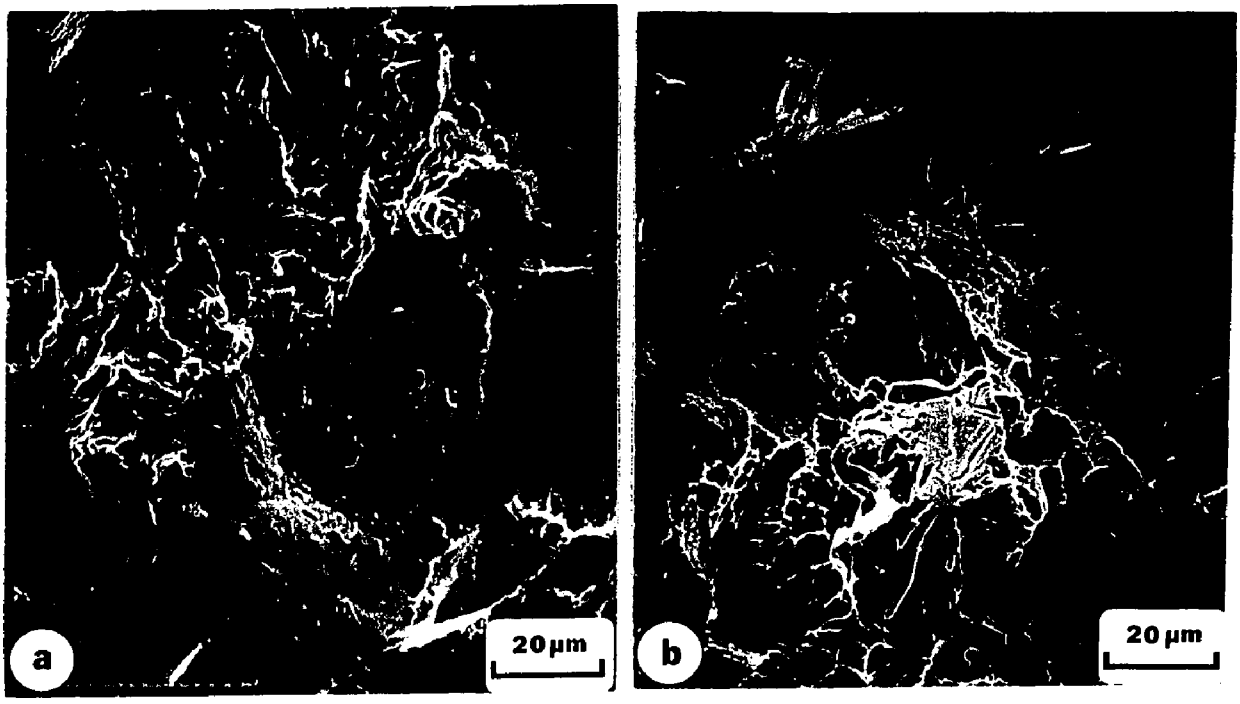

High Stress Initiation Site

High Stress Near Final Failure

Corresponds to point 12 in Fig. 35

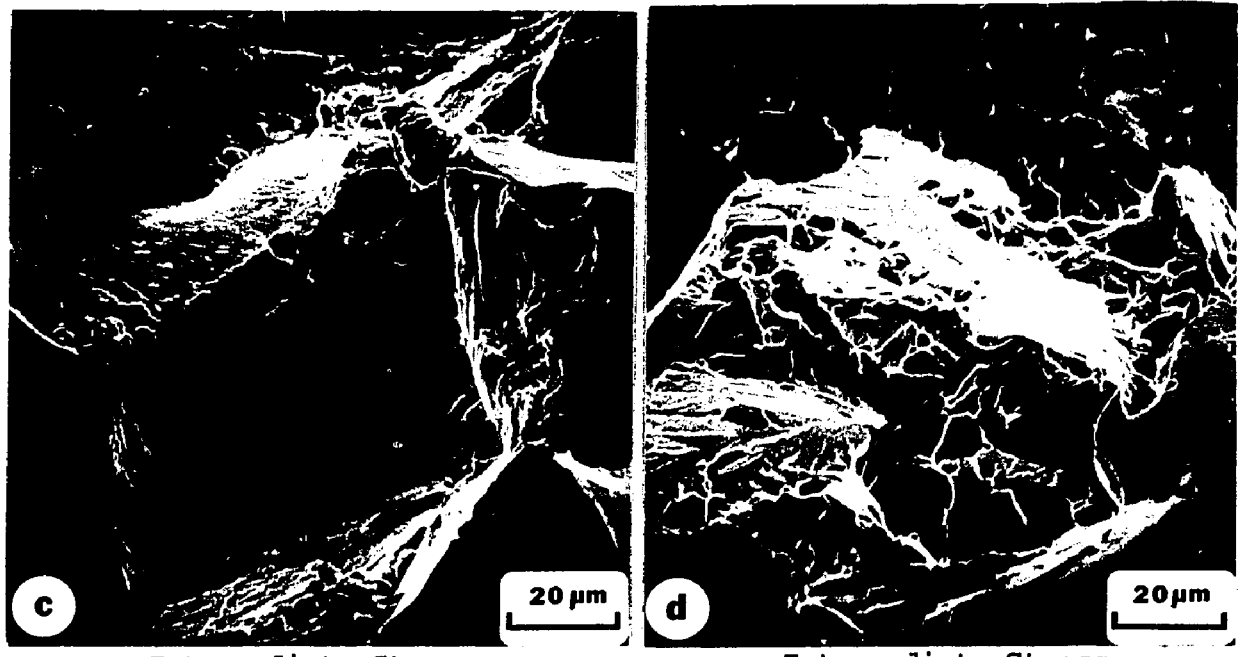

Intermediate Stress Initiation site

Intermediate Stress Near final failure

Corresponds to point 13 in Fig. 35

Fig. 53. Fracture Morphology in Implant test in C10113

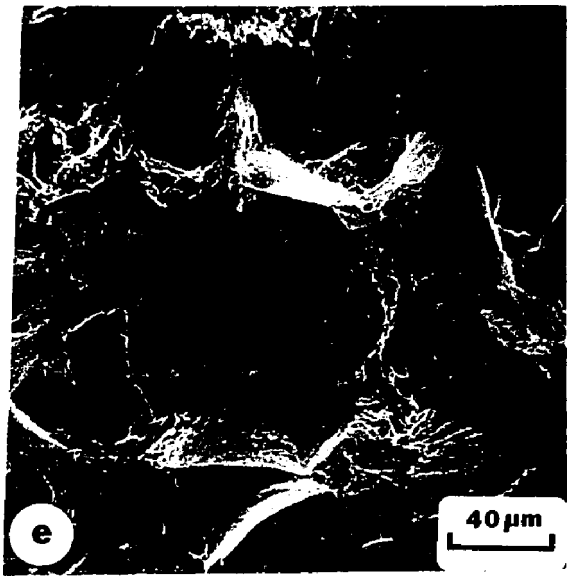

Low Stress - Initiation Site

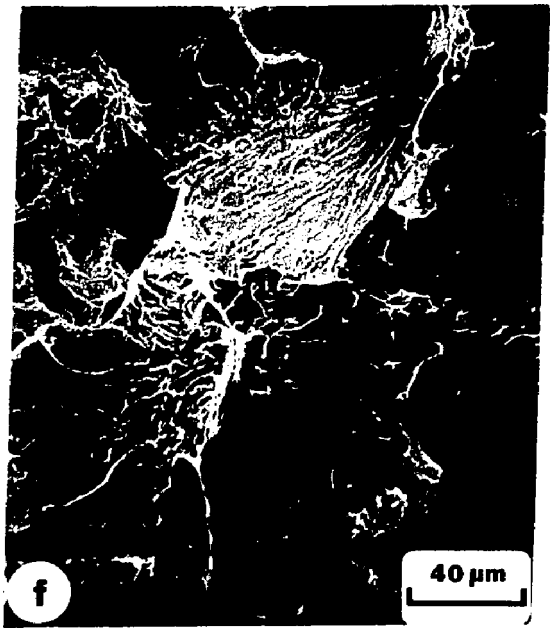

Low Stress - Near Final failure

Corresponds to point 14 in Implant test in Fig. 35

Fig. 53. (cont.) Fracture Morphology in Implant test in C10113

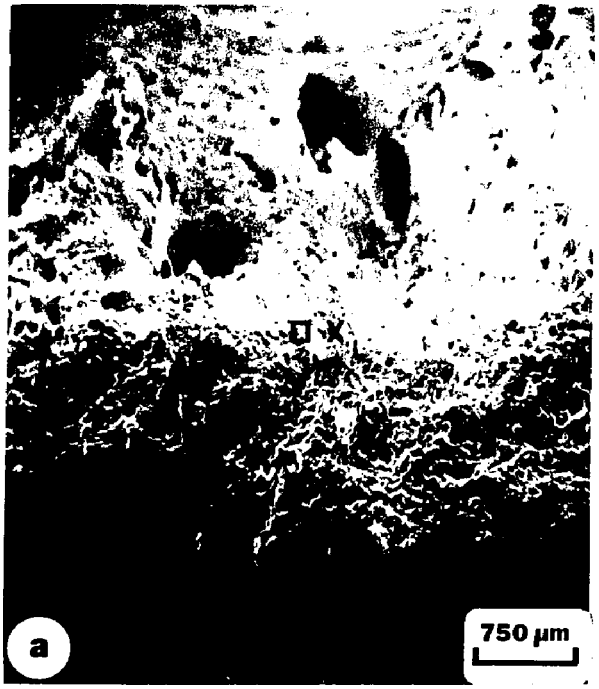

Center of weld. General fracture appearance

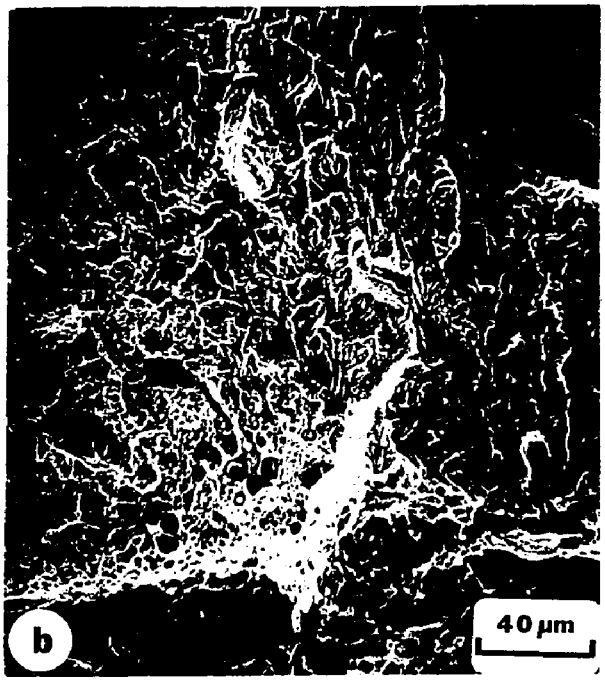

Region Z in figure (a)

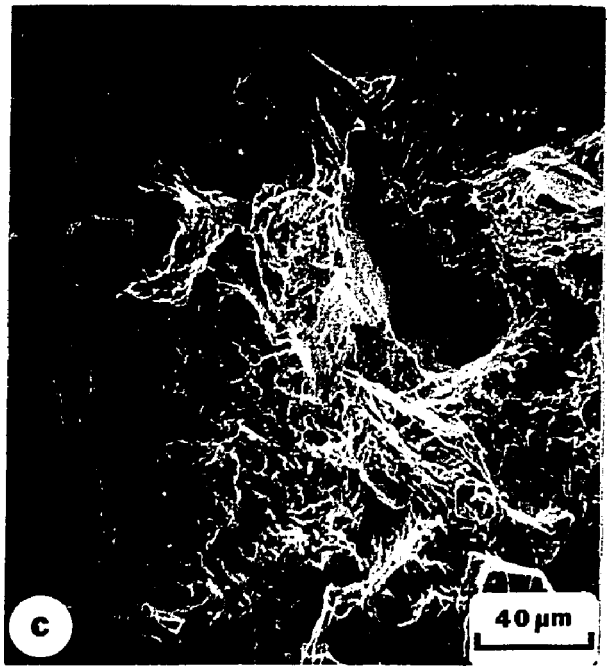

Region Y in figure (a)

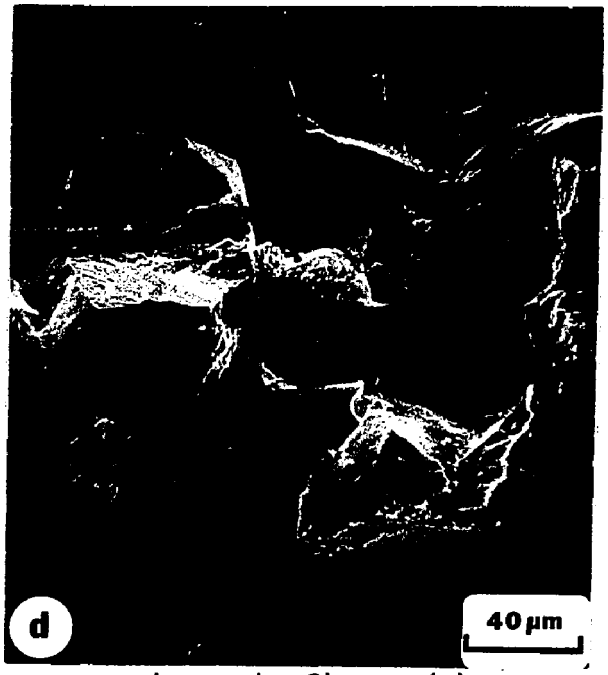

Region X in figure (a)
Close to final fracture

Note: Arrow indicates direction of crack growth

Fig. 54. Fracture morphology in slot weldability test in Heat C10113 welded with E7010 electrode

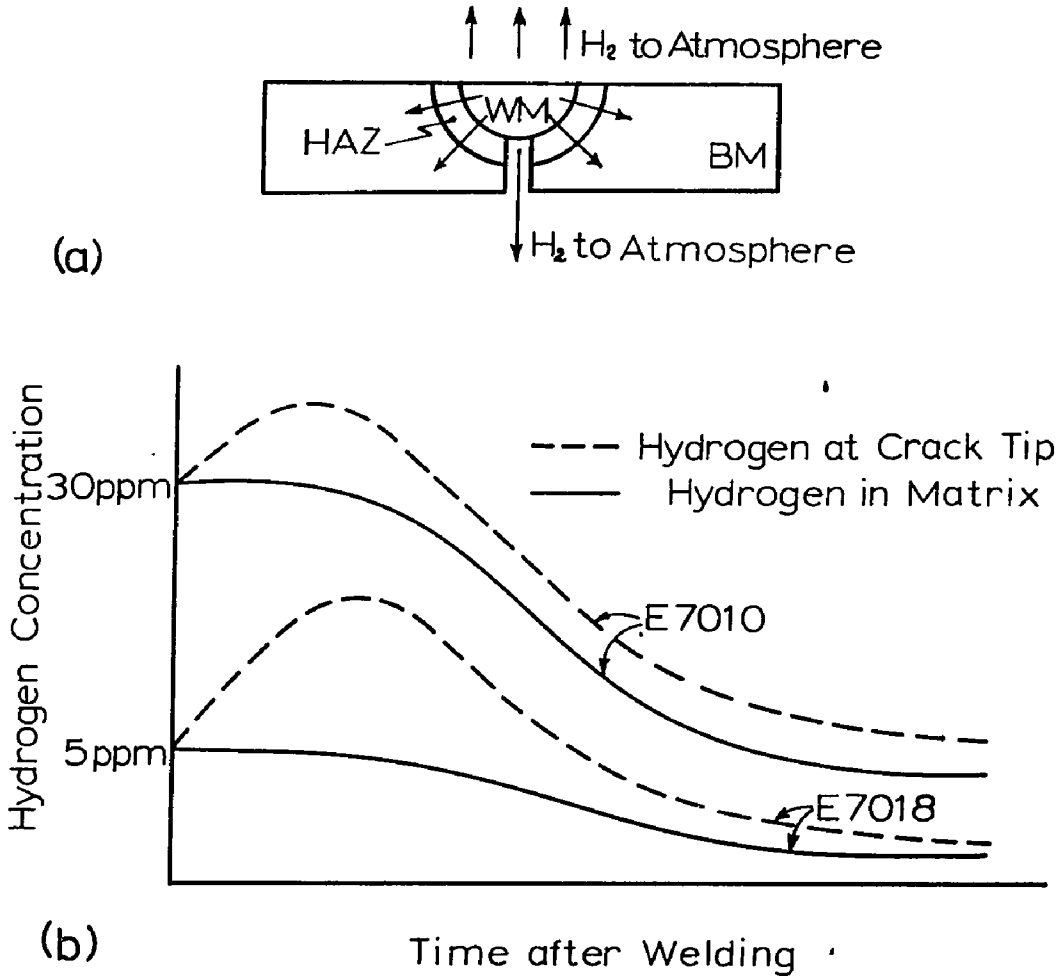

Fig.55 A Schematic of Diffusion Tendencies of Hydrogen in a Weldment.
(a) Escape Paths for Hydrogen.
(b) Variation of Hydrogen Concentration in the Matrix and at the Crack Tip with Time.

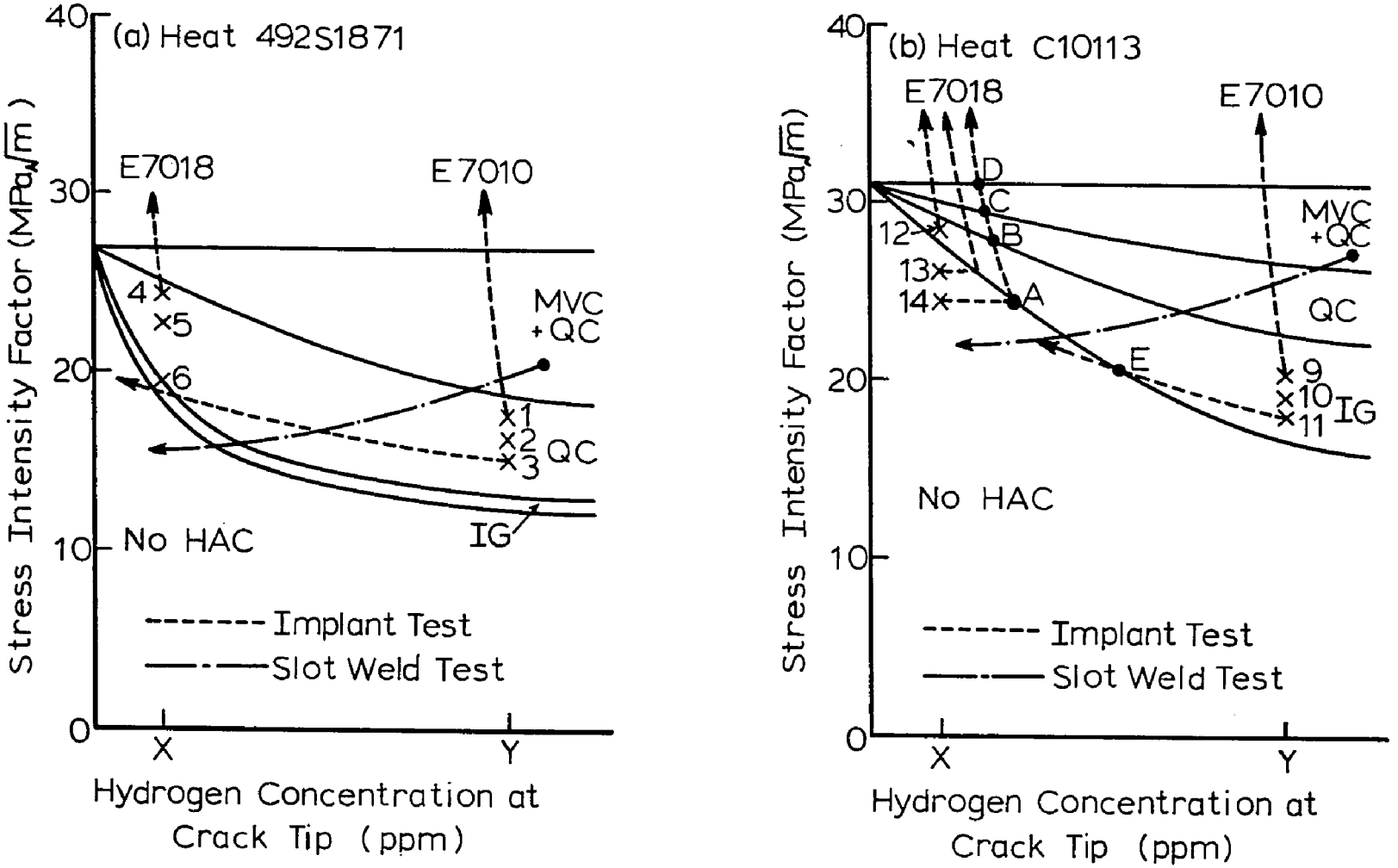

Fig.56 A Schematic of the Combined Effects of Stress Intensity and Hydrogen Concentration at the Crack Tip on the Mode of Fracture.

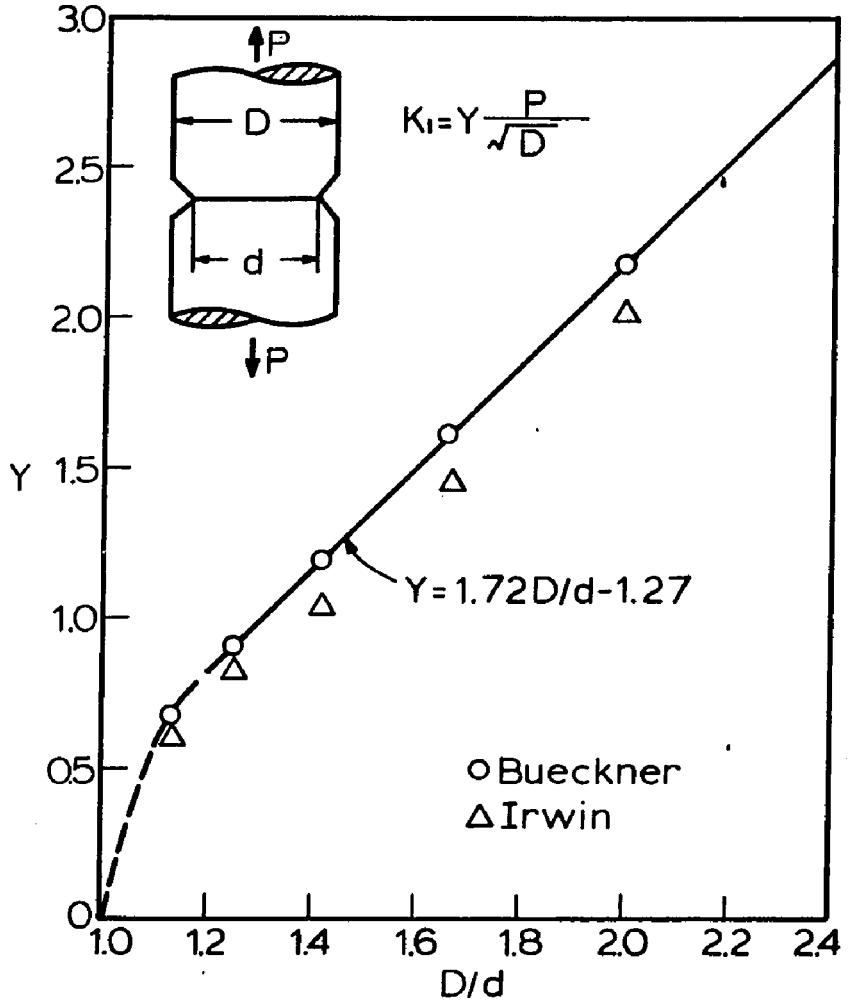

Fig.57 Stress Intensity Factor Solution for a Round Bar with a Notch. (Ref. 131)

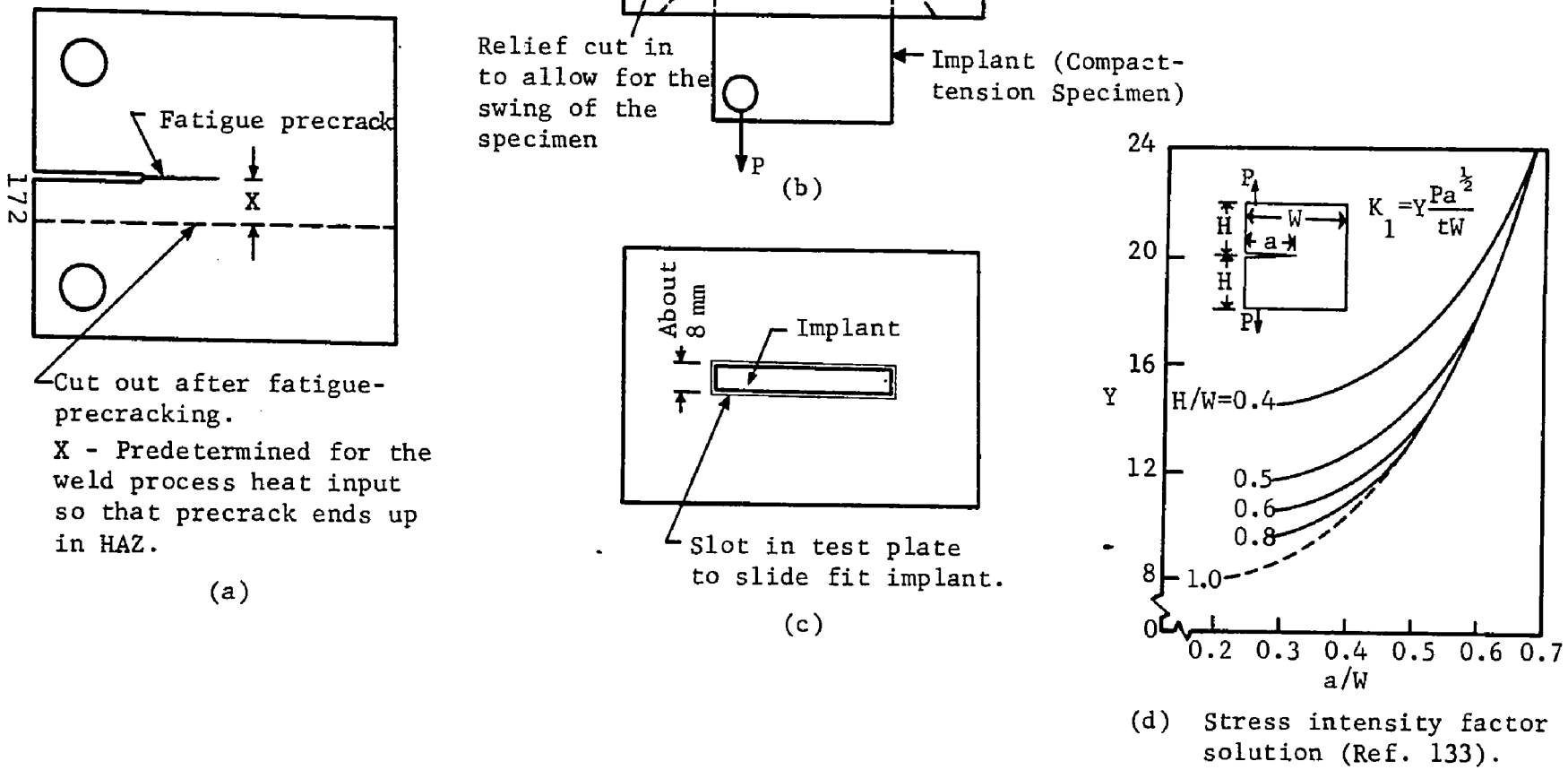

Fig. 58. Suggested Modification of Implant Test

BIBLIOGRAPHY

1. Biederman, N., "Arctic Potential Great", Pipeline and Gas Journal. Vol. 199, No. 8, July 1972, p. 21.
2. Broussard, D. E. and Visser, R. C., "Offshore Pipeline Construction", Ibid. Vol. 199, No. 1, Jan. 1972, p. 34.
3. Hale, D.,"Arctic Energy On Hold", Ibid. Sept. 1978, p. 17.
4. George, N.S., "International Pipeline Construction Forecast: Big, Getting Bigger", Ibid. Oct. 1978, p. 20.
5. Brown, R. J., "North Sea - The Challenge of Offshore Pipelining", Welding Journal, Sept. 77, p. 39.
6. Barkov, A. G., "History of Pipeline Welding - Part II", Ibid. Nov. 1977, p. 23.
7. Wormeli, J. C., "Alyeska - A Welding Milestone", Ibid. Sept. 77, p. 31.
8. Miyoshi, E., Ito, Y., Iwanaga, H. and Yamura, T., "New Development in Weldability and Welding Technique for Arctic - Grade Line Pipe", W.R.C. Bulletin 201, Dec. 1974, p. 31.
9. Barkov, A. G., "Welding High Strength Pipeline Steels" Metal Progress, Vol. 89, No. 4, Apr. 1966, p. 98.
10. Cary, H. B., "CO_2 Pipe Welding in the United States" Welding and Metal Fabrication, Vol. 34, April 1966, p. 138.
11. Lumb, R. F. and Fearnehough, G. D., "Toward Better Standards for Field Welding of Gas Pipelines", Welding Journal, V. 54, No. 2, 1975, p. 63s.
12. I.S.I. Publication 104, "Strong, Tough Structural Steels", London 1967.
13. "Micro-Alloying 75" - An International Symposium on High Strength Low Alloy Steels. 1975. Washington, D.C.

14. Tichauer, P.A., "Submerged Arc Weld in HSLA Line Pipe - A State-of-the-Art-Review", W.R.C. Bulletin 201, Dec. 1974, p. 1.

15. Civallero, M., Parrini, C. and Salmoni, G., "Experience in Development and Welding of Large Diameter Pipes", Ibid. p. 19.

16. "Hydrogen Damage". A metals science source book. American Society for Metals 1977.

17. "Hydrogen in Metals" - Proceedings of an International Conference. Champion. PA, ASM. 1973.

18. "Hydrogen Embrittlement Testing", ASTM. STP 543. American Society for Testing and Materials. 1974.

19. Stout, R. D. and Pense, A. W., "Field Weldability of 5LX Pipeline Steels" - Final Report submitted to American Petroleum Institute. Lehigh University, Bethlehem, Pa., May 1973.

20. Winterton, K., "Weldability Prediction from Steel Composition to Avoid Heat-Affected Zone Cracking", W.J. June 1961. p. 253s.

21. Ito, Y. and Bessyo K., "Weldability Formula for High Strength Steels", IIW Doc. No. 1X-576-68.

22. Tanaka, T., et al., "Evaluation of Girth Welding for Arctic Grade Pipes". The Sumitomo Search No. 18., Nov. 1977, pp. 89-101.

23. Suzuki, H., "Cold Cracking and Its Prevention in Steel Welding", IIW. Doc. IX-1074-78.

24. Fikkers, A. T., "Influence of External Restraint on Cold Cracking". Metal Construction and BWJ. June 1974, p. 188.

25. Gordine, J., "Weldability of a Ni-Cu-Cb Line - Pipe Steel", W.J. Vol. 56, No. 6, June 1977, pp. 179s-185s.

26. Rothwell, A. B., "Weldability of HSLA Structural Steels", Metal Progress. Vol. 111, No. 6, June 1977, pp. 43-50.

27. Gordine, J., "Weldability of Some Arctic Grade Line - Pipe Steels, W.J., Vol. 56, No. 7, July 1977, pp. 201s-210s.

28. Conference report, "Defining Weldability", Metal Construction and British Welding Journal. Jan. 1971, pp. 32-33.

29. Welding Handbook, Vol. 1, Seventh Edition. American Welding Society, Miami, Florida, 1976.

30. Stout, R. D. and Doty, W. D., "Weldability of Steels", 2nd Edition, Welding Research Council, New York, 1971.

31. Kihara, H., Suzuki, H. and Nakamura, H., "Weld Cracking Tests for High Strength Steels and Electrodes", W.J. Vol. 41, No. 1, 1962, pp. 36s-48s.

32. Ozaki, H., Naiman, J., Masubuchi, K., "A Study of Hydrogen Cracking in Underwater Steel Welds", Ibid. Vol. 56, No. 8, Aug. 1977, pp 231s-237s.

33. Bada, T. Yatake, T., Yurioka, N., and Kikuno, T., "Requirements of Steel and Welding Materials for the Prevention of Weld Cracking in Heavy Wall Pipe", Product Research and Development Laboratories, Nipporn Steel Corporation, Aug. 1976, pp. 1-11.

34. Nakano, S., Shiga, A. and Tsuboi, J., "Field Weldability of Line Pipes for Arctic Applications" Research Labs, Kawasaki Steel Corporation, Chiba, Japan. March 1976.

35. Watanabe, M., Satoh, K. and Matsui, S., "Effect of Restraint on Root Cracking of Steel Welds", IIW, Doc. lX-409-64.

36. Satoh, K., et al., "Study on Weld Cracking in Multiple Pass Welds of High Strength Steels", IIW, Doc. lX-678-70.

37. Suzuki, H., Inagaki, M. and Nakamura, H., "Effects of Restraint and Hydrogen on Root Cracking of High Strength Steel Welds", (NRIM TRC test) IIW, Doc. lX-408-64.

38. Granjon, H., "The Implant Method for Studying the Weldability of High Strength Steels", Metal Construction, No. 11, Vol. 1, 1969, p. 509.

39. Bragard, A., Canbo, M., Marquet, F. and Romanini, L., "Application of Implant Tests for Determining Susceptibility to Cold Cracking During Welding of High Strength Steels", IIW, Doc. 1X-905-74.

40. Matsui, S., Inagaki, M., "Recent Trends of Research on Cold Cracking With the Implant Test in Japan", IIW, Doc. 1X-970-76.

41. Christensen, N., "Weldability Testing by the Implant Method", IIW, Doc. 1X-983-76.

42. Christensen, N., "Implant Testing Based on Delayed Fracture", IIW, Doc. 1X-824-73.

43. Ito, Y., Ikeda, M., Nakanishi, M., "Study on Estimation of Lower Critical Stress for Cold Cracking at Welds by Implant Test Method", IIW, Doc. 1X-969-76.

44. Christensen, N., "Weldability Testing by the Implant Method", IIW, Doc. 1X-1037-77, II-827-77.

45. Inagaki, M., Satoh, K., Matsui, S. and Ohkuma, Y., "Application of Implant Test for Cold Cracking", IIW, Doc. 1X-1078-78.

46. Rothwell, A. B. and Bonomo, F., "Weldability of HSLA Steels in Relation to Pipeline Field Welding", WRC Bulletin. March 1977.

47. Hannerz, N., and Ferenc, K., "Influence of Vanadium on the Weldability of Constructional Steels", IIW, Doc. 1X-988-76.

48. Satoh, K., Terasaki, T., and Takagi, O. "Proposal of Displacement-Controlled Implant Test and Its Application to Cold Cracking in Actual Welded Joints", IIW, Doc. 1X-1030-77.

49. Tanaka, J., and Kitada, T., "Implant Test for Studying Cold Cracking", IIW, Doc. 1X-959-76.

50. Hart, P.H.M. and Watkinson, E., "Implant Test Ranks Cr-Mo Hydrogen Cracking Resistance", W.J. Sept. 75, V. 54, No. 9, pp. 288s-295s.

51. Sieverts, A., "Die Aufname Von Gosen Durch Metalle", Zeitschrifft fur Metallkunde.21,1929, p. 37.

52. Zapfee, C.A. and Sims, C.E., "Defects in Weld Metal and Hydrogen in Steel", W.J., Vol. 19, 1940, p. 377s.

53. Beachum, E. P., Johnson, H. H., and Stout, R. D., "Hydrogen and Delayed Cracking in Steel Weldments", W.J., 40, 1961, pp. 155s-159s.

54. Interrante, C. G. and Stout, R. D., "Delayed Cracking in Steel Weldments", Ibid. 43(4), 1964, p. 145s.

55. Smith, N. and Bagnall, B.I., "The Influence of Sulphur on Heat-Affected Zone Cracking of Carbon Manganese Steel Welds", M.C. and BWJ, Feb. (s) 1969, pp. 17-23.

56. Hewitt, J. and Murray, J. D., "Effect of Sulphur on the Production and Fabrication of Carbon-Manganese Steel Forgings", M.C. and BWJ, Feb. (s), 1969, pp. 24-31.

57. "Discussion of Hydrogen Induced Cold Cracking", Ibid., pp. 109-116.

58. Boniszewski, T. and Moreton, Mrs. J., "Effect of Micro-Voids and Manganese Sulphide Inclusions in Steel on Hydrogen Evolution and Embrittlement", Ibid. Vol. 14, No. 6, June 1967, pp. 321-336.

59. Moreton, Mrs. J., Coe, F. R., and Bonizewski, T., "Hydrogen Movement in Weld Metals", Ibid. Vol. 3, No. 5, May 1971, pp. 185-187.

60. Savage, W. F., Nippes, E. F., and Szekeres, E.S., "Hydrogen Induced Cold Cracking in a Low Alloy Steel", W.J. Vol. 55, No. 9, Sept. 1976, pp. 276s-283s.

61. Satoh, K., Ueda, Y., and Kihara, H., "Recent Trends of Research Into Restraint Stresses and Strains in Relation to Weld Cracking", Welding in the World, Vol. 11, No. 516, 1973, pp. 133-157.

62. Masubuchi, K., et al., "Finite Element Analysis of Thermo-Elasto-Plastic Deformations in Butt Welding", IIW, Doc. X-692-73.

63. Fugita, Y., et al., "Welding Stresses With Special Reference to Cracking", IIW, Doc. X-655-72.

64. Toyoda, M., Terasaki, T., Satoh, K., "Local Stresses-Strains in Welds With Particular Reference to Weld Cracking", IIW annual assembly in Dublin, 1978. Colloquium on application of numerical techniques in welding.

65. Matsui, S., et al., "Weld Cracking Susceptibility in Various Groove Shapes", IIW, Doc. lX-1048-77.

66. Krutz, G. W. and Segerlind, L. J., "Finite Element Analysis of Welded Structures", W.J., Vol. 57, No. 7, July 1978, pp. 211s-216s.

67. Masubuchi, K., "Control of Distortion and Shrinkage in Welding", WRC, Bulletin No. 149.

68. Masubuchi, K., "Residual Stresses and Distortion in Welded Aluminum Structures and Their Effects in Service Performance", WRC, Bulletin No. 174.

69. Buhler, H., et al., "The Influence of the Transformation Behaviour in Residual Welding Stresses in Steel" Arch. Eisen. 1974, 45(10), pp 719-728 - English translation by BISI. London. April 1976.

70. Satoh, K., and Matsui, S., "Reaction Stress and Weld Cracking Under Hindered Contraction", Osaka University Technology Report 17-18, 1967-68, pp. 353-375.

71. Satoh, K., et al., "Studies on Structural Restraint Severity Relating to Weld Cracking in Japan", IIW Doc. X-808-76, lX-986-76.

72. Inagaki, M. et al., "Cold Cracking in Multi-Layer Welds of Low Alloy High Strength Steel", IIW, Doc. lX-625-69.

73. Graville, B. A., and Beynon, G., "Free Contraction in Butt, T and Corner Joints", Welding Research International, Vol. 3, No. 2, 1973, pp. 68-81.

74. Sasaki, H., et al., "Effects of Restraint Stress and Intensity of Restraint on Delayed Cracks in the Welds of 80 Kg/mm^2 High Strength Thick Plate Steels", IIW, Doc. IX-784-72.

75. Masubuchi, K. and Martin, D. C., "Investigation of Residual Stress by Use of Hydrogen Cracking", W.J. Vol. 40, 1961, pp. 553s-563s.

76. Rao, N.R.N. and Tall, L., "Residual Stresses in Welded Plates", Ibid, Vol. 40, 1961, pp. 468s-480s.

77. Evans, G. M., "Correlation of the C.T.S. test With the Implant Test", IIW, Doc. II-A-292-71 and IX-814-72.

78. Satoh, K., et al., "Correlation of the Implant Test With the RRC and the TRC Tests", IIW Doc. IX-874-74.

79. Watanabe, K., et al., "Studies of Delayed Crack in Welds of High-Strength Steel", IIW, Doc. No. IX-920-75.

80. Kirihara, S., Onuma, T., Watanabe, K., and Satoh, K. "Studies of Delayed Crack in Welds of High-Strength Steel-Correlation for Method of Various Weld Cracking", IIW, Doc. No. IX-956-76.

81. Horikawa, K., Akazawa, J., Matsui, S. and Ohkuma, Y. "Correlation of Various Weld Cracking Tests", IIW, Doc. IX-966-76.

82. Miyoshi, E., Hasebe, S. and Bessyo, K., "Effect of Copper on the Weldability of Line Pipe Steels", IIW, Doc. IX-968-76.

83. Stout, R. D., "Hardness as an Index of the Weldability and Service Performance of Steel Weldments", WRC Bulletin 189, Nov. 1973.

84. Boniszewski, T., and Watkinson, F., "Effect of Weld Micro-structures on Hydrogen-Induced Cracking in Transformable Steels". Part I and Part II. Metals and Materials, Feb. 1973, pp. 90-96 and March 1973, pp. 145-151.

85. Boniszewski, T., Watkinson, F., Baker, R. G., and Tremlett, H. F., "Hydrogen Embrittlement and Heat Affected Zone Cracking in Low Carbon Alloy Steels With Acicular Micro-Structures", Brit. Weld. J., 12 (7), 1965, pp. 14-36.

86. Boniszewski, T., and Baker, R. G., "Hydrogen Embrittlement in Low Carbon Nickel and Manganese Steels", Brit. Weld. J., 12 (7), 1965, pp. 349-362.

87. Wayman, M. L., and Smith, G. C., "The Hydrogen Embrittlement of Fe-Ni Martensites", Met. Trans. 1, (1970), p. 1189.

88. Bernstein, I. M., "Hydrogen-Induced Cracking in Iron: Morphology and Crack Path Dependence", Met. Trans (1), 1970, p. 3143.

89. Bernstein, I. M., "The Role of Hydrogen in the Embrittlement or Iron and Steel", Matls. Sci. Eng.6 (1970), p. 1.

90. Zapfee, C. A. and Sims, C. E., "Hydrogen Embrittlement, Internal Stress and Defects in Steel", Trans. AIME (145), 1941, p. 225.

91. Tetelman, A. S., "The Mechanism of Hydrogen Embrittlement in Steel", Proc. Fund. Aspects of Stress Corrosion Cracking. Houston, Texas, NACE (1969), p. 446.

92. Petch, N. J., "The Lowering of Fracture Stress Due to Surface Adsorption", Phil. Mag. 1, 1956, pp. 331-337.

93. Petch, N. J. and Stables, P., "Delayed Fracture of Metals Under Static Load", Nature, 169 (1952), p. 842.

94. Troiano, A. R., "The Role of Hydrogen and Other Interstecials in the Mechanical Behaviour of Metals", Trans. ASM, 52 (1), 1960, p. 54-80.

95. Oriani, R. A. and Josephic, W., "Testing of the Decohesion Theory of Hydrogen-Induced Crack Propagation", Scripta Met., 6, (1972), p. 681.

96. Beachem, C. D., "A New Model for Hydrogen Assisted Cracking (Hydrogen 'Embrittlement')", Met. Trans. Vol. 3, Feb. 1972, pp. 437-341.

97. Beachem, C. D., "Electron Fractographic Support for a New Model for Hydrogen Assisted Cracking", Proc. Confce. on Stress Corrosion Cracking and Hydrogen Embrittlement of Iron Base Alloys. NACE, Houston, 1977.

98. Savage, W. F., Nippes, E. F. and Homma, H., "Hydrogen Induced Cracking in HY-80 Steel Weldments", W. J. Vol. 55, No. 11, Nov. 1976, pp. 368s-376s.

99. Savage, W. F., Nippes, E. F., and Tokunaga, Y., "Hydrogen Induced Cracking in HY-130 Steel Weldments", W.J., Vol. 57, No. 4, April 1978, pp. 118s-126s.

100. Embury, J. D., Petch, N. J., Wraith, A. E. and Wright, E. S., "The Fracture of Mild Steel Laminates", Trans. AIME, 239, 1967, pp. 114-118.

101. McEvily, A. J. and Bush, R. H., "An Investigation of the Notch-Impact Strength of an Ausformed Steel", Trans. ASM, 55, 1962, pp. 654-666.

102. Stout, R. D., Vasudevan, R., and Pense, A. W., "A Field Weldability Test for Pipeline Steels", W.J., Vol. 55, No. 4, April 1976, pp. 89s-94s.

103. Beckett, A. S., "Evaluation of API Field Weldability Test", Columbia Gas Transmission Corporation, Nov. 29, 1977.

104. Stightz, R., et al., "Lehigh Slot Weld Testing of X-60 Line Pipe Steels", Republic Steel Research Center, March 23, 1978.

105. Ueno, K., Shiga, A., and Tsuboi, J., "Field Weldability Test for Pipeline Steels", Kawasaki Steel Corporation, Chiba, Japan. May 1977.

106. "Evaluation of API RP 5L7 Recommended Practice for Conducting Weldability Tests on Line Pipe", Report by Natural Gas Pipeline Co. of America - Dec. 22, 1977.

107. Schmid, G. C., "Evaluation of the New Lehigh Pipeline Steel Weldability Test". Armco Research and Technology, Feb. 3, 1978.

108. Smith C., "The Evaluation of API Recommended Practice 5L7 for Conducting Weldability Tests for Pipe Steels", Tennessee Gas Pipeline Report. Nov. 14, 1977.

109. "Evaluation of API Recommended Practice 5L7 for Conducting Weldability Tests on Pipe Steels". The Steel Company of Canada, Ltd., May 30, 1978.

110. "Evaluation of the Lehigh Slot-Weld Test", U.S. Steel Corp. Bulletin, Dec. 11, 1978.

111. Campbell, W. P., "Experiences With HAZ Cold Cracking Tests on a C-Mn Structural Steel", W.J. 55, 4, May 1976, pp. 135s-143s.

112. Sawhill, Jr., J.M., Dix, A. W. and Savage, W. F., "Modified Implant Test for Studying Delayed Cracking", W.J. Vol. 53, No. 12, Dec. 1974, pp. 554s-560s.

113. Metals Handbook, Vol. 11, "Non Destructive Inspection and Quality Control", 8th Edition. American Society for Metals, Metals Park, Ohio, p. 234.

114. Dunegan, H. L., Harris, D. O., and Tatro, C.A., "Fracture Analysis by Use of Acoustic Emission", Eng. Fr. Mech., Vol. 1, 1968, pp. 105-122.

115. Hamstad, M. A., Bianchetti, R., and Mukherjee, A. K., "A Correlation Between Acoustic Emission and Fracture Toughness of 2124-T851 Aluminum", Eng. Fr. Mech., Vol. 9, 1977, pp. 663-674.

116. Liptai, R. G., Harris, D. O., Engle, R. B., and Tatro, C. A., "Acoustic Emission Techniques in Materials Research", International Journal of Non Destructive Testing, Vol. 3, 1971, pp. 215-275.

117. Hartbower, C. E., Gerberich, W. W. and Crimmins, P.P. "Monitoring Subcritical Crack Growth by Detection of Elastic Stress Waves", Welding Journal, Jan. 1968, pp. 1s-18s.

118. Dunegan, H. L., and Tetelman, A. S., "Non Destructive Characterization of Hydrogen Embrittlement Cracking by Acoustic Emission Techniques", Eng. Fr. Mech. Vol. 2, 1971, pp. 387-402.

119. Liptai, R. G., Dunegan, H. L., and Tatro, C. A., "Acoustic Emissions Generated During Phase Transformation in Metals and Alloys", International Journal of NDT, Vol. 1, 1969, pp. 213-221.

120. Bolotin, Y.I., et al., "The Use of Acoustic Emission for Examination of Deformation Processes in Welded Joints", Svar. Proiz. No. 2, 1975, pp. 9-11 (English Translation by BWRA).

121. Hart, S. D., "On the Possibilities for the Use of Acoustic Emission for Non Destructive Testing of Welds and Welded Structures". Welding in the World, Vol. 12, No. 3/4, 1974, pp. 55-58.

122. Dunegan, H., and Harris, D., "Acoustic Emission-A New Non-Destructive Testing Tool". Ultrasonics, July, 1969, pp. 160-165.

123. Arrington, M., "Acoustic Emission", British Journal of NDT, Jan. 1975, pp. 10-14.

124. Hartman, W. F., "Acoustic Emission Detection of Flaws in Butt Welded Plates", Materials Evaluation, Dec. 1974, pp. 259-261.

125. Jolly, W. D., "Acoustic Emission Exposes Cracks During Welding", Welding Journal. Jan. 1969, pp. 21-27.

126. Proc. Third Conference on "Periodic Inspection of Pressurized Components", The Inst. of Mech. Engr., London, Sept. 1976.

127. Romrell, D. M., "Acoustic Emission Weld Monitoring of Nuclear Components", Welding Journal, Vol. 52 (2), Feb. 1973, pp. 81s-87s.

128. Savage, W. F., Nippes, E. F., and Sawhill, Jr., J.M., "Hydrogen Induced Cracking During Implant Testing of Alloy Steels", Vol. 55 (12), 1976, pp. 400s-407s.

129. Krishna, G. V., Air Products and Chemicals, Inc. - Trexlertown, Pa. Private Communications.

130. Rath, B. B. and Bernstein, I. M., "The Relation Between Grain Boundary Orientation and Intergranular Cracking", Met. Trans. 2, p. 2845.

131. Brown, Jr., W. F. and Srawley, J. E., ASTM, STP 410, 1966.

VITA

Ramaswamy Vasudevan was born on February 12, 1949, in Bangalore, India, the son of C. Srinivasa and Rukmini Ramaswamy Iyengar. Following graduation from R. V. High School, Bangalore, in 1963, he joined National College, Bangalore University, to major in science. In 1964, he entered University College of Engineering, Bangalore University, to pursue a degree course in engineering and graduated in 1969 with a Bachelor's degree in Mechanical Engineering. From 1969 to 1971, he was at Indian Institute of Technology, Madras working towards his Master's degree in Metallurgy with specialization in metal joining. From 1972 to 1974, he was at Tohoku University, Sendai, Japan, as a research fellow working in "fusion zone concentration gradients in dissimilar metal weldments". In July 1974, he received a research assistantship to pursue his doctorate in Metallurgy and Materials Engineering at Lehigh University, Bethlehem, Pennsylvania.

Ramaswamy Vasudevan is a member of AWS, ASM, and the Society of Sigma Xi.